TeV astronomy of millisecond pulsars

Brazler, Karen Tracy Susan

Abstract

This thesis is concerned with the detection of pulsed TeV γ-rays from millisecond pulsars. These stars appear to include some very efficient producers of high energy particles, but the mechanisms by which they produce TeV γ-rays are still a matter of debate.

After an introductory section, there is a brief description of the principles used in the atmospheric Cerenkov technique. The design and operation of the University of Durham atmospheric Cerenkov telescopes are reviewed. The main analysis techniques used to search for periodic signals are then described. The effects on periodic signals of binary motion of a source are discussed. These are a particularly important consideration for observations of millisecond pulsars, where high timing accuracy is required.

One of the problems of detecting TeV sources is the cosmic ray background. A means of rejecting background events in TeV γ-ray telescopes is considered in chapter 5. The technique is developed for the Durham Mark III telescope. Substantial rejection of the cosmic ray background is achieved, with minimal loss of source events.

The evolutionary scenarios which lead to the formation of millisecond pulsars are outlined. Two models for γ-ray emission are discussed briefly and applied to six known millisecond pulsars. Empirical results on these and two other pulsars are also presented. In particular, a detection of PSR 1855+09 is reported, and an upper limit to the flux from PSR 1957+20 is derived. All the empirical fluxes are compatible with the emission models, but the 'polar gap' model may be favoured.

The final chapter summarises the results obtained and suggests some directions for future work on the γ-ray emission from millisecond pulsars.

TeV ASTRONOMY of MILLISECOND PULSARS

BY

Karen Tracy Susan Brazier, BSc.

A thesis submitted to the University of Durham in accordance with the regulations for admittance to the degree of Doctor of Philosophy.

DEPARTMENT OF PHYSICS
UNIVERSITY OF DURHAM

AUGUST 1991

Contents

Preface

The Durham Mark III telescope has been operating at Narrabri, New South Wales, Australia, since 1986. The author was a member of the observing team at this site for five dark moon periods. She was also a member of the observing team using the Mark IV telescope on La Palma, Canary Islands, for one dark moon period. In addition, she has been part of the team performing the routine pre-processing of the data.

The author was responsible for the development of the signal to noise enhancement technique described in chapter five. In conjunction with this work, she wrote software to examine and normalise data, and to test event selection criteria.

Together with her colleagues, she investigated the effects on a periodic signal of mis-correcting for binary motion of a source, and developed software to produce graphical representations showing the relationship between the major orbital parameters and the strength of periodicity.

The author analysed data on a number of objects, including the X-ray binary Centaurus X-3 and a number of millisecond pulsars. She studied data on PSR 1855+09 and PSR 1957+20 in detail, and reanalysed archival data on PSR 1953+29. She summarised all the Durham results on millisecond pulsars and made the comparisons with theoretical expectations given in chapter seven.

None of the material contained in this thesis has been submitted previously for admittance to a degree in this or any other university.

Acknowledgements

I would like to thank Professors A.W. Wolfendale and A.D. Martin for the provision of the facilities of the Department of Physics over the last three years, and the Science and Engineering Research Council for my studentship. I thank Professor K.E. Turver for his enthusiastic supervision, and Alan Lotts and the Starlink project, for keeping me in touch with the outside world.

It is a pleasure to thank my colleagues at the Observatory for their help and companionship: Chris Bowden, Stella Bradbury, Alberto Carramiñana, Paula Chadwick, Nigel Dipper, Penny Dunbabin, Pete Edwards, Cyril Hay, Susan Hilton, Eric Lincoln, Vince Mannings, Lowry McComb, Keith Orford and Ken Tindale. Steve Rayner is especially thanked for reading this thesis, and for his memorable Italian cooking in Narrabri.

I would also like to thank all the members of the YTA in the department, whose lunchtime seminars were much appreciated, my family, for wondering what this was all about, and Peter and Graham, for putting up with me for the last year.

Lastly, I would like to thank Richard Bower, without whose love, encouragement and support, I would certainly have been finished before this thesis. This is for him.

Sprich aus der Ferne,
Heimliche Welt.

Clemens Brentano

1778 - 1842

CHAPTER 1

Introduction

1.1) An introduction to cosmic rays

The term 'cosmic rays' is used to describe the highly energetic particles which are incident on the Earth from extraterrestrial sources. Such particles have been the subject of much interest since the beginning of this century. The study of cosmic rays began with a terrestrial discovery. It was observed that the rate of charge leakage in an electroscope could be greatly reduced by enclosing the electroscope in a thick metal shield (Rutherford and Cooke, 1903). This meant that the charge loss must be due to some external, highly penetrating radiation. At first, this was attributed to radioactive materials, but it was found that the intensity of the radiation did not decrease with altitude as expected for radiation of a purely terrestrial origin (Gockel, 1910, Hess, 1911, Millikan and Bowen, 1926, Millikan and Otis, 1926). It was concluded that there was an element of the radiation which was extraterrestrial in origin, and the term 'cosmic radiation' was coined to describe the phenomenon.

Cosmic rays and their origin have been a subject of study and speculation ever since their discovery. The cosmic ray spectrum is now known to extend in energy to beyond 10^{20} eV (Lawrence, Reid and Watson, 1990). The flux of particles at the Earth is highly isotropic and consists mostly of protons. These are deflected over interstellar

scales by the 10^{-6} G Galactic magnetic field even up to 10^{18} eV, so the flux isotropy does not place strong constraints on the location or nature of the sources of cosmic rays. γ-rays, which do not suffer this deflection, make up only $\sim 10^{-4}$ of the overall flux. At first, acceleration in interstellar shocks was favoured as a mechanism for producing cosmic rays. Later, as energetic and compact objects such as neutron stars, black holes, active galactic nuclei and quasars were discovered, the possibility arose that some proportion of the cosmic radiation originated in discrete sources.

To test the hypothesis that cosmic rays are generated in discrete sources, it is necessary to search for local anisotropies in the cosmic ray flux. The locations of the anisotropies can then be compared with the positions of candidate sources. Searching for anisotropies is difficult because the majority of TeV particles are charged and are deflected by the galactic magnetic field over typical stellar distances. Neutrons cannot be studied because they do not survive long enough to traverse interstellar distances without decay. There is no way of directly determining the origin of these particles. The only easily detectable particles which provide us with directional information about their origin are γ-rays. TeV γ-rays are highly penetrating and can survive intergalactic distances without interaction. Thus, even extragalactic sources of TeV γ-rays may be identifiable. The γ-rays from a point source also retain temporal information. This is especially important in the study of variable objects, where the variability can be used to extract much information about the physical processes occurring at the source. Variability can also help to identify weak signals and to associate a signal with a candidate source.

1.2) The discovery of pulsars

As mentioned above, one of the candidate mechanisms for the acceleration of cosmic rays involves neutron stars. Rapidly rotating, magnetised neutron stars (pulsars) are powerful accelerators of particles. Their study has proved to be one of the most fruitful fields of TeV γ-ray astronomy, and it is useful to consider the development of the subject.

The discovery of pulsars in 1967 fuelled much interest in high energy astrophysics and cosmic rays. Jocelyn Bell and Anthony Hewish were involved in a project studying scintillation in cosmic radio signals. Bell noticed that in one part of the sky, the signal varied with extraordinary regularity. After investigation, these pulsations were eventually assigned to a stellar source, possibly a white dwarf or a neutron star, the latter an object whose existence was at that time unproven (Hewish et al, 1967). Three other pulsating sources were also observed by the group in that year, and the new objects were named 'pulsars'.

The physical nature of pulsars was quickly established. Pacini (1967) had already shown that a rapidly rotating neutron star with a strong dipolar field would be a powerful generator of radiated energy, and Gold (1968) independently identified pulsars with rotating neutron stars. The detection of X-rays from the Crab nebula (Fritz et al, 1969) confirmed that pulsars were powerful sources of high energy emission as well as radio radiation. This empirical result opened the way for many more works on the high energy emission from pulsars, among them the possibility that pulsars were responsible for a substantial fraction of

the cosmic ray flux.

1.3) The development of TeV γ-ray astronomy

The original motivation for TeV γ-ray astronomy was therefore to search for the origin of cosmic rays in discrete celestial objects. Candidate sources now include pulsars, active galactic nuclei, quasars, the Galactic centre and other energetic systems. The term γ-ray is generally applied in astronomy to any photon of energy above ~1 MeV, a category which includes photons from a multitude of sources and processes and detected using a number of techniques. These are split into three broad regions: low - high energy, very high energy and ultra high energy. γ-rays in the first of these categories, from ~1 MeV to ~30 GeV in energy, are detected using scintillation detectors, spark chambers, and Compton and Cerenkov detectors. As the primary particles do not penetrate far into the Earth's atmosphere, the detectors are mounted on balloons or satellites. At ultra high energies (above ~ 10^{15} eV, or 1 PeV), where the flux of γ-rays is very low, showers of particles generated during the primary γ-ray's passage through the atmosphere ('air showers') can be detected directly on the ground using large arrays of scintillation detectors. The wide lateral extent of these showers (> 10^4 m^2) means that the count rate of a ground-based telescope is very much increased from the flux at the top of the atmosphere.

It is with the energy band between the two regions mentioned above that this thesis is concerned. At photon energies of between ~ 30 GeV

and ~ 100 TeV, the number of energetic shower particles reaching the ground is too small to be detected by particle detector arrays, whilst the flux at the top of the atmosphere is insufficient to make satellite detectors practical. However, a short, highly collimated flash of Cerenkov light, created when relativistic shower particles interact with the atmosphere, is detectable at ground level. Absorption processes in the atmosphere leave a Cerenkov spectrum at ground level which peaks at the blue end of the visible region. A detector may therefore be constructed very simply using a single optical light collector and a photomultiplier tube mounted at its focus. Cerenkov flashes from the night sky were first observed by Galbraith and Jelley (1953) using the simple combination of a searchlight mirror and a single photomultiplier tube.

Several TeV astronomy groups are currently operating Cerenkov telescopes. These are listed in Table 1.1. The telescopes are all similar in that their main components are one or more large, optical flux collectors and an arrangement of photomultiplier tubes. The differences lie in the techniques used to improve the signal to noise ratios of these simple devices. Most of the groups employ only geometrical arguments to discriminate between the large, isotropic background of protons and the weak flux of γ-rays from point sources, but some attempt to identify the γ-rays directly. Photon- and hadron-initiated air showers are slightly different in structure, because protons and other hadrons give rise to 'daughter' showers which cause irregularities in the Cerenkov shower at the ground. The difference can in theory be used to identify the type of cosmic ray and thus increase the signal to noise ratio of data. The Whipple collaboration have

Telescope location	Group	Operational
Crimea, USSR	Crimea	1965
Gulmarg, India	Bhabha	1983
Nooitgedacht, RSA	Potchefstroom	1985
Albuquerque, USA	California Riverside	1985
Narrabri, Australia	Durham	1986
Pachmarhi, India	Tata Institute	1987
Mt. Hopkins, USA	Whipple	1987
Beijing, China	Acad. Sinica	1987
Woomera, Australia	Adelaide	1988
Pyrenees, France	Saclay	1989
Delingha, China	Acad. Sinica	1990
Albuquerque, USA	Michigan	1988
Xing Long, China	Beijing	1990

Table 1.1

Currently operative atmospheric Cerenkov telescopes

developed the use of the spatial image of the Cerenkov flash to find both the direction of origin and nature of the cosmic ray primary, in order to achieve a high signal to noise ratio (Weekes et al, 1989), whilst a group using high precision timing (Tumer et al, 1990a, 1990b) discriminate according to the showers' temporal profiles. Both of these techniques, however, still suffer from some uncertainties, and neither has become widely used. Spatial imaging, for example, may be effective only over a limited range of zenith angles (Weekes, private communication). Time structure discrimination is a very new technique and the analysis is still reliant on subjective rejection criteria. The Durham group has confined itself through a succession of Cerenkov telescopes to the established method of a restricted angular aperture to decrease the proton noise background component, combined with a fast coincidence arrangement to eliminate contamination by optical starlight photons and electronic noise and to minimise the telescope energy threshold.

1.4) Candidate TeV sources

Except for the case of fast pulsars, predictions of TeV γ-ray emission from astronomical objects have not been abundant, and most candidate TeV sources have been studied only empirically. A large number of sources of various types has been claimed, most of which have been X-ray pulsars, and many in binary systems. To date, only eight sources have been confirmed as TeV sources by two or more independent groups. Notable among them have been the Crab pulsar and nebula (Gibson

et al, 1982a, Weekes et al, 1989), Hercules X-1 (Chadwick et al, 1987, Gorham et al, 1986, Resvanis et al, 1988) and Cygnus X-3 (e.g. Brazier et al, 1990f, Resvanis et al, 1987a, Gregory et al, 1990). The other five are the X-ray binaries Centaurus X-3 (Brazier et al, 1989b, North et al, 1989), Vela X-1 (North et al, 1987, Carramiñana et al, 1989a) and 4U0115+63 (Chadwick et al, 1985c, Resvanis et al, 1987b), and the cataclysmic variable AE Aquarii (Bowden et al, 1991, Raubenheimer et al, 1991). The low and often variable fluxes of TeV γ-rays from point sources are probably largely responsible for the lack of confirmed sources, as most detections are made only after extensive observations of a source. It is particularly important in this field of astronomy to obtain good signal to noise ratios in order to reduce the observation time necessary and to facilitate the detection of weak sources. This thesis is concerned with a means of enhancing of γ-ray signals, and with the detection of TeV γ-rays from millisecond radio pulsars, a recently discovered class of pulsars which include the fastest ones known. Although they have so far been extensively studied only at radio wavelengths, they are predicted to have spectra which peak at γ-ray energies. They may thus be some of the most efficient particle accelerators in the Galaxy.

CHAPTER 2

The Atmospheric Cerenkov Technique

2.1) Introduction

High energy particles entering the Earth's atmosphere do not penetrate to the ground. Instead, they interact with atoms in the upper atmosphere to generate a shower of daughter particles. Many of these are themselves of sufficient energy to propagate this process, so that a cascade of particles with a wide range of energies develops. A large fraction of a cascade is made up of electrons and positrons, which are the particles of most interest to Cerenkov astronomers. This electromagnetic element of the cascade continues to grow via pair production and bremsstrahlung interactions until the mean particle energy becomes too low for further pair creation. Ionisation and Coulomb scattering losses then dissipate the shower. Although very few of the particle trajectories deviate widely from the direction of the primary particle, the long flight through the atmosphere leaves the shower of particles spread over typically 10^4 m^2 at ground level. For this reason, such particle cascades in the atmosphere are termed 'extensive air showers' (EAS).

Atmospheric Cerenkov telescopes operate by detecting a pulse of visible Cerenkov light emitted by the atmosphere as relativistic charged particles in the EAS pass through it. They operate generally with energy thresholds in the TeV region, where large numbers of these

visible photons are produced by a shower and the Cerenkov pulses are much brighter than the ambient night sky for their very short duration. The technique enables high energy cosmic particles to be detected very effectively from the ground, using the atmosphere as an essential part of the detector. The ease of operation is only one of the advantages which Cerenkov telescopes have over other high energy telescopes, which must be operated on balloons or satellites.

2.2) Atmospheric cascades

2.2.1) Photon-initiated air showers

The cascade interactions in air showers generated by incoming γ-rays are almost entirely electromagnetic, so the air shower is composed mostly of electrons, positrons and photons. The electrons and positrons are formed by pair production in the nuclear fields of atmospheric atoms, and the γ-rays are produced in the bremsstrahlung interactions and electron-positron annihilation of these pair particles. The EAS has a smooth, circular cross-section, except for a small elongation caused by deflection of the charged particles in the geomagnetic field.

2.2.2) Hadronic air showers

A hadronic shower is in many respects similar to photon-initiated showers, since a substantial part of it will be electromagnetic. The first interaction will usually be strong, and produces a number of both charged and neutral pions, which carry large fractions of the primary's

energy. Charged pions can interact with atmospheric nuclei to produce further pions and generate small sub-showers of their own, or they will decay into neutrinos and muons. The muons thus formed are highly penetrating and generally reach the ground without further interaction. Neutral pions have a very short lifetime and therefore decay into pairs of photons, which then go on to generate electromagnetic cascades. In general, the air shower initiated by a hadron is less regular than one from a photon, because of its more complicated development and because extreme fluctuations in the energy distribution can occur.

2.3) Cerenkov light in the atmosphere

2.3.1) Production of Cerenkov light

When a charged particle moves through a dielectric medium, it induces polarisation of the charges in nearby atoms. In returning to the ground state, these atoms produce radiation, which for a non-relativistic primary particle interferes destructively and is not seen. If, however, the particle is moving faster than the local phase velocity of light, i.e. $v > c/n$ where n is the refractive index, there is one angle to the particle trajectory at which the radiation interferes constructively, and a hollow cone of light is produced. The creation of Cerenkov light is most effectively illustrated by a Huygens' construction (Figure 2.1). The condition $v > c/n$ implies an energy threshold E_{th} for a particle of given mass:

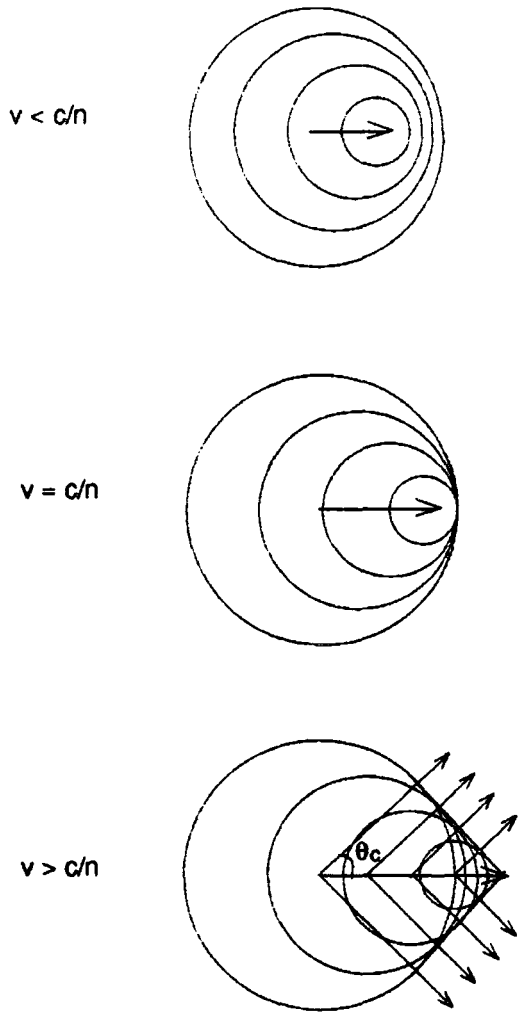

Figure 2.1

Huygens' construction to illustrate the production of Cerenkov light.
θc is the Cerenkov angle.

$$E_{th} = \frac{mc^2}{(1-v^2/c^2)^{1/2}}$$

i.e.
$$E_{th} = \frac{mc^2}{(1-1/n^2)^{1/2}} \qquad - \ 2.1$$

The half-angle of the cone is given by:

$$\cos\Theta = c/vn \qquad - \ 2.2$$

where Θ is known as the Cerenkov angle. Note that the maximum half-angle is reached for ultra-relativistic particles, when $\Theta \sim \cos^{-1}(1/n)$, or $\sim 1.3^\circ$ for visible light in air at N.T.P. Clearly, Cerenkov light cannot be emitted if $n < 1$, and so Cerenkov light is emitted in the atmosphere only in the ultraviolet, visible, infrared and microwave regions. The wavelength spectrum at emission is proportional to λ^{-2}, but is distorted due to strong atmospheric attenuation at short wavelengths. The resultant spectrum at the ground has a maximum in the extreme blue (Protheroe, 1977).

The number of Cerenkov photons emitted is a function of the particle energy. It has been shown (Jelley, 1958) that the number of photons emitted per unit path length between wavelengths λ_1 and λ_2 is

$$\frac{dN}{dl} = \frac{2\pi}{137} \cdot \left[\frac{1}{\lambda_1} - \frac{1}{\lambda_2} \right] \sin^2(\Theta_c) \qquad - \ 2.3$$

where Θ_c is defined in equation 2.2.

2.3.2) Cerenkov light from extensive air showers

Since the threshold particle energy for Cerenkov light production is proportional to the particle mass, electrons produce nearly all the Cerenkov light from air showers. For electrons at sea level, E_{th} = 21 MeV which is exceeded by around 85% of electrons at the shower's maximum (Roberg and Nordheim, 1948). The shower propagates through the atmosphere at nearly the vacuum speed of light and tends to advance ahead of the Cerenkov photons. The progress of the shower electrons, however, is slowed by Coulomb scattering, which also increases the lateral spread of the shower. The resultant flash of Cerenkov light at the ground is a smooth 'pancake' of light, the *light pool*. The photon density in the light pool is typically 100 m^{-2}, over an area of 10^4 m^2 for a cosmic γ-ray with a energy of a few hundred GeV (Browning and Turver, 1977).

The angular width of the Cerenkov flash is determined mostly by the spread of particle trajectories in the air shower. Since most of the Cerenkov photons are produced where the number of particles is greatest ('shower maximum'), the characteristic angular spread of the Cerenkov flash represents roughly the angular width of the shower at this point, as seen from the ground. The geomagnetic broadening of the shower has little effect on the Cerenkov light except to spread it over a slightly wider area, with a corresponding reduction in the peak photon density (Browning and Turver, 1977). At the zenith, the Cerenkov photons are expected to arrive at 0.5 - 0.7° to the source direction (Kenter, 1989). The angles may be expected to be smaller at large zenith angles, where the shower maximum is more distant, although broadening of the flash, primarily by Rayleigh scattering, must also be considered (Protheroe,

1977). A larger degree of attenuation will also occur here.

The thickness of the light pool yields a characteristic light flash duration of 2-3 ns. This very short timescale is of great use in identifying EAS Cerenkov flashes above the ambient starlight.

The Cerenkov flashes from air showers produced by cosmic γ-rays and protons are essentially fairly similar. The major difference between the two types is that the less orderly showers resulting from incident protons yield Cerenkov flashes at the ground which appear broader and less regular than their photon-initiated counterparts. Because of the energy lost to muon sub-showers and because the shower develops later, the Cerenkov flashes are also weaker than flashes from γ-rays of similar energy. The angular spread of the Cerenkov light is, however, very similar to that of a photon-initiated flash, and it is therefore difficult, with a conventional Cerenkov telescope, to determine the nature of the primary particle from the Cerenkov light alone.

2.4) Astronomy with the atmospheric Cerenkov technique

Cerenkov telescopes enable astronomy to be carried out in a region of the electromagnetic spectrum which would otherwise be inaccessible. Up to ~ 30 GeV, satellite telescopes operate successfully with spark chamber instruments, such as the EGRET instrument aboard the Gamma Ray Observatory satellite. The primary and inevitable limitation of any space telescope is its size. The flux of incident photons decreases with increasing enegry, and at energies approaching 1 TeV, the background flux of incident particles is only ~ 10^{-3} cm^{-2} s^{-1} $ster^{-1}$.

At these energies, a small detector would not be able to make sensitive measurements in typical satellite lifetimes.

At PeV energies and above, the EAS particles can be detected at ground level using arrays of scintillators, opening up to study the highest energies known. A large number of particle detector arrays now exist around the world. They are used both to study the EAS as a probe of very high energy interactions, and to search for point sources of ultra high energy (UHE) photons.

Cerenkov telescopes fall between these two categories, in a gap in the energy spectrum where the flux is too low for satellite observations and the EAS particles are not detectable at ground level. Instead, the flashes of Cerenkov light associated with EAS are detected. That the peak of the atmospheric Cerenkov spectrum is in the visible region greatly facilitates the design of Cerenkov telescopes. A simple light collector with a photomultiplier tube at its focus is sufficient to detect Cerenkov flashes from the night sky. The narrowness of the Cerenkov cone enables directional information to be retained. Although the $\sim 1^{\circ}$ spread of the light does not permit very high directional precision by the standards of astronomy at lower wavelengths, it is easily sufficient to associate TeV sources with known celestial objects. As with particle detector arrays, the atmosphere acts as an amplifier for a Cerenkov telescope, multiplying both the number of particles to be detected and the effective area of the telescope by many orders of magnitude, transforming the low intrinsic flux into a worthwhile count rate.

Existing Cerenkov telescopes vary considerably in sophistication and efficiency, ranging from simple light collectors to 'cameras' which

form images of the Cerenkov flashes in an attempt to identify the nature of the primary particles. The telescopes built and operated by the Durham group since 1981 have detected a large fraction of all TeV point sources. In the following chapter, their design, construction and operation will be described.

CHAPTER 3

The Durham Cerenkov telescopes

3.1) Philosophy of the Durham telescopes

The design philosophy of the Durham Cerenkov telescopes is straightforward. Cerenkov flashes produced by cosmic ray air showers are focussed by simple light collectors and detected by photomultiplier tubes. No attempt is made to discriminate *directly* between hadronic cosmic rays and gamma rays, but full use is made of the spatial and temporal anisotropies which characterise point sources. If a single photomultiplier tube (PMT) is used in such a system, the gain must be kept very low to minimise the background count rate due to starlight. In order to detect true Cerenkov flashes above the ambient starlight of the night sky whilst retaining a high gain (i.e. low γ-ray energy threshold), the Durham telescopes are designed with three paraxial flux collecting dishes, each with an assembly of PMT's at the focus. The three adjacent, but independent dishes must simultaneously register a Cerenkov event within a tight ($\sim$ 5 ns) coincidence time, t, for the event to be recorded. This 'fast coincidence' system, combined with a narrow field of view, has been shown to be particularly efficient (Patterson and Hillas, 1989). The accidental coincidence rate, R, for a triplet of PMT's is given by

$$R = 3! \times n^3 \times t^2 \qquad - \quad 3.1$$

where n is the number of counts per second registered by a single PMT. Typically, n is kept at less than 50 kHz in the currently operative Mark III and Mark IV telescopes, so the rate R is at most only a few counts per hour. This is negligible compared with the background cosmic ray flux, which contributes ~ 2 counts per *second*. It is therefore a reasonable assumption that all events registered are Cerenkov flashes initiated by high energy cosmic particles.

The major pollutant of any gamma ray signal is therefore the large, isotropic background of hadronic cosmic rays, which gives a signal to noise ratio ~ 1:20 in the Durham telescopes, even for a fairly strong gamma ray source. The effect of this background is limited in the current telescopes by restricting the effective telescope aperture to around 0.9° FWHM, approximately matching the expected angular spread of the Cerenkov photons. A means of further reducing the effective aperture to maximise the signal to noise ratio will be discussed in detail in chapter 5.

3.2) The Dugway experiment: the Mark I and Mark II telescopes

The first University of Durham Cerenkov astronomy project was sited at Dugway Proving Ground, Utah, USA (40° N, 113° W, 1450 m above sea level), where it operated from 1981 to 1984. It consisted of an array of four small telescopes positioned at the apices and centre of an equilateral triangle. Each of the telescopes was composed of three parabolic, 1.5 m diameter searchlight mirrors, paraxially co-mounted on an alt-azimuth mount. A single 5" diameter RCA 4522 photomultiplier

tube was placed about 8 cm behind a 5 cm diaphragm in the focal plane of each mirror. The Dugway telescopes were designed with the detection packages some centimetres from the focal plane to avoid any problems arising from the non-uniformities in the quantum efficiency across the large photomultiplier cathode.

The geometry of the telescopes gave a nominal 1.75° FWHM aperture, which was increased to an effective 2.2° when the angular extent of Cerenkov flashes was included (Dowthwaite, 1987). Since each flux-collector was served by a single, on-axis PMT, no off-axis information was recorded. The energy threshold was estimated from a comparison of the count rate of the telescopes (typically 15 c.p.m. per telescope) and computer simulations to be around 1.0 TeV at the zenith.

The four telescopes operated independently, but common timing also permitted inter-telescope coincidences to be recorded. Up to four independent datasets could therefore be constructed, each containing only events registered by one, two, three or four of the telescopes. Multiple telescope events were of interest as the effective aperture was smaller for these events than for those registered only by an individual telescope, so that the signal to noise ratio was higher in these subsets of the data. The two-telescope events were found to form a particularly useful dataset.

In mid-1983, the primary mirrors on one of the telescopes were replaced by purpose-built, aluminium mirrors. The 5" photomultipliers were also replaced, by 2" RCA 8575 tubes. The improved telescope had an effective field of view for Cerenkov light of only 1.8° FWHM and an enhanced light collection efficiency. Despite the reduced aperture, the count rate of this "Mark II" telescope was 11 c.p.m at the Zenith,

corresponding to a new energy threshold of 800 GeV (Chadwick, 1987). The Dugway telescopes are described in detail in Dowthwaite (1987) and Chadwick (1987).

3.3) The Mark III telescope

3.3.1) The Narrabri site

The Mark III telescope has been operated since October 1986 at a site near Narrabri, New South Wales, Australia (150° E, 30° S, 260 m a.s.l). The site was chosen because its latitude is suited to observations of most Southern Hemisphere Galactic sources and because the weather is stable and dry, with a high percentage of clear nights, essential if large datasets are to be collected and if observations are to be made throughout the year. The site is in a forest, so that the average wind speed is only a few knots, which is an important consideration for a large, unprotected and lightly engineered telescope.

3.3.2) The flux collectors

The collecting area of a Cerenkov telescope is primarily determined by the area covered by the light pool of an extensive air shower. The limiting radius is determined by the fall-off in photon density with distance from the shower centre. For a telescope with a 1° field of view, showers within a radius of ~ 50 m will be detected on-axis, giving a total area of ~ 10^4 m^2 (Browning and Turver, 1977). The telescope sensitivity is dependent on the gain of the detectors, which in turn is

determined by the maximum permissible counting noise from background starlight. The collecting area of the Mark III telescope has been optimised to give the maximum count rate with a low energy threshold (Brazier et al, 1989a). The flux collectors are three large, approximately parabolic dishes constructed from a total of 130 small circular sections of spherical mirror with a common focus (Figure 3.1). The mirrors are surfaced with anodised aluminium, which is about 80% reflective (Weekes, private communication) and has shown no appreciable degradation in the five years since they were installed. The total reflecting area is 34 m^2, and the γ-ray threshold energy of the telescope is estimated to be 250 GeV at the Zenith. The telescope has a count rate near the Zenith of ~ 120 counts per minute, falling as roughly $\cos^{2.35}\theta$, where θ is the zenith angle (Chadwick, 1987).

3.3.3) Telescope pointing

The telescope is steered on an alt-azimuth mount to an attitude resolution of 0.09°. It is operated in three modes, according to the type of source under study:

i) In a drift scan, the telescope remains at a fixed position while the object under study passes through the field of view. This mode is useful for observing extended objects, such as the Galactic Centre, but is inefficent for observations of point objects.

ii) The most common mode of observation is tracking, in which the telescope tracks the position of a point source across the sky. This mode is most efficient for studies of point sources, and is used to

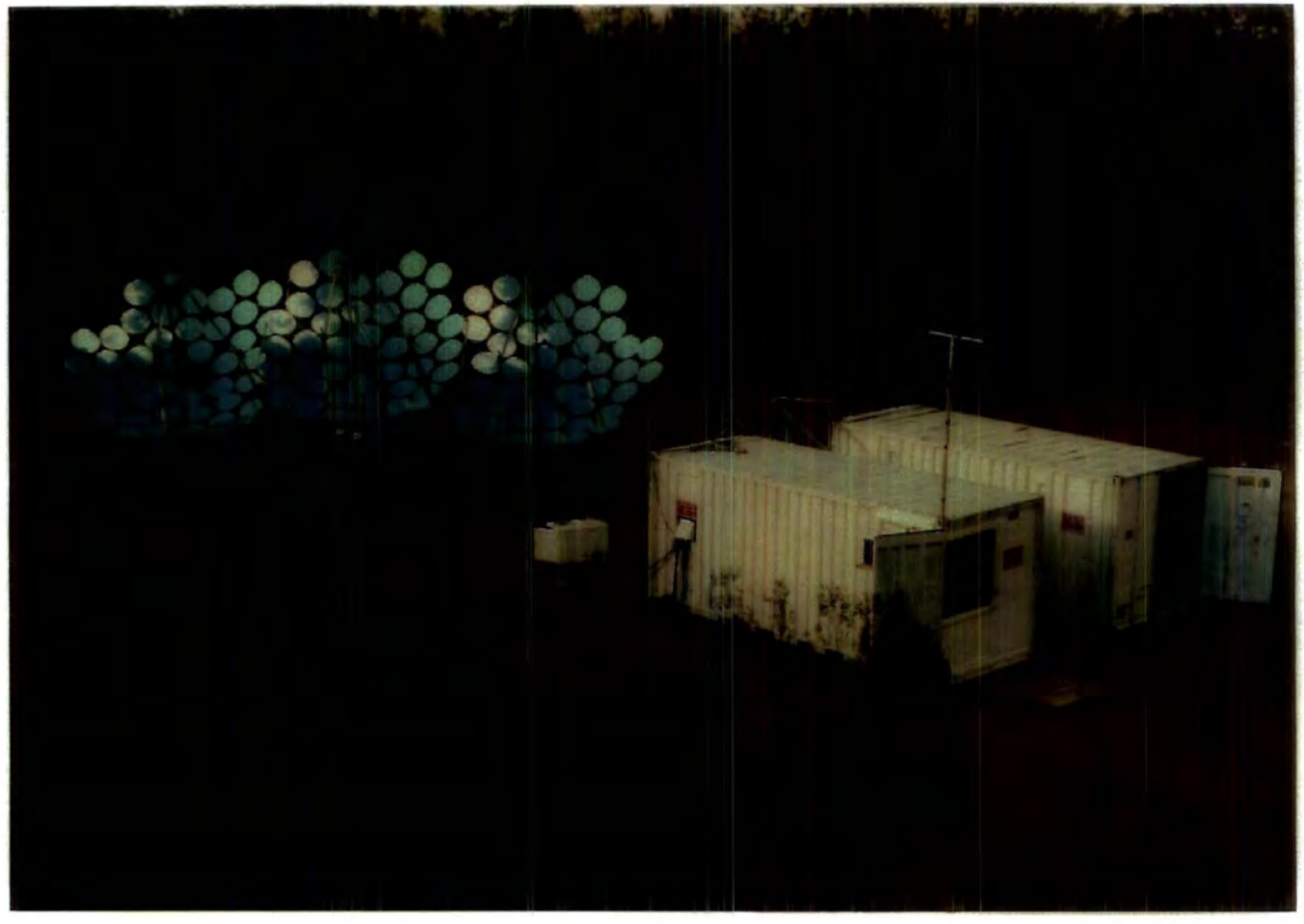

Figure 3.1

The Mark III telescope at the Narrabri site.

maximise the number of on-source counts when studying periodic sources.

iii) For point-like, but generally non-periodic objects, the telescope tracks the source position, but is steered every two minutes to a position two degrees away in azimuth, so that different photomultiplier tubes observe the source and the centre ones observe the background sky. The movement in azimuth only is important to prevent systematic differences on the on- and off-source count rates due to different zenith angles. The 'chopping' mode is useful because it enables on- and off-source count rates from each of the two channels to be compared directly, without gaps in the on-source dataset.

The accuracy of the telescope pointing is monitored routinely using a closed-circuit television camera (CCTV) with a 5° x 8° field of view, mounted below the central dish. Checks are made several times per dark moon period that twelve bright stars, chosen to give even zenith and azimuth coverage of the sky, appear in the correct 'on-axis' position on the CCTV screen when the telescope is steered to their coordinates. Routine checks are also made to ensure that the camera and telescope axes remain parallel, by ensuring that the maximum of the central channel anode currents and the camera's target position coincide when the telescope is pointed towards a visible star. The camera then provides a convenient means of continuous monitoring of the telescope pointing during observations.

3.3.4) The photomultiplier tube assemblies

Each focal plane detector package consists of a filled hexagon of seven RCA 8575 2" photomultiplier tubes (PMT's). This tube was chosen for its stable gain under high illumination, reasonable internal noise rate and fast risetime of ~ 2 ns (comparable to the risetime of the Cerenkov flash). In addition, it has a short warm-up time of only a few minutes and shows very little aging of the photocathode material after extensive use. In order to maintain a constant PMT gain, the night sky illumination of each tube is supplemented by light from a green LED, which is controlled by a feedback loop to maintain a constant PMT anode current. By this simple method, the anode currents of the PMT's are kept constant to better than 1 μA throughout an observation, even when moderately bright stars (magnitude ~ 4) pass through the field of view. The additional noise caused by this illumination has a negligible effect on the accidental coincidence rate (Brazier et al, 1989).

The telescope geometry gives each PMT a nominal field of view of 0.9°. Measurements of the aperture function have been made by noting the variation in PMT anode currents as the telescope scanned across a star. They show that the FWHM aperture is 1.1° after optical smearing of the image (Brazier et al, 1989). The outer ring of PMT's is positioned 2° off-axis. The tubes are arranged in hexagons, which are orientated such that two of the outer tubes observe the same zenith angle as the central one (Figure 3.2). This is essential for the observations made in the 'chopping' mode, when the two alternate positions for the on-source channels must subtend similar zenith angles. The outer ring, known as the 'guard ring', has two functions:

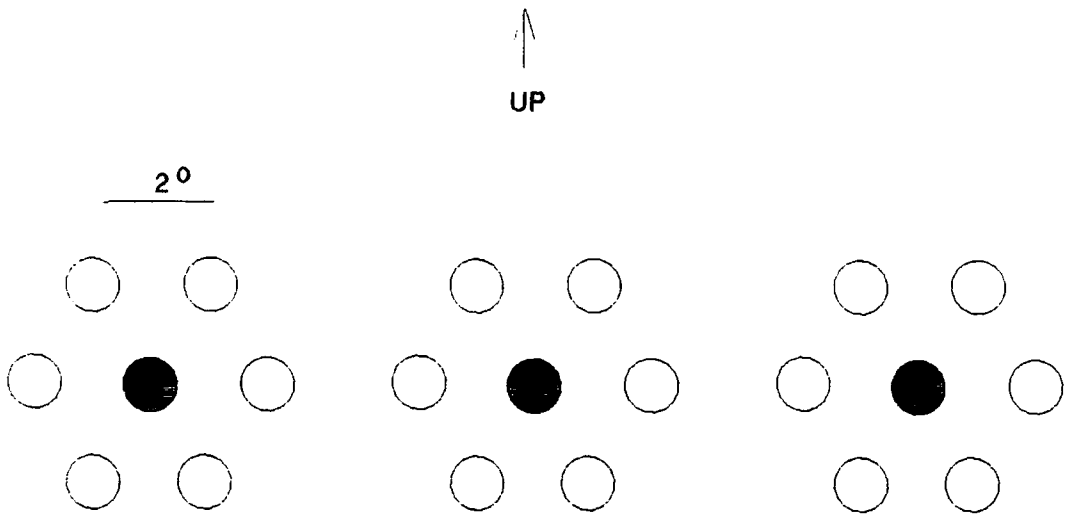

Figure 3.2

Photomultiplier tube configuration in the Mark III and Mark IV telescopes. Each hexagon corresponds to one mirror dish. The three filled circles together form the centre channel. The open circles are guard ring tubes.

i) it provides independent and comprehensive off-source sky coverage during observations, and

ii) the rejection of showers detected simultaneously by the on-source and one or more off-source channels may be used to narrow the effective telescope aperture, resulting in a considerable enhancement of the signal to noise ratio This will be discussed in detail in Chapter 5.

3.3.5) Event recognition and data recording

A set of three corresponding PMT's (one in each dish) is referred to as a 'channel'. After signal amplification, each of the tubes in a channel must show a signal exceeding a fixed threshold of 50 mV, before an event is recorded. The record of a Cerenkov flash consists of temporal, directional and amplitude information about the flash, and details of the telescope performance. The time of the event is recorded to a resolution of 1 μs, together with information on which PMT trios have exceeded the 50 mV threshold, which channel was directed towards the source, target and actual pointing positions, the anode currents of the central channel and the outer channel which observes the source in chopped observations, and, lastly, the digitised responses of each of the 21 PMT's, in the form of charge x time integrals (QT's). The last of these pieces of information is a list of the charges registered by the 21 PMT's, each integrated over a 30 ns gate time. The integration is performed by fast analogue-digital converters, and scaled to 10 bit resolution. As the lowest bits represent only night sky noise, only the 8 most significant bits are stored. The gate time of 30 ns is wide enough to encompass a full Cerenkov flash, but sufficiently short for

the chance of significant noise contributions to be very small.

The dead time of the data collection process is 0.35 ms. However, the arrival times of up to 16 events occurring during the dead time may be recorded. No further information about such events is recorded, but the dead time for the reduced data collection is only 6 μs. This system allows intense, short bursts of events to be noted and their time structures examined.

In addition to the information recorded for each event, pointing information and the PMT anode currents are recorded every two minutes. The rates at which each PMT exceeds the 50 mV threshold and the coincidence rate for each PMT trio are also monitored automatically throughout observations, together with weather information (wind speed, humidity, and temperature). The observers assess sky conditions regularly. Details of the design, construction and operation of the Mark III telescope may be found in Chadwick (1987) and Brazier et al (1989).

3.4) The Mark IV telescope

The Mark IV telescope was designed to be, and initially operated as a Northern Hemisphere counterpart of the Mark III. It was operated from June to October in 1988 and 1989 at the Observatorio del Roque de los Muchachos on La Palma, Canaries (18° E, 28° N, 2500 m a.s.l.). Since May 1990, it has been operated at the Narrabri site in Australia.

The major difference between the telescopes is their flux collecting area, and thus their energy threshold. The Mark IV telescope

is smaller than the Mark III, with only 54 mirrors and a total reflective area of 18 m^2. It also has a slightly smaller angular aperture, of 0.8°. On La Palma, the energy threshold was estimated to be 400 GeV in 1988, with a count rate approaching 100 counts per minute at the Zenith. Simultaneous observations of a source made by the two telescopes in Narrabri show that the Mark IV telescope has a relative count rate of ~ 55%. Assuming an integral cosmic ray spectral index of -1.65, this leads us to estimate the threshold at this lower altitude to be around 100 GeV higher than the threshold of the Mark III telescope (assumed to be 250 GeV).

3.5) Operation of a two-telescope observatory

The operation of two telescopes at the Narrabri site allows us to make observations in either of two ways:

3.5.1) Independent operation of two telescopes

The Mark IV telescope is located approximately 100 m south of the Mark III. At large zenith angles, showers appear elongated on the ground. If both telescopes observe an object at large zenith angle many showers will register on both telescopes. Below around 40°, the number of independent events registered on the Mark IV becomes small, and more efficient use of this telescope is made by observing another source. When the reduced count rate of the Mark IV telescope is also taken into account, it is concluded that it is generally more profitable to observe

different objects with the two telescopes.

3.5.2) Operation of two telescopes in tandem

The exception to this general rule is the study of transient sources. Here, the benefits of confirmation of a burst of excess counts by an independent telescope are especially important. The Mark III telescope is the primary telescope in such observations, because the Mark IV has a poorer sensitivity. Small effects evident above noise in data from the Mark III telescope may therefore not be distinguishable in that from the Mark IV. However, confirmation from the independent dataset is valuable in observations of strong, but short-lived effects. Dual obserations have recently proved useful in observations of AE Aquarii, in which a burst of γ-rays was detected by both telescopes (Bowden et al, 1991).

3.6) Timekeeping

3.6.1) Relative time

It is imperative in studies of fast pulsars that a good timing standard be kept. In Dugway, the time standard was an oven-controlled crystal accurate after correction to one part in 10^9. The clock was regularly synchronised to an off-air radio signal from station WWV at Fort Collins, Colorado. UTC was known to 0.3 ms, and relative arrival times in different telescopes were accurate to better than 1 ns (Chadwick, 1987). It was intended that the Mark III telescope should

have timing sufficiently accurate to retain phase in a 1 ms pulsar over one year. A Rubidium atomic oscillator is used for this purpose. The drift rate of the oscillator is monitored closely by checks against an off-air radio signal. As the clock was initially synchronised using radio station VNG, its signals are used for monitoring whenever possible. This station broadcast until mid-1988 from Lyndhurst, Victoria. Since 1989, it has been broadcasting from Llandilo, New South Wales. In the interim period, a signal broadcast by the Royal Australian Navy in Jervis Bay, Australian Capital Territory, was used. Ideally, the checks are made at the same time of day, as small diurnal variations in the delay are observed. The most significant of these concerns the nature of the VNG signal, which consists of a number of 1 ms pulses. The detection threshold is set to intercept the first pulse under normal conditions. If the amplitude of the signal decreases significantly, or if there is noise in the signal, the first pulse to exceed the threshold may be an integer number of milliseconds later. Such anomalies are easily seen and corrected. Sub-millisecond variations are also seen, which are not systematic and may be attributed to atmospheric effects.

Since an oscillator which loses power and is restarted is unlikely to retain its original drift rate, such interruptions are avoided. The phase relationship between successive time series spanning a restart is also dificult to determine. The clock is therefore supplied with backup support batteries which can power it in case of mains power failure for up to two to three days. In the five year lifetime of the experiment, the clock has been restarted only once, and relative event times are known to around one part in 10^{11}. The drift rate is now measured to be

(0.059 ± 0.0008) ms per day, following a restart in October 1990. Previous to this it had remained at (0.027 ± 0.0007) ms per day since since initialisation in early 1987. The rate of change of the drift rate is too small to have been measured.

3.6.2) Absolute Time

Until January 1991, absolute time (Universal Coordinated Time, UTC) estimates rested on measurements of the transit delay time from the radio transmitters to the Anglo Australian Telescope, 90km away. On 14th January 1991, a new measurement was made by transporting an atomic clock to the Australia National Radio Observatory at Parkes, New South Wales, for comparison with the timestandard there. The latter device keeps UTC to within a few nanoseconds. A Rubidium clock originally used for timekeeping in the Mark IV telescope on La Palma was available for this trip and acted as a portable standard. Here a direct measurement of the clock offset from Universal Time was possible. Five pieces of information were needed: the VNG - Narrabri clock and Narrabri - portable clock offsets at the time of the UTC measurement, the Narrabri and portable clock drift rates, and the offset between the portable clock and the Parkes time standard. The portable clock was monitored closely for several days, so that a local fit to its apparent times was possible. The Narrabri Rubidium clock was monitored against VNG as usual, and the linear fit from the whole month's measurements was used to interpolate to the test time. This clock's behaviour in January 1991 is plotted in Figure 3.3. The fit for the month gives the most accurate measurement of the delay on a given day. The measurement at

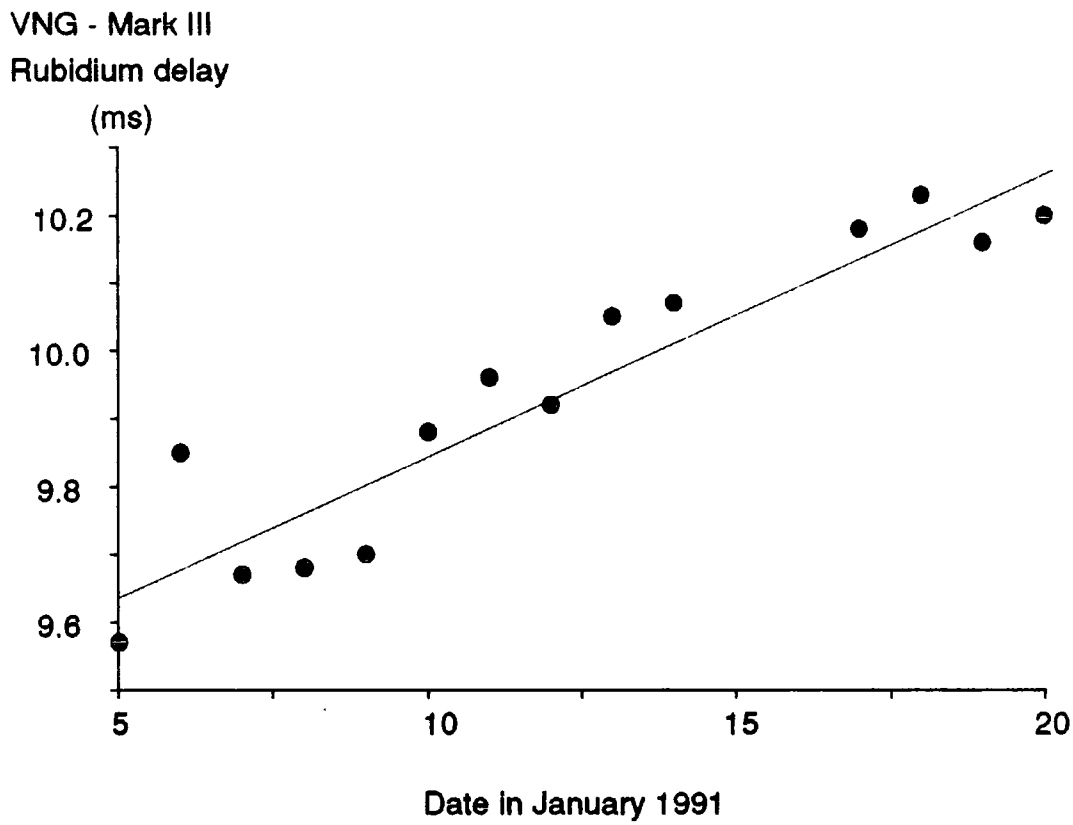

Figure 3.3

The VNG off-air - Narrabri Rubidium clock delays measured in January 1991. Only measurements made in the early evening have been included. The calculated delay at the time of the absolute time measurement at Parkes is 10.02 ms.

Parkes was made at 10:30 EST on 14th January 1991. The offsets for the two clocks were interpolated to this time and found to be:

$$\text{Narrabri Rb - VNG} = (10.02 \pm 0.02)\ \text{ms}$$

$$\text{Portable Rb - Narrabri Rb} = (0.174 \pm 0.005)\ \text{ms}$$

The offset from the Parkes time standard was found to be:

$$\text{Portable Rb - Parkes} = (12.5690 \pm 0.0005)\ \text{ms}$$

This leads us to conclude that the transit time between the VNG transmitter in Llandilo, New South Wales, and Narrabri is 12.569 - 0.174 - 10.02 = (2.38 ± 0.03) ms, which is entirely consistent with the distance to the transmitter. The new result has enabled us to know absolute time to around 30 μs for current data. By matching the off-air delays and drift rates across the period of RAN radio checks and the two eras of VNG measurements, absolute time is known to better than 10 ms (Rayner, private communication).

3.7) Quality control

3.7.1) Weather monitoring

The atmosphere is an essential part of all atmospheric Cerenkov telescopes. The data quality is therefore reliant on climatic conditions. The weather on the Narrabri site is monitored and recorded automatically throughout all observations. In addition, the observers

watch sky conditions closely and record the presence and degree of cloud cover, the sky clarity, and, in summer months, whether any lightning is visible. The weather records permit a high degree of quality control to be exercised before analysis is undertaken. It should be stressed that the majority of observations are made in good conditions, and that very few must be rejected on the basis of data quality, but in order to demonstrate the precautions taken to ensure that only good data is analysed, the problems which can arise will be described here.

Poor data is generally caused by poor weather. There are four main problems: lightning, cloud, wind and humidity.

3.7.2) Lightning

Lightning in Narrabri is generally confined to the Australian summer. Nearby lightning causes electrical pickup in the telescope's sensitive electronics. If a storm is seen to be affecting the telescope, the observation is ended and precautions are taken to protect the electronics from a lightning strike close by. The telescopes can also be optically sensitive to distant lightning flashes, which can cause short bursts of spurious events. Although these are very seldom obvious above the general count rate, they may seriously disrupt analysis of the data by introducing false periodicities. Confirmation of lightning activity during observation permits the rejection or truncation of the affected dataset. However, an efficient means of rejecting lightning-induced events also exists. This will be described in Chapter 5.

3.7.3) Cloud

Cerenkov light is not transmitted through cloud. If intermittent or light cloud is present, variations in the count rate will occur, and these may introduce spurious, long-term periodicities into the data. It is usual under these circumstances to observe fast pulsars (p < few seconds), since the periodic analysis at short periods will not be adversely affected by the relatively slow variations introduced by intermittent cloud cover. Observations of unpulsed sources are not attempted unless the sky is clear of cloud.

3.7.4) Wind

The Mark III telescope's size, shape and light engineering make it susceptible to steering difficulties in high winds. As the wind speed on the Narrabri site is usually less than 6 kts, this is not frequently of concern. Only occasionally, when the wind gusts to > 12 kts, can the telescope be seen to move from its target position by a small amount. Manual steadying of the telescope is then sufficient to restore stable pointing. Only under very severe conditions (> 15 kts), is it necessary to end an observation on the Mark III telescope. The smaller Mark IV telescope is very little affected by high winds. The wind tolerance of both telescopes is greatly increased if they are observing sources at small zenith angles, as their horizontal cross-sections are greatly reduced. The telescopes are fitted with audible and visual alarms to warn observers of pointing errors and/or high winds.

3.7.5) Humidity

Condensation on the telescope mirrors is a frequent problem in cool, still, humid conditions, but can be easily predicted and corrected before it affects the telescope performance. After some experimentation, a technique has been devised which very effectively prevents condensation. The mirrors are sprayed with a solution of a high quality liquid detergent, which by reducing surface tension prevents the formation of droplets and leaves the mirrors covered with a clear, aqueous film. This method allows the count rate to remain normal throughout a night. Without treatment, the scattering of light by the condensation would greatly reduce the count rate of the telescope.

In winter, the mirrors can become cold enough for the film of detergent and water to freeze. In this case, the mirrors may be sprayed with methanol, which dissolves the frost. This restores the count rates temporarily, but the mirrors may eventually freeze again. Future telescopes may be designed with heated mirrors to circumvent this problem.

3.8) Data processing

3.8.1) Information recorded

The raw data from a night's observing consists of three types of data file. 'Run Start' files are recorded at the beginning of the night and contain a description of the weather, the observers' names, the Civil and Julian dates of the start of the night's run and a telescope

status record. 'Source Start' files are written before each individual observation of a source. They contain the name of the source and it celestial coordinates, the start time of the observation, the terrestrial position of the observatory, the telescope steering offsets and any comments made by observers. The third file is the 'Data File'. This contains the event records, which have been described in section 3.3.5. All these files are stored on 67 Mb 3M DC600 data tapes in the Mark III telescope, and on a 20 Mb hard disk in the Mark IV.

3.8.2) Data formatting and reduction of event times to the Solar System barycentre

The pre-analysis data processing proceeds as follows. Since analysis routines do not require information on the telescope status, this latter part of the event records is stripped off, and the remaining information - the time of each event, a list of PMT's exceeding the fixed threshold (the 'fire pattern'), and the pulse integrals - is formatted into individual source observation files.

The second stage of processing transforms the event times to the Solar System barycentre, to remove the systematic effects of the telescope's terrestrial motion. In order to recover pulsar periodicities, it is necessary to remove the Doppler effects on the period imposed by the Earth's motion, by reducing times to the Solar System barycentre. 'Barycentring' involves three corrections: a component to allow for the orbital position of the Earth, one to correct the times from the position of the telescope to the centre of the Earth, and a correction to allow for the relativistic effects on the observers'

timescale due to the Earth's motion and due to the difference in gravitational potential between the position of the telescope and the Solar System barycentre. Barycentring is performed using the JPL DE200 Earth Ephemeris. A similar correction to this is necessary for the periodic analysis of data from binary sources, wherein the times taken for photons to travel across the binary orbit must be removed. This is not made as part of data pre-processing because of uncertainties in, and not infrequent updates of the available orbital ephemerides (see chapter 4).

3.8.5) Data storage and archiving

After the routine processing precedures, the files are suitable for analysis. The files are stored on 60 Mb hard disks for short-term access and are archived on 3M DC 600 data cartridges. The raw data and formatted data are also archived on 3M cartridges.

CHAPTER 4

Data analysis techniques

4.1) Introduction

Many potential VHE gamma ray sources are radio or X-ray pulsars, which show a regular periodicity. This periodicity may be used to advantage in the analysis of VHE γ-ray data. Because of the high cosmic ray background, it is difficult to detect a weak, steady count rate excess in the direction of a source or a stronger, but short-lived, transient effect. The means of searching for unpulsed emission in VHE data taken with the Durham telescopes have been comprehensively described by Rayner (1989). Where there is a known periodicity in the emission from a source, it is often more fruitful to search data for evidence of periodicity. As well as making use of the telescopes in their most efficient mode of operation (tracking), the detection of periodicity in TeV gamma rays can provide important clues as to the origin of the high energy emission. In this chapter, the techniques used by the Durham group to search for periodic emission will be discussed.

4.2) Tests for periodicity

Since gamma ray fluxes are small in comparison with the hadronic background, it is rarely possible to observe periodicity in data merely from a visual inspection of time variations in the count rate. However, a number of well-established statistical tests exist which test for periodicity in data. An extensive review of the tests and their possible uses in VHE astronomy may be found in de Jager (1987). The Rayleigh test in particular is widely used in the field of VHE γ-ray astronomy. Its application to the field was first suggested by Gibson et al (1982a) because it is the test least dependent on knowledge of the shape of the pulse phase distribution (also called the 'light curve'). The Durham group routinely uses the Rayleigh test on data on all candidate periodic sources except for those pulsars whose period is extremely well known. More powerful, less general tests can be applied in the latter cases. The Rayleigh test has been described by Mardia (1972) and Batschelet (1981). It is briefly reviewed below.

4.2.1) The Rayleigh Test

The Rayleigh test was designed to test for cyclic phenomena. It does not require knowledge of the absolute times at which peaks in a phase distribution occur, but instead is able to detect periodicity from relative event times alone. This is an advantage in VHE γ-ray astronomy, since knowledge of absolute phases is generally precluded by uncertainties in pulsar ephemerides and in absolute event arrival times. Neither does the test involve any arbitrary division of data into phase

bins, which could split a signal between bins and which requires an assumption on the length of the duty cycle. Essentially, the test looks for a correlation between event phases and a sine wave at the test period. This period is the fundamental in the Fourier series, which will dominate for all light curves except those with very narrow peaks. Although the test is therefore most powerful for broad phase peaks, it is sensitive to all except very narrow peaks. It is thus useful for testing for non-uniformities of phase in data where the shape of the deviation is not known. The following outlines its use in VHE γ-ray data analysis.

Each event in a dataset is ascribed a phase at the test period. A unit vector is created with the phase of the event, and the vectors from all events are added. The modulus of the resultant vector is divided by the number of events, yielding a normalised value, R, between 0 and 1. R is then tested for significance. If n is the number of events in the dataset, then the statistic $2nR^2$ is distributed approximately as a Gaussian (i.e. χ^2 with two degrees of freedom).

For a trial period p, the phase angle of an event at time t_i (assuming that terms in higher derivatives of the period are negligible) is:

$$\theta_i = \frac{2\pi}{p} t_i - \frac{2\pi}{p^2} \frac{dp}{dt} t_i^2 \quad (\mathrm{mod}\ 2\pi) \qquad - \ 4.1$$

To calculate the magnitude, R, of the resultant vector, φ, we have

$$n^2R^2 = \left[\sum_{i=1}^{n} (\cos\theta_i) \right]^2 + \left[\sum_{i=1}^{n} (\sin\theta_i) \right]^2 \qquad - \ 4.2$$

The probability of nR^2 arising by chance is then given for large n ($n > 100$) by $\exp(-nR^2)$.

The Rayleigh test is clearly not a suitable test for a bimodal distribution, since the opposing vectors will cancel. Such distributions are found where there are both a pulse and an interpulse in the light curve. If an interpulse is predicted, however, the test may be made at the half period to avoid this problem.

Once the existence of a signal has been established, it is useful to estimate the gamma ray flux. In order to do this, it is necessary to calculate the signal strength as a fraction of the cosmic ray background flux. It should be noted that the Rayleigh test is primarily designed as a hypothesis test, and the magnitude of the Rayleigh vector is not a particularly reliable estimator of the signal strength, S. However, an unbiased estimate of the signal strength may be made from the relation (Mardia, 1972, de Jager, 1987)

$$S = 2\left[\frac{nR^2 - 1}{n - 1}\right]^{1/2} \qquad - \quad 4.3$$

Clearly, if n and $nR^2 >> 1$, then $S \approx 2R$.

A more accurate calculation of signal strength is made if the mean strength yielded by data from a number of observations is determined. If the data comprise only one observation, the data may be split into a number of shorter subsections, with the same result. Because the relative phase between the sections is lost, the period can no longer be so well determined from the divided data.

4.3) Searching over a range of periods

It is frequently necessary to search for periodicity over a range of trial periods. The period of a source at the time of an observation may not be well known, either because of irregularities in the period derivative of the object, or because of measurement uncertainties in the available ephemeris. If this is the case, it is necessary to search for periodicity at a number of periods in a range about the estimated period. A figure showing Rayleigh probability or power against test period is termed a periodogram.

4.3.1) Independent periods: the Fourier interval

Tests of a dataset at two periods arbitrarily close together will obviously yield correlated Rayleigh vectors. Let the first test period be p. If the second period is increased from p, then the phases of events will alter systematically. At a period $p + \delta p$, the phase shift of the last event is equal to one cycle, and coherence is lost. The new period $(p + \delta p)$ is therefore independent of the original period, p. The separation δp between independent periods is known as the Fourier interval. It is calculated as follows. Suppose that a observation is made for T seconds and that the data are tested for periodicity at a period p. If A is a constant, such that

$$\frac{T}{p} = A \qquad - 4.4$$

then the Fourier interval is δp, such that

$$\frac{T}{p - \delta p} = A + 1 \qquad - \ 4.5$$

$$= \frac{T + p}{p} \qquad - \ 4.6$$

In general, p will be the spin period of a pulsar. Since pulsar periods are shorter than ~ 300 s, while most observations last for more than 4000 s, we have $p << T$, and the Fourier interval is

$$\delta p \approx p^2/T \qquad - \ 4.7$$

In a period search, each independent period must be tested. In order to calculate the final significance of a result, it is important to know and allow for the number of independent periods at which the test has been made. The number of Fourier intervals sampled in a period range $p_1 - p_n$ is

$$T/p_1 - T/p_n \qquad - \ 4.8$$

In practice, it is usual to test more than once per independent interval, since the Rayleigh probability may minimise anywhere between the bounds of an interval. De Jager et al (1989) and Orford (1990) have considered the factor by which derived chance probabilities must be reduced to allow for this oversampling. Their treatments of the problem are numerical and analytical respectively. Both conclude that the

oversampling factor tends to three as the number of trials within each interval increases. It is normal practice to make three samples per interval, and to assume a conservative oversampling factor of three.

4.4) Treatment of multiple observations

In order to gain maximal benefit from a series of observations, it is desirable to combine the data in some way. The data from multiple observations can be combined either retaining or disregarding the relative phase between them. Each of these two methods is commonly used. Relative phases between datasets must be disregarded when the object under study is known to behave erratically, when its behaviour has not been well studied, or when the dataset covers several years and the cumulative uncertainties in event times are a significant fraction of the test period. These problems are usually associated with binary and millisecond pulsars. For maximum sensitivity, relative phase should be retained between datasets whenever possible.

4.4.1) Combining datasets without retention of relative phases

Event timing in the Mark III and Mark IV telescopes is sufficiently accurate to maintain phase on a one millisecond pulsar over one year. However, unless an accurate, contemporary ephemeris is available, the expected phase relation between observations made some time apart cannot be known. In this case, the Rayleigh test is applied to each observation separately, and the results are combined statistically

according to the method of Eadie et al (1971). If the data taken in an observation i are tested for periodicity, the Rayleigh probability at the test period is P_i. Then the Rayleigh probabilities for all observations can be combined as a logarithmic sum, C:

$$C = -2 \log_e \prod_{i=1}^{n} (P_i) \qquad - \ 4.9$$

where n is the number of observations. C is then distributed as χ^2 with 2n degrees of freedom.

The Fourier interval for period searching in this method is that of a single dataset. In VHE gamma ray astronomy, observations are seldom of equal length, and so the Fourier interval (equation 4.7) is not a constant. However, in order to combine probabilities, it is essential that the same series of test periods is applied to each dataset. The Fourier interval appropriate to the longest observation (i.e. the smallest Fourier interval) should always be used to define the test periods.

4.4.2) Combinations of datasets retaining phase information

If the test period is very well known, then phase may be maintained between observations. In this case, the data from a series of observations are combined 'in phase' to produce a single, large dataset. Because the effective length of the dataset is now very much increased, the period resolution is greatly improved, and the degrees of freedom incurred by phase loss in a phaseless combination of data are avoided. The signal strength, however, is less well defined than that found from

a phaseless combination of datasets, as described in section 4.2.1.

A single observation lasts typically for three hours, and sucessive observations are taken days or even months apart. This leaves the summed dataset with small 'windows' of data, interspersed with large and often regular gaps. The gaps introduce beats between any periodicity in the data and integral numbers of days and/or months. The resulting periodogram thus has a minimum chance probability at the fundamental period, with a series of 'alias' minima either side, modulated by an envelope of width $p^2/[T(\text{one observation})]$. If the signal is small, it can be difficult to distinguish the fundamental period from the aliases, unless a very accurate prediction is available. The aliases also cause complications in estimating the number of independent trials made. Clearly, there is a correlation between the Rayleigh vectors at aliasing periods, but how this reduces the effective number of trials is not yet well understood.

4.5) Recovery of periodicity from pulsars in binary orbits

4.5.1) Introduction

Just as it is necessary for the recovery of stellar periodicities to reduce a series of arrival times to the Solar System barycentre, so it is necessary to unify the changing travel times incurred by photons emitted from a moving source in a binary orbit. This process is known as 'focussing'. In this section, we will demonstrate how focussing is achieved and discuss the implications for the recovery of periodicity when there is an uncertainty in the available ephemeris. Only circular

orbits will be discussed, since none of the binary systems studied in this thesis have orbital eccentricities greater than 3×10^{-2}.

4.5.2) Reduction of event times to a common reference plane

A point on a circular orbit can be described as (a, Φ) where a is the radius and Φ is the position angle with respect to the ascending node (Figure 4.1). In the case of a binary stellar orbit, the inclination of the orbit, i, is an additional and usually unknown variable. i is defined as the angle between the plane of the orbit and the plane of the sky. This factor limits the information discernible from pulsar timing data. It is generally not possible in timing analyses to distinguish between a small orbit viewed side-on, and a larger orbit at a smaller inclination. It is thus only possible to know the product asini, i.e. the radius of the orbit projected along the line of sight. Figure 4.1 shows the projected orbital elements of a binary pulsar taking this into account.

The time taken for light to travel from a point (asini,Φ_i) on the orbit to a reference plane perpendicular to the line of sight is

$$t_i = \text{asini}.\sin\Phi_i.c \qquad - 4.10$$

where for convenience we have taken the plane to be that which includes the system's barycentre. Any other plane would introduce a additional constant in the travel times. Note that if asini is measured in light seconds, as is conventional, then c = 1. In the focussing of event times, the travel time is subtracted from each time, according to the

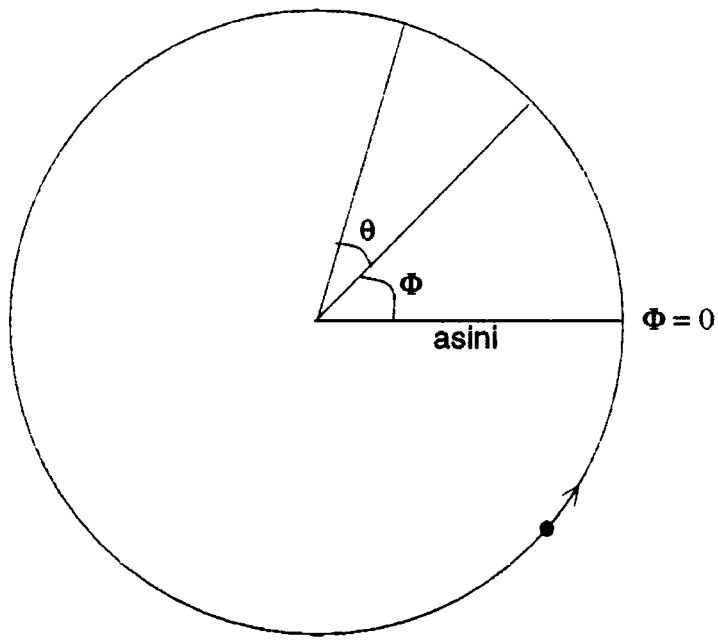

Figure 4.1

The main orbital parameters used in time corrections. Φ is defined here as the orbital phase of the pulsar at the beginning of an observation and is measured with respect to the descending node. θ is the angular duration of the observation.

full reference ephemeris for the binary system. This correction is made *after* reduction of event times to the Solar System barycentre.

4.5.3) Uncertainties in orbital parameters

It is sometimes found that the ephemeris of a binary system is not known well enough to reduce the data to within one Fourier interval of the pulsar period. Coherent periodicity in the incorrectly focussed data may be reduced and spread across several Fourier intervals, or it may be moved to another period, depending on the orbital parameters of the particular binary. In focussing data using a poor orbital ephemeris, it is imperative that the uncertainties in the perceived pulsar periods are understood, so that an appropriate search range in periods or in the orbital parameters may be chosen. Consider the focussing correction described above, applied to data on a pulsar in a binary system. The data correspond to a section of the pulsar orbit. Let the first event in the observation have a time T_1 and the last event be at T_2. In order to reduce the times in the dataset to the reference plane described above, we have a transformation:

$$T_2 - T_1 \rightarrow T_2' - T_1' \qquad - 4.11$$

where $$T_2' - T_1' = T_2 - T_1 - (a\sin i.\sin\Phi)_1 + (a\sin i.\sin\Phi)_2 \qquad - 4.12$$

If the values of asini and Φ are varied, the transformation of the event times will change. Suppose that there is a test period, p. If the transformed duration is decreased by the change, then any

periodicity at p will instead be perceived at a smaller period, and vice versa. Assuming that the segment of the orbit covered in an observation is small, we can deduce the sampling interval in time series duration, as before. Let

$$\frac{T_2' - T_1'}{p} = A \qquad - 4.13$$

Then let δT be an increment in T such that

$$\frac{T_2' - T_1' + \delta T}{p} = A + 1 \qquad - 4.14$$

Then

$$\delta T = p \qquad - 4.15$$

This is the change in the transformed duration of the observation necessary to change the perceived periodicity by one Fourier interval in period, i.e. by p^2/T. Since the transformation is determined by the orbital parameters, we can use equations 4.12 and 4.15 to find the associated intervals in asini and Φ.

4.5.4) The sampling interval in orbital radius

Consider the circular orbits shown in Figure 4.2. Let Φ be the orbital phase of the beginning of an observation and $\Phi+\theta$ be that of the end. Let orbits (i) and (ii) differ only in asini, such that the difference in corrections for the binary position causes the perceived period to change by one Fourier interval. Then from equations 4.12 and

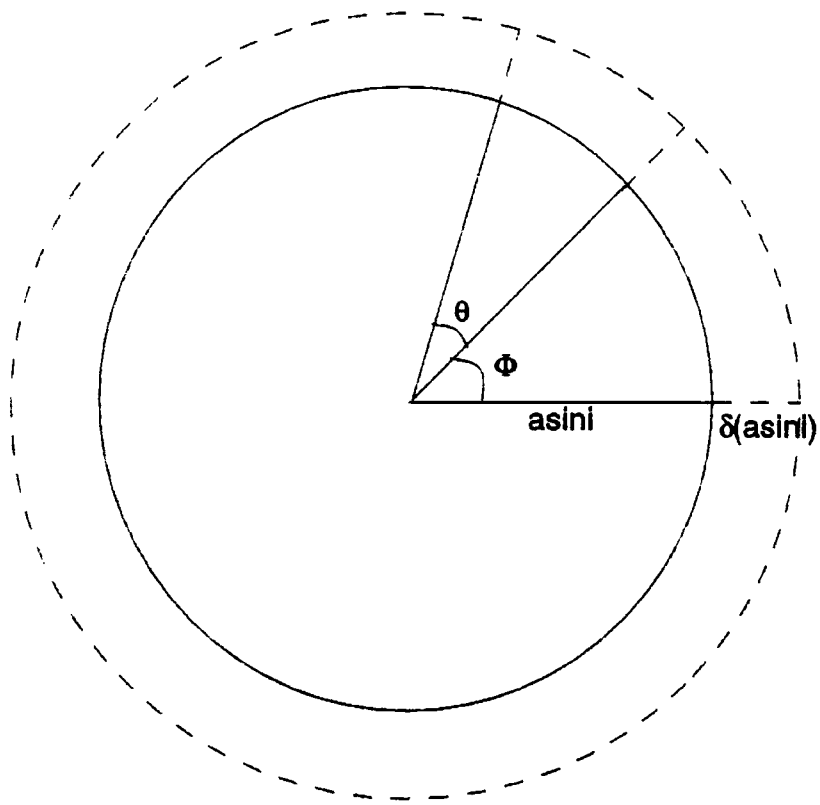

Figure 4.2

Orbital geometry with a small increase in the projected semi-major axis, asini. Φ is the orbital phase at the start of an observation; $\Phi + \theta$ is the phase at the end.

4.15,

$$(a\sin i.\sin(\Phi+\theta) - a\sin i.\sin(\Phi))_{ii}$$
$$- (a\sin i.\sin(\Phi+\theta) - a\sin i.\sin(\Phi))_{i} = p \qquad - 4.16$$

$$\Rightarrow \quad [(a\sin i)_{ii}\sin(\Phi+\theta) - (a\sin i)_{ii}\sin(\Phi)]$$
$$- [(a\sin i)_{i}\sin(\Phi+\theta) - (a\sin i)_{i}\sin(\Phi)] = p \qquad - 4.17$$

$$\Rightarrow \quad [(a\sin i)_{ii} - (a\sin i)_{i}][\sin(\Phi+\theta) - \sin(\Phi)] = p \qquad - 4.18$$

Let the increment in asini be $\delta(a\sin i)$. Then the sampling interval in asini is:

$$\delta(a\sin i) = \frac{p}{\sin(\Phi+\theta) - \sin(\Phi)} \qquad - 4.19$$

Note that if an observation is symmetric about a conjunction with the companion star (phases 0.25 and 0.75 with respect to the ascending node), then $\sin(\Phi+\theta)$ approaches $\sin(\Phi)$, and the sampling interval in asini tends to infinity.

4.5.4) The sampling interval in orbital phase

The geometry of an orbit in which the orbital phase, Φ, is altered by an amount $\delta\Phi$ is shown in Figure 4.3. Then, if Φ is the only parameter varied, the interval between independent orbits may be derived similarly to above. Note that the angular duration of the observation,

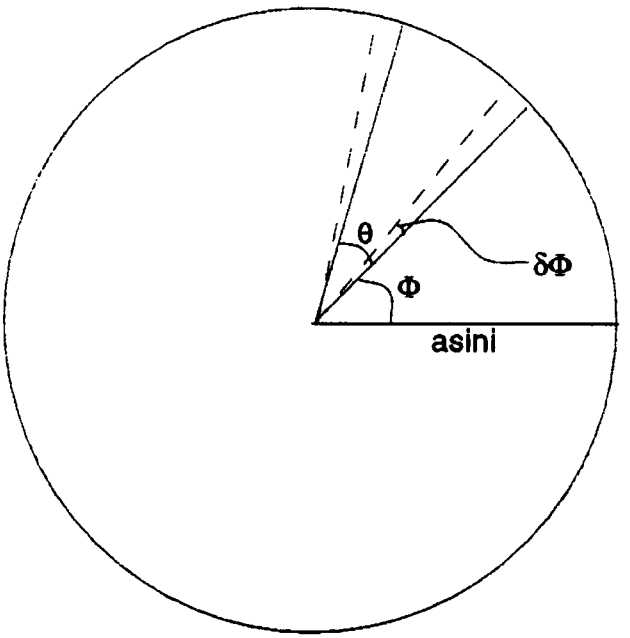

Figure 4.3

The orbital parameters with a small change in the orbital phase, Φ. The symbols are defined as in Figure 4.1.

θ, is fixed if the orbital period is held constant.

$$a\sin i.\sin(\Phi+\theta+\delta\Phi) - a\sin i.\sin(\Phi+\delta\Phi) - a\sin i.\sin(\Phi+\theta) - a\sin i.\sin(\Phi) = p \qquad - 4.20$$

$$\Rightarrow \quad \sin(\Phi+\theta+\delta\Phi) - \sin(\Phi+\delta\Phi) - \sin(\Phi+\theta) + \sin(\Phi) = \frac{p}{a\sin i} \qquad - 4.21$$

$$= \cos(\delta\Phi)\{\sin(\Phi+\theta) - \sin(\Phi)\} + \sin(\delta\Phi)\{\cos(\Phi+\theta) - \cos(\Phi)\} - \sin(\Phi+\theta) + \sin(\Phi) \qquad - 4.22$$

Rearranging and squaring,

$$\cos^2(\delta\Phi)\{\sin(\Phi+\theta) - \sin(\Phi)\}^2 = [-\sin(\delta\Phi)\{\cos(\Phi+\theta) - \cos(\Phi)\} + (\sin(\Phi+\theta) - \sin(\Phi)) + (p/a\sin i)]^2 \qquad - 4.23$$

After some manipulation, it then follows that

$$A\sin^2(\delta\Phi) + B\sin(\delta\Phi) + C = 0 \qquad - 4.24$$

where:

$$A = \{2 - 2\cos(\theta)\}$$

$$B = -2\{\cos(\Phi+\theta) - \cos(\Phi)\}\{\sin(\Phi+\theta) - \sin(\Phi) + (p/a\sin i)\}$$

$$C = (p/a\sin i)^2 + 2p\{\sin(\Phi+\theta) - \sin(\Phi)\}/a\sin i$$

Hence, the Fourier interval in phase, $\delta\Phi$, can be calculated.

4.5.5) Sensitivity to other orbital parameters

Although the full orbital ephemeris for a binary system also contains other parameters, these are less directly connected to the time transformation, and small changes generally have similar or identical effects to those caused by shifts in the radius and orbital phase. For instance, a movement of the ephemeris epoch (the time of passage of the star across a reference phase of the orbit) is directly equivalent to a change in the orbital phase. Likewise, an uncertainty in the orbital period, or the inclusion of an orbital period derivative, primarily affects the phase of an observation.

4.5.6) Focussing with a matrix of test parameters

The sampling intervals in the radius of the orbit and in the orbital phase of an observation can be used to determine the adequacy of an ephemeris, and to show whether a deviation from the reference ephemeris is significant. An ephemeris is sufficiently accurate if the maximum period shift which can be accommodated by its errors is smaller than one Fourier interval. A deviation from the reference ephemeris which is much larger than a sampling interval must be explained in some other way. This may be of especial significance in sources such as X-ray binaries, where it is possible that VHE γ-rays are not produced at the same location as X-rays or radio emission.

An (asini x Φ) matrix of test orbits can be formed about the reference values if the orbital parameters are insufficiently well known. The Rayleigh test is then applied to the data focussed according to each test orbit. It is interesting to note that the intervals are not fixed, but depend on the starting phase/time and the duration of an observation. Two observations are therefore likely to have similar, but not identical dependences. Obviously, there will be large variations in sensitivity between binary systems with very different orbital and pulsar parameters. In particular, binaries containing short period pulsars will have unusually small orbital sampling intervals. In addition, for binaries with orbital periods as short as a few hours, a substantial section of the orbit may be sampled in a single observation. In the latter case, the curvature of the orbit will become important, and the approximation to a short, linear section of the orbit is no longer strictly valid. The most extreme effects of curvature are found in composite datasets in which phase has been retained. Such datasets may span several orbital periods. Allowance for orbital uncertainties is not required for the analysis of any composite, phased dataset on any object discussed in this work.

The number of independent trials made over an orbital sampling matrix is not a simple multiplication of the number of orbital intervals sampled. The time correction is made only along the line of sight (y) direction, and the (x,y) frame (where x is in the plane of the orbit and perpendicular to the line of sight) is the frame of the corrections. This is why the contour plots of Rayleigh probability in an (asini,Φ) matrix are seen to curve (e.g. Figure 4.4) and why the sense of the curvature changes with orbital phase: it is merely a reflection of the

transformation from polar to Cartesian coordinates. However, since ephemerides must be quoted in terms of polar coordinates, it is more useful to sample in these same coordinates.

The orbital Fourier intervals derived in this section are of great use in assessing the adequacy of an ephemeris and for choosing a suitable sampling range if one is deemed necessary. The exact number of degrees of freedom used in testing over a matrix of orbital parameters, however, should not be found from the number of intervals calculated above, especially if a range of test period is included or if the effects of curvature are important. The calculations do not include estimates of the effects of curvature in the orbit, nor do they consider oversampling. For these reasons, it is concluded that the number of degrees of freedom incurred in testing over a matrix of orbits is best found from simulations.

CHAPTER 5

A technique for the reduction of cosmic ray background noise

5.1) Introduction

Ground-based VHE γ-ray astronomy can be severely hampered by the large, isotropic background of cosmic ray protons, which smothers any but the largest γ-ray flux. The difficulty lies in the general similarity between the Cerenkov flashes generated by these protons and those from TeV γ-rays. Careful telescope design is clearly vital if the signal to noise ratio is to be optimised and weak sources are to be detected. When optimising the signal to noise ratio of his data, the Cerenkov astronomer is led to choose one of two options. Either he can attempt to identify the γ-rays directly using precise measurements and models of the temporal or spatial characteristics of the Cerenkov flashes, or he can rely on the most distinctive feature of γ-rays from discrete sources, anisotropy. Enhancement techniques have been exploited by a number of groups, with varying degrees of success.

5.1.1) Spatial imaging

The first technique considered here is that of distinguishing between protons and γ-rays by the spatial and angular characteristics of the Cerenkov flashes. Hillas (1985) has modelled the images expected of hadron- and γ-ray initiated Cerenkov flashes, and has shown that there

is a detectable difference between the two types of Cerenkov image, with protons yielding a broader, less regular image than γ-rays. The Whipple collaboration exploit these results using the single dish of the 10 m diameter Mount Hopkins telescope. They image Cerenkov flashes using an array of photomultiplier tubes as a 109 pixel 'camera'. The imaging technique allows the group to reject all but 2% of their full dataset as being unlike photon images, and has produced startling sensitivity to TeV γ-rays from the Crab Nebula (Weekes et al, 1989, Lang et al, 1990). It is still not clear, however, whether imaging is a universally applicable technique. A number of convincing signals were reported by this group using an earlier detector package with only 37 pixels and a more conventional analysis technique. None of these datasets has responded to the application of current imaging techniques and the original claims have been formally withdrawn (Macomb et al, 1990, Reynolds et al, 1990). The withdrawal of these earlier claims demonstrates the collaboration's faith in the imaging technique, but the failure to enhance signals from sources other than the Crab Nebula has not yet been explained.

5.1.2) Pulse shape discrimination

A second method for direct discrimination between types of primary particle uses the temporal characteristics of the Cerenkov flashes. As the lateral structure of a photon-initiated air shower is symmetric, it will yield a short, bright pulse of Cerenkov light. The time profile of a proton shower with the same energy, however, reflects the irregular nature of the air shower. The small sub-showers may appear as one or

more observable sub-pulses in the tail of the Cerenkov light profile, and the tail itself may be extended. Because of the energy diverted to these subsidiary processes, the peak intensity of the flash is lower. Tumer et al (1990a, 1990b) have investigated the feasibility of discerning shower type from the temporal profile of the Cerenkov pulse ('pulse shape discrimination'), with promising results. They rejected events with sub-pulses or extended tails by visual examination of the pulse shapes, and retained only 8% of events as potential γ-rays. As a result, emission from the Crab Nebula was detected from observations totalling only 200 minutes. It is hoped that a less subjective, but otherwise similar method of reducing the number of background events by pulse shape analysis will soon be developed.

5.1.3) Narrow aperture telescopes

A simpler method of signal enhancement does not attempt to determine the type of particle initiating an air shower, but involves the use only of directional information. The diffuse cosmic ray background is composed almost entirely of protons. These are significantly deflected in the Galactic magnetic field over typical Galactic distances (a few kpc) and lose any directional information they may once have had, with the result that the cosmic ray proton flux at the Earth is highly isotropic. Superimposed on the background are small γ-ray fluxes from point-like sources, which have travelled along straight trajectories and form local anisotropies in the background cosmic ray flux. Directional information can therefore be used profitably to reject air showers which do not come from the direction of

the source and thus to increase the signal to noise ratio of a telescope. It is most simply achieved by designing a telescope to have a narrow field of view. A telescope with a 1° field of view, for example, would be able to reject immediately 90% of the events seen by a wide-field (~3°) telescope. (Imaging telescopes have wider apertures in order to capture the full width of the Cerenkov flash.) Narrow aperture telescopes do not distinguish between hadronic and γ-ray showers, and thus cannot reject background showers coming by chance from the area of sky containing a source. The minimum noise level is therefore probably higher than in direct discrimination methods, but the method is much more reliable and easier to employ than more intricate techniques. It is therefore only this characteristic of anisotropy which the Durham telescopes currently employ in maximising signal strengths.

5.2) Principles of event selection in the Durham telescopes

5.2.1) The fields of view of the Mark III and Mark IV telescopes

In the Durham telescopes, the only selection of air showers is based on a measure of their alignments with the source direction. Whereas background showers are distributed randomly across the sky, VHE γ-rays arriving from a point source will be perceived as showers with a finite angular spread of $< 1°$ but always centred within about 0.5° of the source. The spread arises because Cerenkov flashes from showers centred some distance from the telescope appear slightly off-source. A field of view matched to the expected angular size and spread is clearly desirable. The Mark III telescope has a field of view of width 0.9°

(FWHM), and the Mark IV has one of 0.8°, which approximately match the width of Cerenkov flashes. The small difference between the two telescopes arises because the Mark IV has a slightly larger focal length. The narrow field of view ensures that only showers centred within ~ 1.5° of the source direction are recorded, while as much as possible of the light from an on-source shower is still collected, keeping the energy threshold as low as possible.

5.2.2) The guard ring

Each central PMT is surrounded by a 'guard ring' of photomultiplier tubes, with fields of view centred 2° off-source. This separation is sufficient for Cerenkov flashes registered only in the guard ring channels to be considered off-source, so the ring provides a continuous measure of the background flux in the region around the target direction. The simultaneous coverage of the background flux is of extreme importance in the validation of results.

In addition, the guard ring gives a means to discriminate against off-source showers from near to the source direction, as stated in Chapter 3. The discrimination is possible because some showers are registered by two or more channels, indicating that their arrival directions probably lay between the areas of sky covered by the channels. It is assumed for the rejection of off-source showers that any shower which is registered above the discrimination threshold in both the on-source and one or more off-source channels arose unacceptably far from the source direction and was initiated by a background cosmic ray. Without the guard ring, such showers could not

be distinguished from on-axis showers. Examples of showers deemed on- and off-source using the guard ring are shown schematically in Figure 5.1.

This simple and highly successful selection criterion is now a well-established and routinely used analysis tool. It has been demonstrated empirically with both the Mark III and Mark IV telescopes that no γ-ray signals detected from point sources have observable components in the rejected datasets (e.g. Brazier et al, 1990a, 1990f). One source detected by the Mark III telescope is the X-ray binary star Centaurus X-3. A γ-ray signal from this star is detectable in data taken near the ascending node of the binary orbit. The signal is pulsed at the X-ray pulsar period, and appears only in the guard ring-selected data (Figure 5.2). The rejection of a large number of intermediate off-axis events which contain no evident γ-ray signal considerably improves the sensitivity of the telescopes to signals from point sources.

The technique, which is based only on a single, fixed threshold, has proved its efficiency. It is used in all analyses of data on point sources, with a consistent enhancement of γ-ray signals. Typically 40 - 50% of the events recorded by the centre channel of the Mark III telescope are rejected by this method. The rejection on the Mark IV telescope is only about 20%, because smaller images of the Cerenkov flashes give the channels a wider effective separation on this telescope. In 1991, the separation of the guard ring channels has been reduced to 1.5° in both telescopes. The hardware selection technique now rejects around 50 - 60% and 40 - 50% of events in the Mark III and Mark IV telescopes respectively.

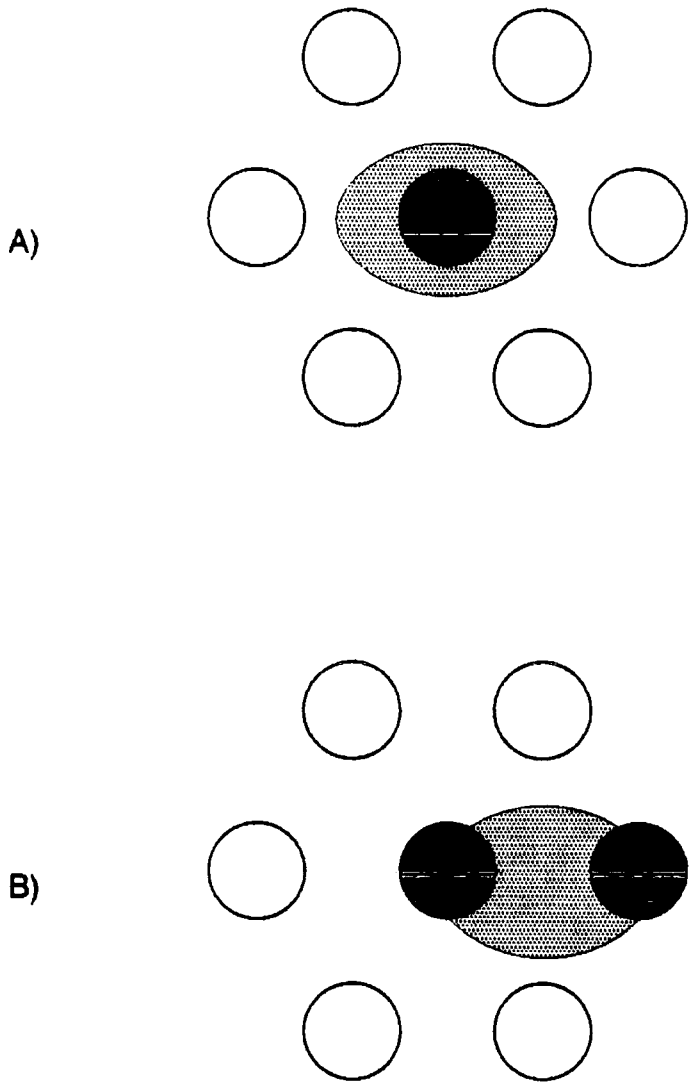

Figure 5.1

Schematic view of the telescope responses to Cerenkov flashes arising A) on-axis and B) off-axis. The light flash (shaded grey) is registered above threshold in the black channels.

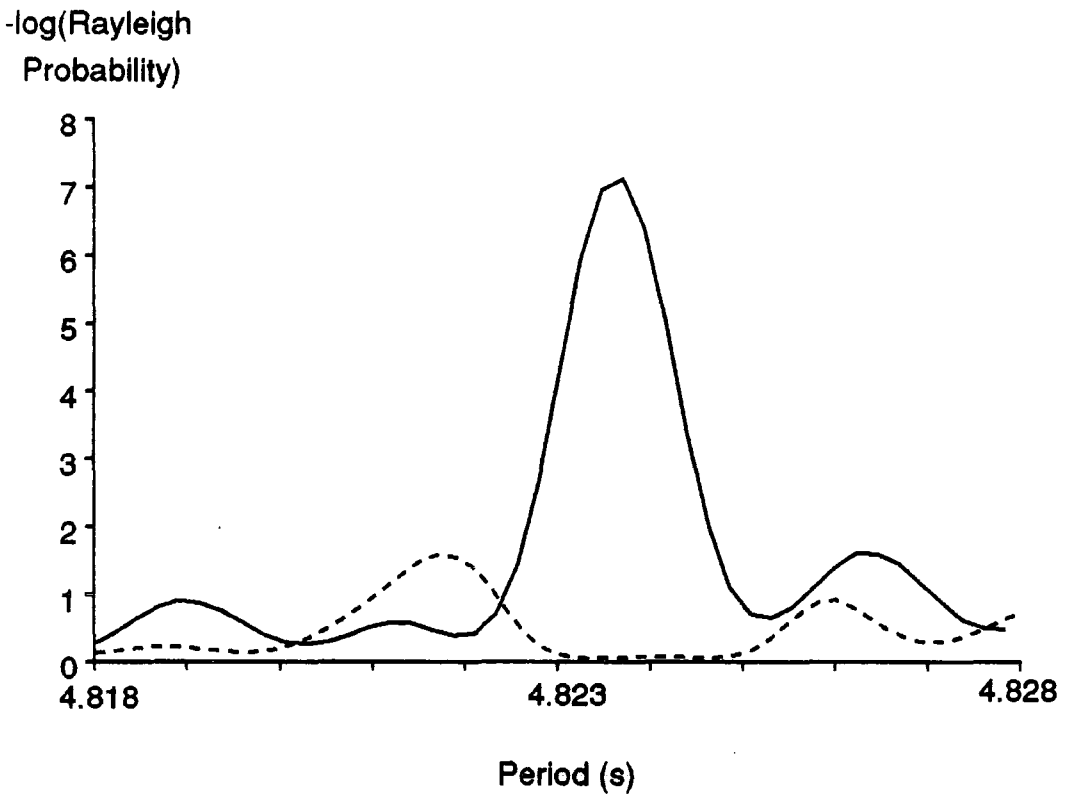

Figure 5.2

Rayleigh probabilities for chance occurrence of periodicity in on-axis data (solid line) and in the off-axis data rejected using information from the guard ring channels (dashed line). The data is on Centaurus X-3.

5.2.3) Limitations of the hardware discrimination system

The success of the selection indicates that the angular offset of the guard ring is sufficient to provide an effective rejection of background events, although it is not possible from this evidence alone to say whether the separation is ideal. The very simplicity of the event selection system described above also means that it is to some extent limited. For example, in order to alter the frequency of coincident events between pairs of channels, it would be necessary to alter the PMT separations physically or to tailor the threshold voltages. When the effects of intensity variations between Cerenkov flashes are considered, the disadvantage of a fixed threshold becomes clear. A small shower which just exceeds the threshold in the central channel could have a substantial fraction of its light falling on one of the off-source channels and yet not be registered in this second channel. As a consequence, the shower would be accepted as an on-axis event. A larger shower with the same or even a smaller fraction of light falling on the off-source channel would exceed the threshold in both channels and automatically be rejected. The shape of the cosmic ray spectrum defines that the majority of events are registered near the threshold, so a fixed threshold system will inevitably result in the incorrect acceptance of an excess of near-threshold events.

There is also a decrease in the fraction of events rejected by the fixed threshold system with an increase in the zenith angle of observation, as illustrated in Figure 5.3. The decrease is due to a simple geometric effect. A shower which appears low on the sky has traversed a greater distance through the atmosphere than one at the Zenith, so, as shower maximum occurs near the same depth for both

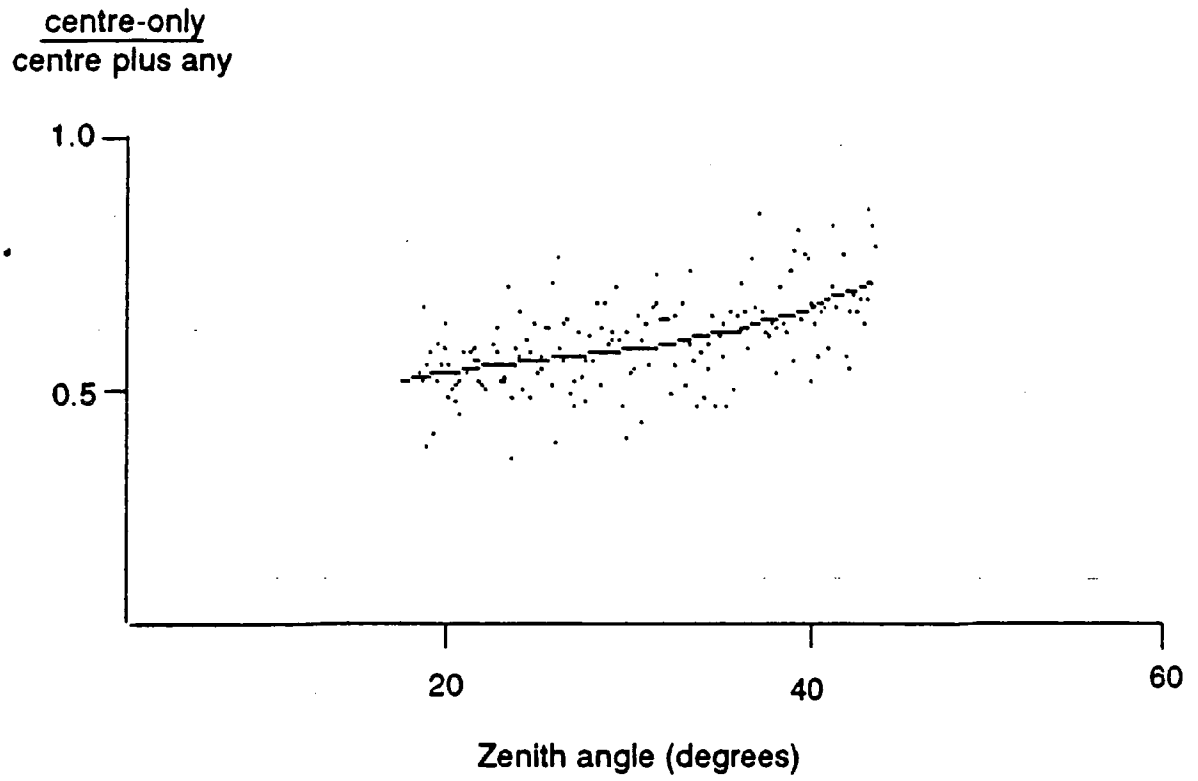

Figure 5.3

The fraction of events accepted under the hardware selection system, as a function of zenith angle.

showers, the maximum for the first shower is further from the observer. The effect is translated into a smaller image of this point, seen as a more compact Cerenkov flash. To some extent, the tightening of the flash will be counteracted by increased scattering of the light in the atmosphere, which spreads the light pool. Note that atmospheric attenuation at high zenith angles causes the intensity of the flashes to be diminished, resulting in a decrease in the total number of events counted and a corresponding increase in the energy threshold.

5.3) Digitised records of the Cerenkov flashes: pulse integrals

5.3.1) Recording and digitisation of the PMT responses

In addition to the pattern of hardware threshold responses, the record of every event includes the digitised response of each photomultiplier tube in the form of a pulse integral. Whereas the hardware threshold is only a indicator of the maximum intensity, the pulse integral is a measure of the total amount of light entering a tube during a short (30 ns) time interval. The recording of pulse integrals proceeds as follows.

An incoming signal from the photomultiplier tubes is amplified and then split along two paths. One half of the signal is sent to the 50 mV discriminators and then to a logic unit which determines whether a triple coincidence (i.e. a Cerenkov event) has occurred. The other half is sent to commercial LeCroy digitisers to be digitised in the form of pulse integrals. If the coincidence unit registers an event, the gates in the digitisers are opened for 30 ns to allow a capacitor to be

charged by the incoming signal. The signals are passed through delay cables prior to this to ensure that the gate time includes the whole of the Cerenkov pulses. The output of the digitiser is a TTL pulse, whose length is proportional to the charge in the signal integrated across the gate time. The output is then scaled. Finally, the digitised pulse integrals are written to the recording tape at the end of the event, each in the form of an 8-bit word. A schematic view of the process is shown in Figure 5.4.

5.3.2) Performance of the digitisers

The digitisers for the four primary channels (the centre plus three alternate outer channels) were installed in October 1986 and have been operational since that time. The remaining three channels and their associated recording electronics were installed in July 1987. The performance of the digitisers is monitored nightly, and they have functioned correctly throughout the lifetime of the experiment. The monitoring takes two forms, both of which may be done by observers at the telescope, so that any fault could be rectified without undue delay. Firstly, the observers check at the beginning of each night's observing that the digitisers continue to give a non-systematic, fluctuating output. Secondly, in order to ascertain that the outputs correspond to Cerenkov light flashes from the night sky, the outputs from each of the three PMT's in a channel are compared with each other and with the hardware fire pattern. A correlation between the PMT's in a channel would be expected only if the pulse integrals describe real phenomena seen by the PMT's on the sky. An example of the 1:1 intra-channel

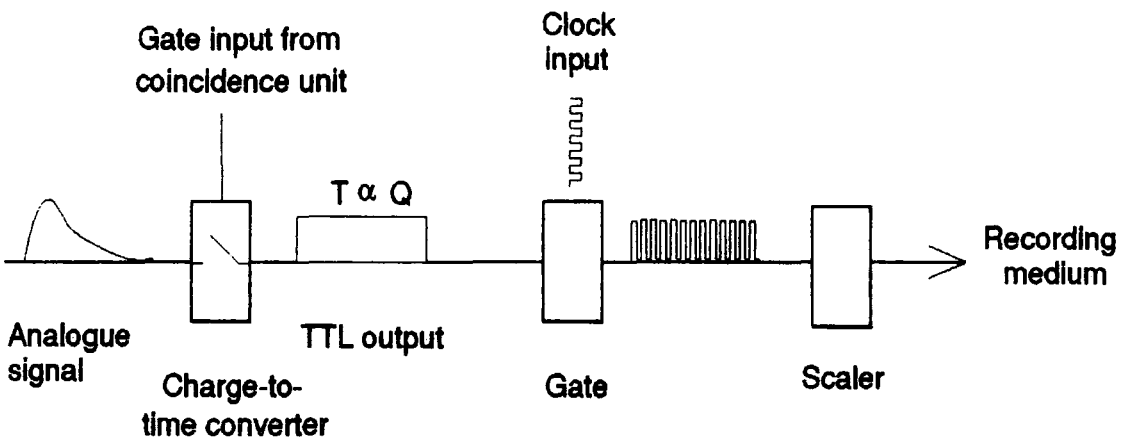

Figure 5.4

Schematic representation of the process which records the pulse integrals.

correlations is shown in Figure 5.5. The scatter originates in real variations in the Cerenkov light across the three dishes of the telescope. The offset from zero is very simply corrected (see section 5.5). The comparison with the hardware responses is merely a check that large pulse integrals in a channel correspond to a fixed-threshold event in that channel.

The stability of the digitisers in the Mark III telescope permits the extraction of a large quantity of information from the pulse integrals. The Mark IV telescope also contains pulse digitisers, but their quality is poor in comparison with those of the Mark III telescope, as they are not recorded by commercial electronics. All the development work and the uses of the pulse integrals described in this chapter apply to the Mark III telescope only.

5.3.3) Form of stored pulse integrals

The pulse integrals are stored in processed datasets as strings of integers. To minimise storage space, early datasets were stored with seven (initially four) pulse integrals, each of which was the average of the three integrals in a channel. Files are now stored with all 21 individual integrals, to allow studies of the detailed behaviour of the light flashes. Directional event selection, however, is performed on the averaged integrals to minimise local fluctuations in individual PMT responses.

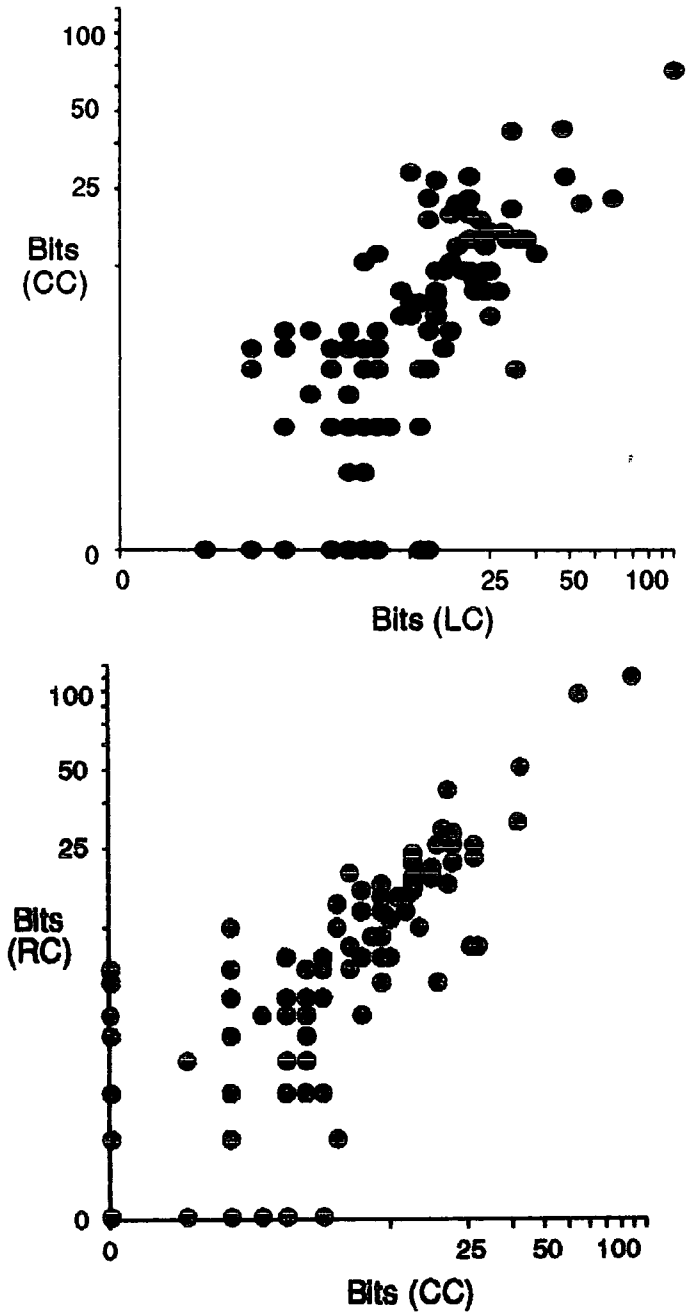

Figure 5.5

Comparisons between the left, centre and right PMT QT's on the centre channel (labelled LC, CC and RC respectively). The strong correlations between the responses of different PMT's indicates that they represent Cerenkov flashes from the night sky.

5.3.4) Use of the pulse integrals

Since events are recorded only when the 50mV discrimination threshold has been exceeded, there is inevitably some correlation between the 'fire pattern' and the pulse integrals. For example, the 50 mV threshold corresponds to a normalised pulse integral of approximately 10 bits. The latter are, however, electronically independent, and also contain a wealth of further information. The great advantage of the pulse integrals over the hardware threshold system is that they provide a 'grey scale' of event sizes. They are not used to identify genuine source events in real time, but may be used to advantage at a later stage of data processing as a flexible and powerful extension of the the fixed threshold selection. The following sections describe an investigation of their ability to identify unwanted events on a directional basis.

5.4) Development strategies for event selection

The development of an event selection criterion using the pulse integrals is divided into three parts. Firstly, the integrals must be normalised across all photomultiplier tubes to remove any systematic bias introduced by the digitising electronics or by the individual tube responses, so that subsequent event selections will discriminate uniformly. The spectrum of pulse integrals obtained from a tube may be characterised most simply by the position of the mode and the width of the distribution. If a comparison is to be made between the integrals registered on different channels, these two parameters must be matched

across all tubes in any given source observation and ideally across all observations of a source.

Having achieved a set of pulse integrals which conform to a uniform spectrum, the optimal event selection criterion may be ascertained. The main requirement is that it selects showers centred on the source direction without a significant bias against either very small or large showers. In order to test selections on real data, a dataset containing a known γ-ray signal is needed. The preferred selection will be that which gives the strongest combination of background rejection and signal enhancement.

Lastly, the chosen selection criterion will then be applied to potential and established γ-ray signals to test its efficiency. This will also determine whether a single criterion is applicable to all sources. It might be expected that there may be some dependence on zenith angle or on sky brightness. Some allowance for these factors must be permitted. If the chosen selection works efficiently at enhancing signals, then all real signals will be strengthened, while spurious ones will be weakened and rejected.

5.5) Normalisation of the pulse integrals

Typical spectra of raw pulse integrals from the Mark III telescope are shown in Figure 5.6. The data are taken from an observation of the Vela Pulsar, which was chosen for studies of the pulse integrals because of its high event total and the large range of zenith angles it covers (34°). It does not contain a detectable flux of γ-rays. All non-dead-

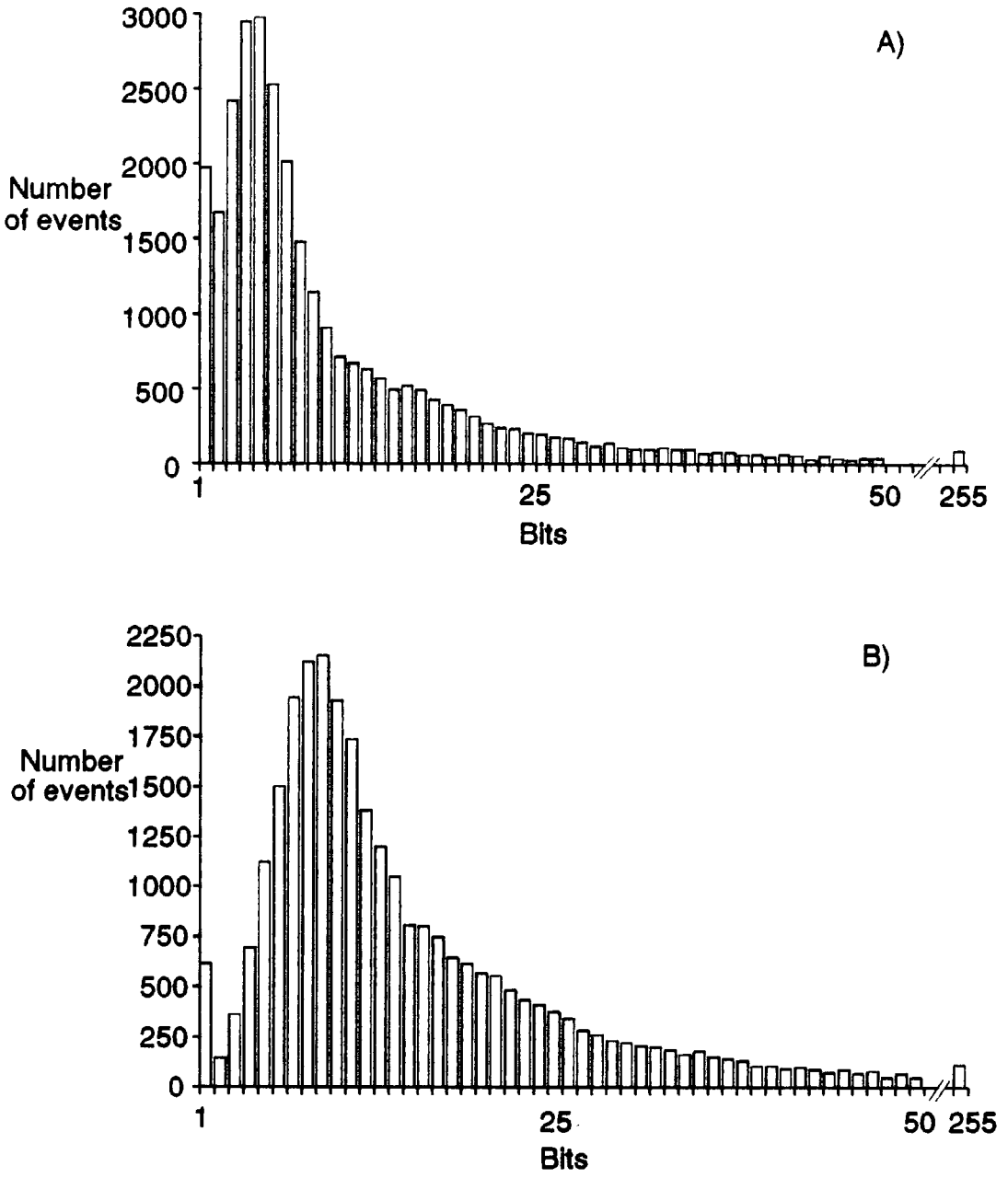

Figure 5.6

Two examples of spectra of pulse integrals, from an observation made on 7th March, 1989. The target object was the Vela Pulsar. The spectra are taken from A) the left and B) the right central PMT's.

time events in the data file have been included in the spectra, regardless of whether they exceeded the discrimination threshold in the tube shown. It can be seen that the spectrum is smooth and single-peaked, as would be expected, and that very few events are bright enough to approach the limit of the digitisers at 255 bits.

For normalisation purposes, a spectrum of pulse integrals can be characterised in terms of a 'pedestal' and the 'gain'. The pedestal is defined here to be a fixed offset from the position of the distribution peak, the mode. A value of (peak - 3) is chosen, since very few events occur with pulse integral values smaller than this. As long as the pedestal lies below nearly all events and is at a fixed position, its absolute value is unimportant. Use of the pedestal allows the position of the spectra to be normalised to a common, easily recognisable point. The mode is preferable over other measures of the average because it is important that if an irregular spectrum should occur, no weight be given to the irregularity. An example of an irregular spectrum is shown in Figure 5.7. In this figure, the spectrum peak lies close to zero. Since negative values of pulse integral cannot be accommodated, all sub-zero values appear at a value of 0. In the example shown, there are enough sub-zero events for the false peak at 0 to lead to an incorrect identification of the pedestal. In practice, the peak is only permitted to occur anywhere in the range 1-99, and is always found to be between 2 and 15. Individual tubes have characteristic pedestals, regardless of the object observed.

The normalised spectra corresponding to Figure 5.6 are shown in Figure 5.8. For convenience in graphical representation, the spectra have been normalised to have a peak at 10 bits. The simple method of

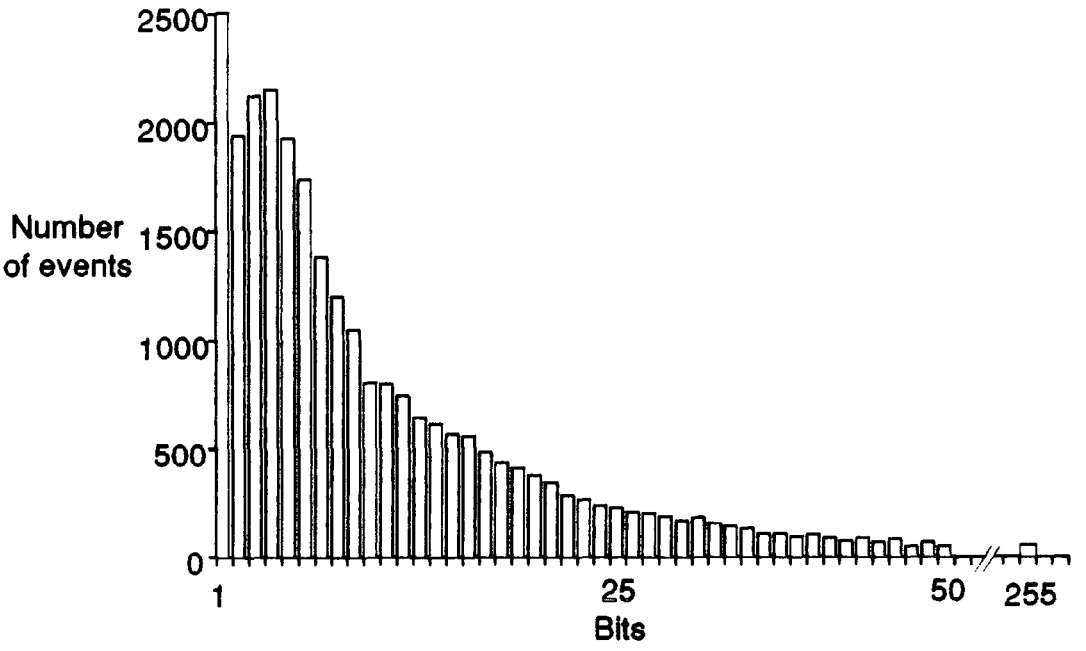

Figure 5.7

An example of a pulse integral spectrum showing where a false peak could occur. The peak at zero is merely a consequence of the small pedestal.

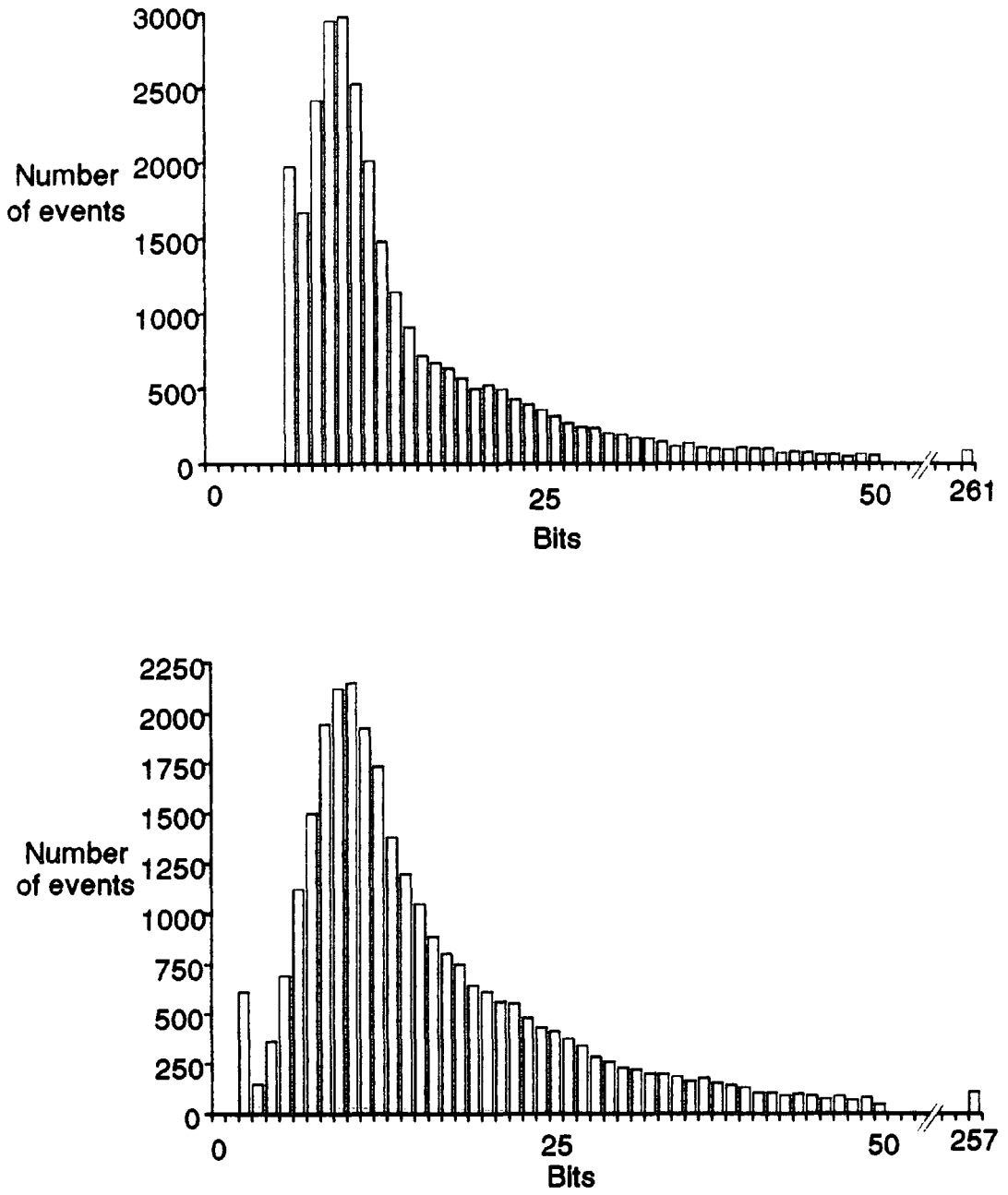

Figure 5.8

The normalised spectra corresponding to the raw spectra shown in Figure 5.6. The spectra have been brought to a common position by unifying the pedestals.

alignment described above has been successful in bringing the spectra to a common position. The definition of the peaks is such that the position of the pedestal in similar spectra would very seldom be uncertain by more than 1 bit. Since this is also the resolution limit, more accurate methods of aligning the spectra such as spline fitting would not yield a significant benefit unless the dataset were very small (< 1000 events). Full datasets usually contain several thousand events.

It is also apparent that the widths of the two spectra are very similar. After comparing the spectra from all tubes, it is found that the inter-tube gain variations for observations of a given source are less than ~ 15%. Because of the quantised nature of the digitised pulse integrals, the height of any bin in the histogram distribution cannot be changed. It is therefore not possible to map the spectra onto a single distribution using a simple scaling factor. Since the vast majority of events are close to the distribution mode, and especially since the quantised nature of the pulse integrals cannot be lost, the spread in gains will have only a small effect, and so no correction is made to the distribution widths.

Small, additional variations between sources may be expected and are attributed to different operating voltages and to zenith effects on the incoming showers. This effect is generally negligible for observations of any one object.

5.5.1) Zenith angle effects on the pulse integrals

The effects of zenith angle on pulse integral spectra have been investigated using the observation of the Vela pulsar used for Figures

5.6 and 5.8. During this observation, the object crossed an unusually large range of zenith angles, from 13° to 47°. Any effect which zenith angle might have on the spectrum of Cerenkov flashes might therefore be expected to be particularly noticeable in this dataset. In order to search for an effect, two sections of 5000 events were extracted from the data, one covering the zenith range from 13° to 20° and the other from 40° to 47°. The resultant spectra are plotted in Figure 5.9 for each of the three PMT's in the central channel. There is only a small difference between the two sets of spectra, which appears as a tendency for recorded showers to be smaller at large zenith angles. The difference is very much smaller than the inter-tube variations and zenith angle effects will therefore be limited to the geometrical effects seen in the hardware system.

5.6) Possible noise rejection criteria using the pulse integrals

Having achieved a set of normalised spectra, we must now devise an efficient criterion for rejection of off-axis events. The new selection system will supplement rather than replace the existing system of event selection. The most simple candidate selections fall into two categories. Either the selection will follow the lines of the hardware discrimination system and demand that an event be rejected if an off-axis channel exceeds some fixed threshold, or the selection can be made on the basis of the *fraction* of the signal occurring in outer channels.

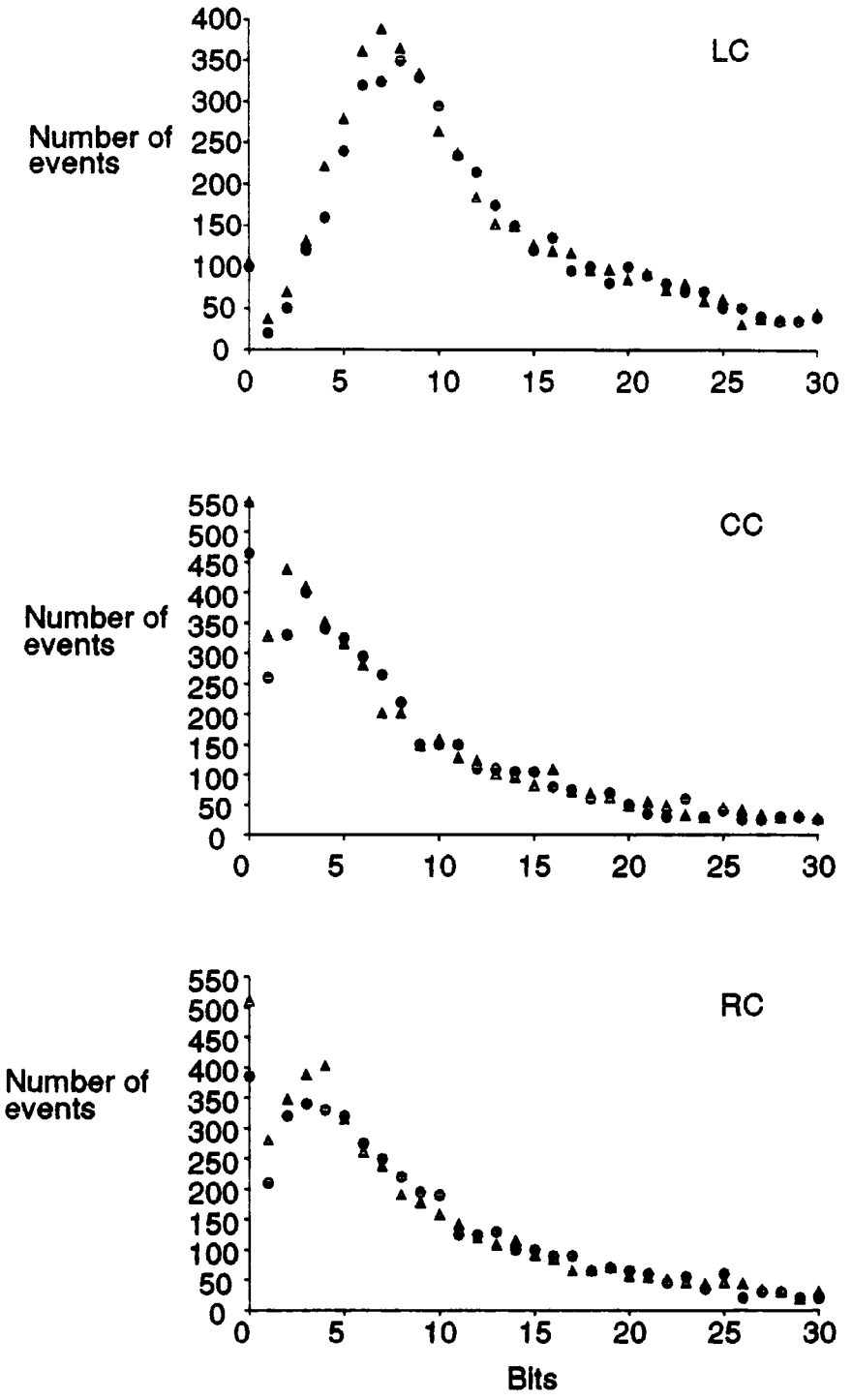

Figure 5.9

Comparison between the pulse integral spectra for different zenith angles of observation. The data is taken from the observation of the Vela Pulsar made on 7 March 1989. Triangles represent data taken at large zenith angles, and circles, data taken at small zenith angles.

5.6.1) Fixed threshold rejection

A direct pulse integral equivalent to the hardware threshold would reject events on the basis of any one off-axis response exceeding a fixed threshold. An approximate match would be achieved by a (pedestal-subtracted) discrimination threshold of 10 bits. An alternative criterion might use the sum of all off-axis integrals. Both of these will be subject to exactly the same limitations as the hardware selection itself. Instead, a criterion involving the *relative* amplitudes of on- and off-axis responses is desirable, to remove the biasing towards the acceptance of small showers inevitably imposed by fixed thresholds.

5.6.2) Rejection by relative response

The relative amplitude of a pulse integral in a given channel is a direct measure of the fraction of the shower's Cerenkov light falling on that channel. Consider the simple example in which all the light falls on two channels. Then a relative amplitude of 50% in the one of the channels would imply that a third of the total light had fallen on that channel. In reality, the relative amplitude does not have such a simple translation, but, since different channels sample separate parts of the sky, it does provide a simple mechanism for estimating the direction of propagation of the shower. Moreover, the amplitude of the shower does not introduce a bias. Relative amplitudes of the on- and off-axis pulse integrals provide precisely the information needed to reject background showers on a directional basis, regardless of their size. A form of selection is therefore chosen which utilises this information.

Having decided upon the general form of selection, we must now determine how best to make use of the information afforded by the guard ring channels. It is sometimes observed that light from an incoming shower has fallen on three or more channels. If we are to obtain maximum efficiency in our selection criterion, it is therefore reasonable to assume that the sum of two or more off-axis responses could be required to exceed the fractional threshold instead of only one.

The extra efficiency gained by a multiple channel selection criterion is ultimately dependent on the frequency of events which it will affect. If the hardware selection has already been applied, around 80% of events are sufficiently biased towards two of the channels for a selection requiring an excess in only one off-axis channel to be as effective as more complicated criteria. This is similar to the dominance of single- and double-channel events in the fire pattern, in which only 25% of events have a greater multiplicity than 2. For this reason, the pulse integral selection criterion is restricted to the simple form:

$$\text{Accept if (each off-source)} \times C\% \leq \text{(on-source)} \qquad - \ 5.1$$

where C is the threshold percentage. This selection is not subject to the systematic irregularities inherent in the hardware selection system and described above.

5.6.3) Expected behaviour of genuine and spurious signals

Candidate signals are divided into two types: those which arise from stellar γ-rays and those which arise in the background noise by chance. By applying a series of pulse integral selections at increasingly severe thresholds, it is possible to distinguish between these. If the signal is real, the number of γ-rays will be approximately conserved as the threshold is decreased to an optimum, and the strength of the signal will increase steadily within the diminishing dataset. Beyond the optimal percentage, source events will also begin to exceed the threshold, so that event rejection will be random and the percentage strength will stop rising. If the candidate signal is spurious, noise and signal will have been treated similarly throughout, with no upwards trend in the signal strength and a systematic increase in the Rayleigh probability.

A sustained decrease in the probability is therefore indicative of a real flux from the source under study, and a sustained increase likewise suggests that the supposed signal is a statistical fluctuation in the phase distribution. Thus, the flexibility of pulse integral selection gives it the power to reject conclusively spurious signals accepted by the hardware cut, as well as to confirm and strengthen real detections.

5.7) A case study: Centaurus X-3

5.7.1) The X-ray binary Centaurus X-3

Centaurus X-3 was discovered as a bright X-ray source in 1967 (Chodil et al, 1967) and was later identified as a 4.8-second pulsar in an eclipsing binary system (Giacconi et al, 1971, Schreier et al, 1972). The pulsar is believed to be accreting via an accretion disc from an O-type supergiant companion. The orbit is seen at high inclination and at some phases of the orbit, absorption dips indicate that matter passes across the line of sight. Absorption features in the X-ray flux near inferior conjunction (when the neutron star is directly in front of its companion) and near the ascending node have been interpreted as evidence for an accretion wake (Tuohy and Cruise, 1975, Pounds et al, 1975). The source also shows irregular fluctuations in X-ray intensity on timescales from seconds to months (Giacconi et al, 1971, Pounds et al, 1975). On a timescale of months, the source alternates between high states, lasting for between one and four months, and low states, which last from two weeks to two months, during which time the flux remains *lower* than the high state eclipse level (Schreier et al, 1976). It is thought that these transitions are related to variations in the intensity of the companion's stellar wind.

The source has been observed by various X-ray experiments since its discovery. The two most recent measurements of the pulsar period have been made with the Ginga and Mir-Kvant satellites (Makino et al, 1987, Gilfanov et al, 1989). The orbital parameters were last measured with the SAS-3 satellite (Kelley et al, 1983a) and are listed in Table 5.1.

Semi-major axis	(39.636 ± 0.003) lt-sec
Eccentricity	0.0004 ± 0.0002
Epoch of mid-eclipse	JD 2443870.38910 ± 0.00002
Orbital period	(180325.2 ± 0.7) s
Orbital period derivative	$-(1.02 \pm 0.05)_{\lambda} \times 10^{-8}$ ss^{-1}

Table 5.1

The orbital parameters of Centaurus X-3, as given in Kelley et al, 1983. Note that the detection of eccentricity is marginal and that the longitude of periastron is not given. A more recent observation with the Mir-Kvant module was too short for a determination of the orbital parameters (Gilfanov et al, 1989).

5.7.2) Durham VHE observations of Centaurus X-3

Centaurus X-3 was observed with the Mark III telescope in good weather conditions on a total of 84 occasions, from January 1987 to February 1991. A further 6 good weather observations were made with the Mark IV telescope in January and February 1991. All of the data taken with the Mark IV telescope and the majority of that taken with the Mark III telescope were taken in the tracking mode; some of the 1988 Mark III data were taken in the chopping mode. A summary of all data suitable for analysis is presented in Table 5.2.

5.7.3) Analysis strategy

The data were focussed to the binary's barycentre according to the ephemeris of Kelley et al (1983a). No correction for the very slight orbital eccentricity was made, as the longitude of periastron is unknown. The sensitivity of this slow pulsar to variations in orbital parameters is very weak, and the data were therefore focussed to an exact, circular orbit.

A search for periodicity in the data was made using the Rayleigh test. Only events selected as on-source by the hardware system were used. Where the observations were taken in the chopping mode, only the data taken with the central channel on-source were analysed, to maximise the signal enhancement gained by use of the guard ring responses.

A preliminary analysis was made using all the data available from the 34 observations made between January 1987 and June 1989. At the time of the analysis, the most recent measurement of the pulse period was that of Makino et al (1987). They measured the period to be

Table 5.2

Observing log for Centaurus X-3, showing the duration and orbital phase of all good observations.

Date	Steering mode	Duration (hrs)	Mid-phase
Mark III observations:			
280187	Tracking	2.5	0.28
290187	Tracking	2.3	0.76
310187	Tracking	2.5	0.72
010287	Tracking	2.5	0.20
020287	Tracking	2.5	0.69
040287	Tracking	2.5	0.63
060287	Tracking	2.5	0.59
070287	Tracking	2.0	0.08
290487	Tracking	3.0	0.80
030587	Tracking	3.0	0.72
190587	Tracking	2.0	0.33
200587	Tracking	3.5	0.83
210587	Tracking	3.0	0.32
220587	Tracking	4.0	0.78
230587	Tracking	3.3	0.25
240587	Tracking	3.5	0.74
250587	Tracking	3.5	0.21
260587	Tracking	3.5	0.69
270587	Tracking	3.5	0.17
280587	Tracking	4.0	0.66
290587	Tracking	3.5	0.13
300587	Tracking	3.7	0.62
310587	Tracking	3.3	0.09
170188	Chopping	2.0	0.90
180188	Chopping	3.3	0.36
190188	Chopping	3.0	0.85
200188	Chopping	3.7	0.32
210188	Chopping	3.3	0.79
220188	Chopping	4.7	0.27
240188	Chopping	2.7	0.25
250188	Chopping	4.7	0.71

150288	Chopping	4.5	0.79
170288	Chopping	4.3	0.74
190288	Chopping	4.3	0.69
240288	Chopping	5.3	0.09
250288	Chopping	4.5	0.58
260288	Chopping	4.5	0.08
110588	Tracking	3.5	0.86
130588	Chopping	3.5	0.83
150588	Tracking	4.0	0.80
190588	Tracking	3.0	0.77
050688	Tracking	3.3	0.85
070688	Chopping	3.0	0.82
060189	Tracking	3.0	0.98
090189	Tracking	2.0	0.43
140189	Tracking	4.0	0.80
160189	Tracking	3.0	0.78
020289	Tracking	3.0	0.88
010389	Tracking	3.7	0.77
270489	Tracking	3.0	0.06
280489	Tracking	4.0	0.55
290489	Tracking	4.0	0.06
300489	Tracking	2.0	0.52
010589	Tracking	2.0	0.00
020589	Tracking	4.0	0.49
030589	Tracking	3.0	0.96
040589	Tracking	3.0	0.44
050589	Tracking	3.0	0.90
280589	Tracking	5.0	0.92
290589	Tracking	4.7	0.40
010689	Tracking	3.0	0.84
070689	Tracking	1.7	0.71
290190	Tracking	2.0	0.90
300190	Tracking	4.0	0.36
310190	Tracking	4.5	0.84
230290	Tracking	2.0	0.84
240290	Tracking	1.7	0.31
250290	Tracking	1.7	0.78
260290	Tracking	1.7	0.27
010390	Tracking	3.0	0.70
040390	Tracking	2.5	0.16

140590	Tracking	1.0	0.08
150590	Tracking	2.7	0.56
210590	Tracking	2.5	0.45
240590	Tracking	2.0	0.84
100191	Tracking	1.5	0.63
110191	Tracking	2.0	0.14
140191	Tracking	4.7	0.58
150191	Tracking	3.0	0.07
180191	Tracking	3.0	0.50
080291	Tracking	3.0	0.50
110291	Tracking	2.5	0.01
190291	Tracking	4.5	0.79
210291	Tracking	3.0	0.81
Mark IV observations:			
140191	Tracking	2.0	0.61
150191	Tracking	2.5	0.05
170191	Tracking	2.0	0.01
180191	Tracking	2.3	0.49
110291	Tracking	2.0	0.00
190291	Tracking	4.0	0.75

(4.8230 ± 0.0002) s in May-June 1987, contemporary with the early Durham observations. No measurement of the short-term period derivative was made.

Centaurus X-3 has exhibited a non-uniform variation in its pulse period since the time of its discovery. It has been observed to have intervals both of rapid spin-up and of relative stability, with a long-term period derivative of the order of -3×10^{-11} ss^{-1}. The absence of a contemporary measurement of the period derivative makes it necessary to test the data over a range of possible periods. For the preliminary analysis, it was assumed that the period derivative was no more than twice the long-term value, which would induce a maximum period shift over one year of 2 ms. The period search range was therefore limited to ± 2 ms from the X-ray period. For the longest observation (five hours), this corresponded to a range of approximately ± 2 Fourier intervals.

The most sensitive searches for periodicity involve combining all available data. For such an uncertain period, it would clearly not be wise to to try to retain pulse phase over a year's data. However, the assumption that the period change is comparable with the Fourier interval of a single observation does permit a phaseless combination of the data. Thus, the individual observations were tested for periodicity separately and the Rayleigh probabilities were combined statistically, according to the method described in section 4.4.1. The combined periodogram would be expected to show periodicity if the period changed by less than one Fourier interval.

Two combinations of data were tested in this manner. The database was combined as a whole, to test for a steady flux of pulsed γ-rays, and a search was also made for an orbitally modulated flux. There are many

reasons to expect that any emission might be confined to a limited section of the binary orbit, stemming from X-ray observations of this source and TeV observations of similar ones. From X-ray observations of eclipse ingress and egress, it has been concluded that the companion of Cen X-3 has an extended atmosphere, and absorption dips around the ascending node suggest streams of material associated with mass transfer to the neutron star (Tuohy and Cruise, 1975). If, as has been suggested, the absorbing matter is the site of VHE γ-ray production via interactions with particles accelerated near the pulsar, then the X-ray modulation may well be reflected in some way in the VHE γ-ray flux.

More suggestions of orbital modulation in the VHE flux come from TeV observations of other X-ray binaries. There is evidence that the emission from a similar binary, LMC X-4, is modulated with the orbital period (Chadwick, 1987, Brazier et al, 1990d). The low-mass binary Hercules X-1 shows a modulation with a longer, 35-day X-ray period due to precession of the accretion disc (Gorham, 1986), and Cygnus X-3 (Dowthwaite et al, 1983) is only detectable for a small part of the 4.8 hr X-ray cycle. There is good reason to expect similar behaviour in Cen X-3.

5.7.4) Preliminary results

All the data were tested for periodicity about the pulsar period and the results were combined. The resultant periodogram is shown in Figure 5.10. The wide range of test periods in this plot is included only for display purposes. The probability that the data are uniform in phase is 0.1. Thus, there is no evidence of periodicity at the pulsar

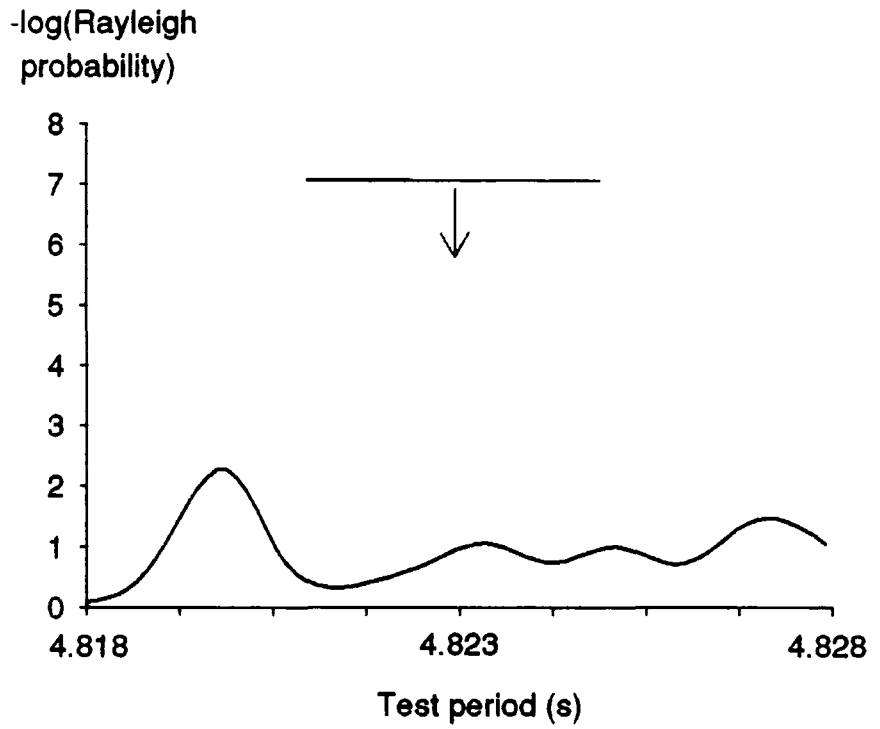

Figure 5.10

Periodogram in the region of the pulsar period for all data taken up to the end of 1988. The Ginga measurement of the period (arrowed) and the search range (horizontal bar) are indicated. There is no evidence of periodicity at the pulsar period.

period in this complete dataset.

The data were then divided into 10 subsets, according to the orbital phase of the middle of each observation. Phase zero was taken to be at the ascending node. The sections do not define absolute bounds, since a typical observation of three hours covers 6% of the 2.1 day orbit and the observations were not subdivided. The data in each phase section were tested for evidence of periodicity at the pulsar period, with the results summarised in Table 5.3. The data in the section immediately after the ascending node (Φ = 0 - 0.1) show significant periodicity. The probability of the periodicity arising by chance is 1.1×10^{-5}, which reduces to 1.3×10^{-3} after allowance for the division of the data into orbital sections and the range of test periods. The periodogram corresponding to this subset of data is shown in Figure 5.2. The extended period range is again shown for display purposes only. Note that in an early presentation of this result (Carramiñana et al, 1989b), a small error in the phase calculation was made. The correct phases are quoted here, and are advanced by 5% from the original calculations.

It is interesting that this region of the orbit is also the site of X-ray absorption dips, which have been interpreted as indicating an accretion wake. It is possible that the VHE γ-rays originate here. If hadrons emitted from the vicinity of the central pulsar are incident on the accretion wake, TeV γ-rays may be produced via π° decay. Charged particles would be significantly deflected in the pulsar magnetic field and would lose any timing information. The detection of coherent pulsations has therefore prompted the suggestion that the incident particles may be neutrons (North et al, 1989). If the wake is the site

Orbital Phases	Observations	No. Events	Chance Prob.
0.0 - 0.1	12	33687	1.1×10^{-5}
0.1 - 0.2	1	2684	3.7×10^{-2}
0.2 - 0.3	0	0	-
0.3 - 0.4	4	23970	4.7×10^{-1}
0.4 - 0.5	5	26970	3.3×10^{-1}
0.5 - 0.6	6	27355	4.2×10^{-1}
0.6 - 0.7	1	5411	4.2×10^{-2}
0.7 - 0.8	0	0	-
0.8 - 0.9	4	23201	6.3×10^{-1}
0.9 - 1.0	6	34204	5.0×10^{-1}

Table 5.3

The chance probabilities of periodicity at the pulsar period in 10% sections of the binary orbit. There is significant periodicity in the phase band 0.0 - 0.1.

of emission, coherent periodicity would place stringent constraints on the geometry of the emitting region.

Note that the observed X-ray absorption features are time-variable, lasting only for a few months, similar to the timescale for the low/high state transitions. The VHE flux, if dependent on this accreting matter, may thus also be highly variable on this timescale. Since the orbital phase of X-ray absorption is not fixed, it may also be expected that the phase of TeV γ-ray will also move by a few per cent on timescales of months.

5.7.5) Use of the Cen X-3 data in tests of event selection criteria

The Centaurus X-3 data provide a γ-ray signal on which to test selection criteria. Within the phase region 0.0 - 0.1, the emission is strongest in the phase band 0.02 - 0.07, for which the combined chance probability is 2×10^{-7}. Three individual observations display significant periodicities. These are the observations taken on 29th April 1987, 22nd May 1987 and 21st January 1988. Of these, that of the 22nd May, 1987, is the longest and also contains the most significant level of periodicity (chance probability 7×10^{-4}). This dataset was chosen for tests of the selection criterion suggested in section 5.6.2.

In order to test the effectiveness of the criterion, the data were subjected to a series of selections at increasingly severe thresholds, ranging from 50% to 25%, where the threshold percentage is defined in equation 5.1. The dataset remaining after a particular cut was then tested for periodicity at the pulsar period. The numbers of events remaining and the Rayleigh probability of periodicity for each selected

dataset are shown in Table 5.4. Contrary to expectation for a random event selection, there is a systematic drop in the probability to a minimum of 2×10^{-5}, and then increases. This is the behaviour predicted for a genuine signal (section 5.6.3). The minimum occurs at a cut of 30%, i.e. when no guard ring channel shows a digitised response larger than 30% of that occurring on the centre channel. The order of magnitude improvement represents a significant gain in sensitivity over the hardware selected dataset.

The success of the cut on this single night does not prove that the relative integral selection is universally effective. A 30% cut was therefore applied to the data from all seven observations in the Φ = 0.02 - 0.07 phase band. Figure 5.11 shows the result of subjecting the data to a 30% integral selection as well as the hardware selection. The decrease in peak Rayleigh probability over the original result is a factor of approximately three, to a final probability of 7.9×10^{-8}. This reduction would not be expected if the enhancement applied to the 22nd May 1987 dataset had not been successful when applied to the other six.

The above improvement in sensitivity permits us to detect periodicity in some observations where previously none was observable. In Figure 5.12 are plotted the periodograms for each of the seven observations in the 0.02 - 0.07 phase range. Also marked is the Ginga X-ray period. Periodicity at the Ginga period is visible in six of the observations. Interestingly, the period does not move significantly from the Ginga period between 1987 and 1988. Such a constant period is not consistent with the long-term period derivative of Centaurus X-3, but in the pulse period history of the star (Figure 5.13), the period

Selection		No. events	Prob.	R (%)
1		12057	1.2×10^{-3}	2.4
2		7449	6.6×10^{-4}	3.1
3	50%	6494	1.4×10^{-3}	3.2
	45%	6063	2.7×10^{-4}	3.7
	40%	5695	3.6×10^{-4}	3.7
	35%	5107	1.6×10^{-4}	4.1
	30%	4475	2.1×10^{-5}	4.9
	25%	3735	9.0×10^{-5}	4.9

Table 5.4

The event totals and Rayleigh periodicities of data accepted under a series of hardware and pulse integral cuts. The data are taken from the observation of Cen X-3 made on 22nd May 1987. The event selections are :

(1) All events which have exceeded the hardware threshold in the centre channel, regardless of the guard ring responses.

(2) Events which have exceeded the hardware threshold only in the centre channel.

(3) Events which are in (2) and also have no guard ring channel with an average pulse integral above the shown percentage of the central one.

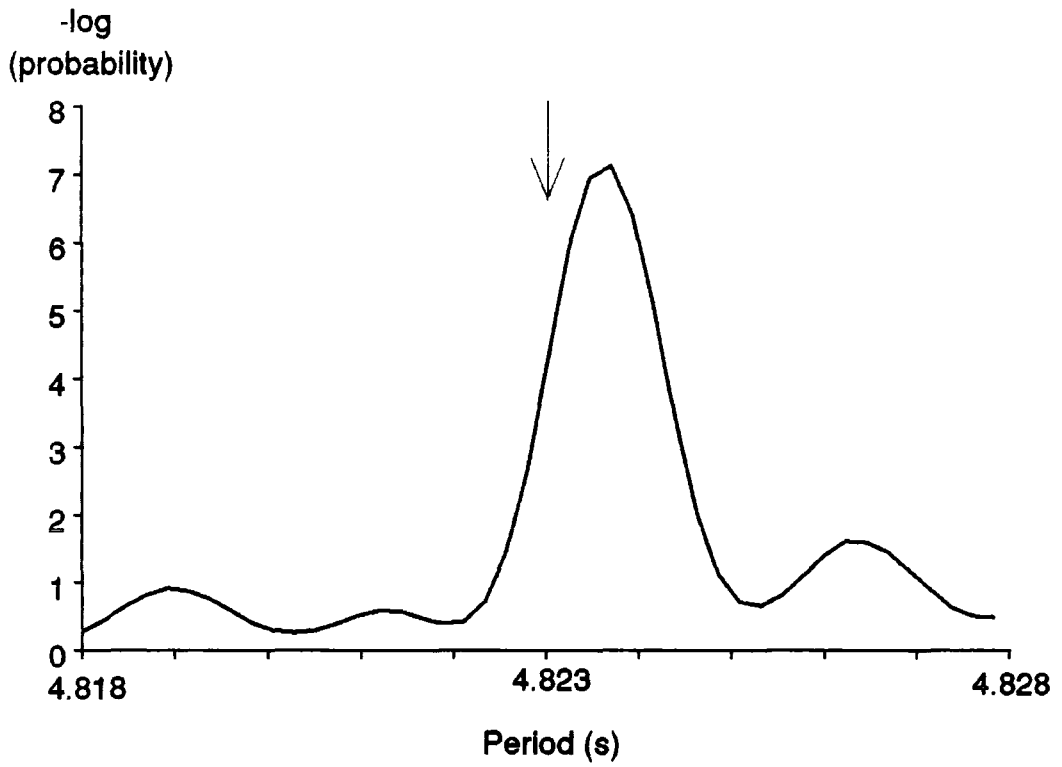

Figure 5.11

The chance probability of periodicity at the test periods shown in the 1987 - 1988 data on Cen X-3. The observations included are all those in the 0.02 - 0.07 phase band, where phase zero is the ascending node. The data have been subjected to pulse integral selection at a threshold of 30%.

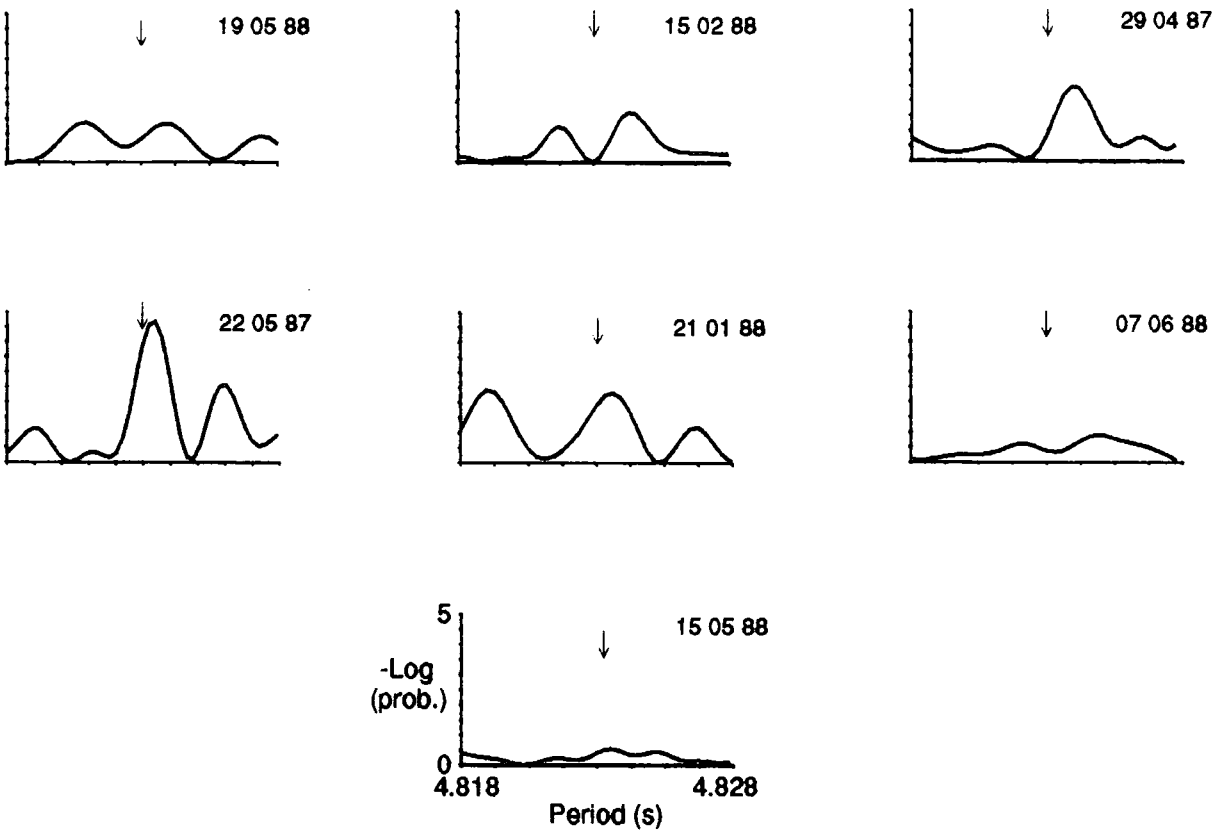

Figure 5.12

Periodograms in the region of the Cen X-3 pulsar period (arrowed) for each of the observations made of the orbital phase region 0.02 - 0.07. The axes are labelled as indicated for the dataset of the 15th May 1988. Note that the search range is smaller than that displayed, with a width of 4 ms about the pulsar period.

has at times remained stable to within a millisecond for over a year. It would appear from the enhanced Durham data that this was the situation for the years 1987 - 1988. In fact, a subsequent X-ray period measurement at 4.82259 s (Gilfanov et al, 1989) confirmed that the period had indeed remained unusually constant over the interval 1987-1989. This measurement and the summed Durham result are included in Figure 5.13. The Durham measurements are clearly fully consistent with the two contemporary X-ray periods (Brazier et al, 1989b, 1990a). Descriptions of the detection of Centaurus X-3 can also be found in Brazier et al (1989c, 1990b, 1990c).

5.7.6) Other TeV observations of Centaurus X-3

Centaurus X-3 was also observed by the Potchefstroom group during 1987-1989. They observed periodicity near the ascending node, but in the orbital phase band 0.95-0.05 (where the ascending node defines phase zero) (North et al, 1989, 1990). The latter half of this phase band overlaps the 0.0 - 0.1 band in which the Durham result appears. The data in the 0.95 - 0.05 phase band included three observations, of which only the first and third showed significant periodicity in their search range. The two periods were 4.827 s and 4.817 s respectively. In none of the observations was any significant periodicity detected at the X-ray period of 4.823 s. The authors concede that the periods detected are not consistent with the X-ray measurements. However, they derived a period derivative which would link their two observed periods and used this to combine all three observations, yielding an overall Rayleigh probability of 2×10^{-4}. This probability does not include any

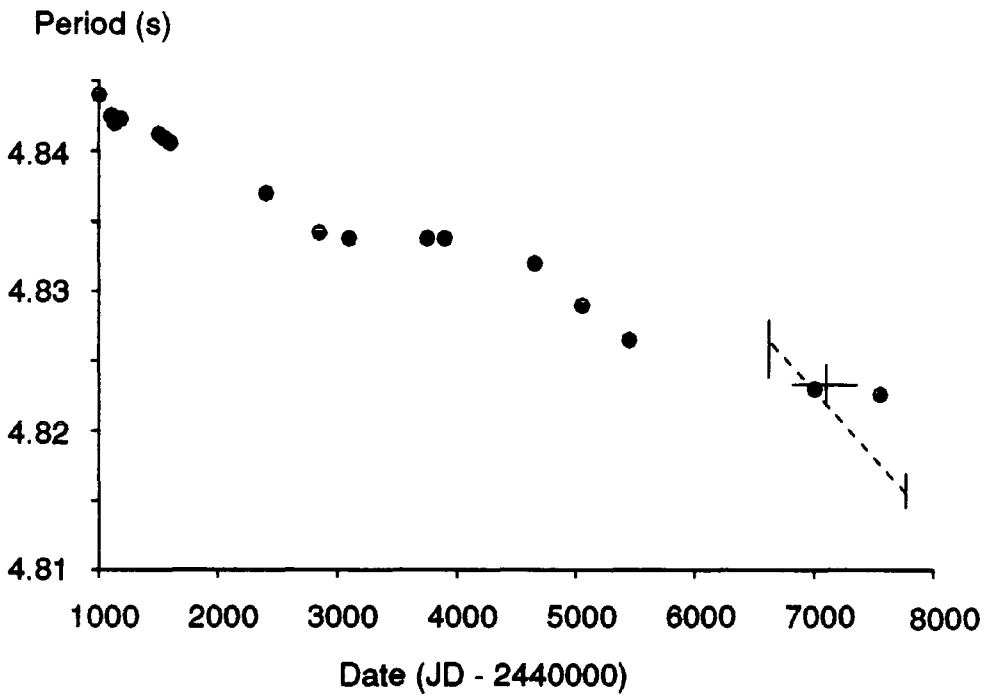

Figure 5.13

The pulse period history of Centaurus X-3. References for the various X-ray measurements can be found in Gilfanov et al, 1989. Also shown are the Durham (solid cross) and Potchefstroom (dashed line) VHE results.

allowance for the freedom used in choosing an appropriate period derivative. Given that the calculated period derivative of 10^{-10} ss^{-1} is an order of magnitude larger than the contemporary X-ray period derivative ($\sim 8 \times 10^{-12}$ ss^{-1}) and is in disagreement with the more significant Durham results, the validity of the result remains in some doubt.

5.7.7) Recent observations of Centaurus X-3 from Narrabri

A further 46 good weather observations of Cen X-3 were made with the Mark III telescope between 1989 and 1991. All the data were subjected to hardware selection and a pulse integral selection at the optimal 30% level determined above[1]. In none of the observations, including five in the phase band 0.02 to 0.07 is there any evidence of periodicity at the period of 4.823 s. This is unlikely to be due to a shift in the rotation period of the pulsar, as the search period ranges were widened in the analysis to allow for this. The lack of a detectable flux in the 1989 - 1991 data may, however, be due to variations in the source luminosity. It is not known whether Cen X-3 was in a low or high state during the months of the observations.

Five of the six observations made with the Mark IV telescope were made simultaneously with Mark III observations, but the data were analysed separately, because those from the Mark IV telescope were not suitable for pulse integral event selection. Only one of the observations (19th February, 1991) was made when the neutron star was

---

[1] Data taken with the new guard ring offset of 1.5° will necessitate a re-evaluation of the optimum threshold.

near the ascending node of its orbit. There is no evidence for periodicity in this or any other of the Mark IV datasets.

5.8) Application of pulse integral event selection to other data

A number of radio and X-ray pulsars have been conclusively or tentatively detected with the Mark III telescope. These include the X-ray binaries LMC X-4 and SMC X-1, the millisecond radio pulsar PSR 1855+09 and the Galactic Bulge source GX 339-4 (Brazier et al, 1990d, Bowden et al, 1990). Pulse integral selection was applied to data on each of these in turn. The data were tested in each case after event selection at five thresholds, to determine whether the optimum threshold varied between objects or zenith angles. The percentage threshold was then fixed for all future observations of these objects.

5.8.1) LMC X-4

LMC X-4 is a massive X-ray binary located in the Large Magellanic Cloud. It contains a pulsar of spin period 13.5 s (Kelley et al, 1983b) and has an orbital period of 1.4 days (Chevalier and Ilovaisky, 1977). It was observed with the Mark III telescope in November 1986 and January-February 1987. Early data taken in November 1986 could not be enhanced, because no off-axis data were available, but the remaining dataset from 1987 included 7 observations with off-axis records. A γ-ray signal was observed at the 13.5 s pulsar period in the three of these observations taken near the maximum of the 1.4 day X-ray cycle

(Chadwick, 1987, Brazier et al, 1990d). The probability of the periodicity arising by chance was 8.5×10^{-5}.

The pulse integral enhancement technique was applied to the three datasets which showed a γ-ray signal. A range of five thresholds from 50% to 25% were applied to the data, with the results tabulated in Table 5.5. At a threshold of 45%, the Rayleigh probability minimised, with a factor of 4 reduction in probability over the original result. Although not significant after the five trial cuts, this is an improvement on the original result, and in addition, the optimal percentage derived from these data can now be routinely applied to further data on this object.

5.8.2) SMC X-1

SMC X-1 is another extra-galactic X-ray binary. It has a pulsar period of 0.71 s, spinning up steadily via accretion from the companion. Although its large distance (50 kpc) makes it appear not unusually bright, it is the one of the most intrinsically luminous stellar X-ray sources known.

An extensive series of observations of this object has been made with the Mark III telescope. Some of the longest observations were made in July 1987. The data of three of these (23^{rd}, 29^{th} and 31^{st}) show periodicity at the pulsar period. These three datasets were subjected to selections with a range of thresholds, with the results tabulated in Table 5.6. As with Cen X-3, there is an improvement in the Rayleigh probability, in this case by a factor of 14. The significant enrichment gained is of additional importance in the detection of this variable and distant source.

Selection		No. events	Prob.	R (%)
1		13527	6.6×10^{-5}	2.6
2		8577	1.4×10^{-4}	3.2
3	50%	6838	3.8×10^{-5}	3.8
	45%	6039	3.5×10^{-5}	4.1
	40%	5337	9.2×10^{-5}	4.2
	35%	4179	4.5×10^{-3}	3.6
	30%	3131	3.0×10^{-2}	3.4
	25%	2060	1.9×10^{-1}	2.8

Table 5.5

The effects of hardware and pulse integral selections on data on LMC X-4. The observations were made on 26/01/87, 29/01/87 and 02/02/87 and show periodicity at the pulsar spin period. There is a maximum enhancement of the signal at a pulse integral cut of 45%. The event selections are:

(1) All events which have exceeded the hardware threshold in the centre channel, regardless of the guard ring responses.

(2) Events which have exceeded the hardware threshold only in the centre channel.

(3) Events which are in (2) and also have no guard ring pulse integral above the shown percentage of the central one.

Selection		No. events	Prob.	R (%)
1		23528	6.2×10^{-5}	2.2
2		14711	2.1×10^{-5}	3.1
3	50%	11488	2.5×10^{-6}	3.6
	45%	10659	1.9×10^{-6}	3.8
	40%	9952	1.5×10^{-6}	3.9
	35%	8747	2.1×10^{-6}	4.3
	30%	7508	4.9×10^{-6}	4.5
	25%	5918	4.4×10^{-5}	4.6

Table 5.6

The effects of hardware and pulse integral selections on data on SMC X-1. A subset of the substantial dataset on SMC X-1 was subjected to a range of pulse integral cuts. The optimum percentage cut occurs at 40%. As in Table 5.6, the event selections are:

(1) All events which have exceeded the hardware threshold in the centre channel, regardless of the guard ring responses.

(2) Events which have exceeded the hardware threshold only in the centre channel.

(3) Events which are in (2) and also have no guard ring pulse integral above the shown percentage of the central one.

5.8.3) PSR 1855+09

Unlike the majority of VHE γ-ray sources, PSR 1855+09 is a non-accreting radio pulsar. It is a 5.4 ms binary pulsar with a low mass companion, situated ~ 400 pc from the Solar System. It has been observed from Narrabri from 1987 to 1990. The detailed results of the analysis of the data are presented in Chapter 7. Of the 56 observations of the source made with the Mark III telescope, one showed a very high level of periodicity (Rayleigh probability = 2×10^{-5}). This observation alone was subjected to selections at a range of thresholds, with the results shown in Table 5.7. At a threshold of 45%, the Rayleigh probability drops to a minimum of 2×10^{-6}, even though 46% of the events have been rejected. The optimum cut was subsequently applied without further trials to all data on this source, with the positive results described in Chapter 7.

5.8.4) GX 339-4

GX 339-4 is one of the Galactic bulge sources. It is considered to be in an accreting binary and is a black hole candidate. The inclination is close to zero, so that few orbital effects are observed. In 1987, possible detection in optical data of a 1.13 ms periodicity in this source was reported (Imamura et al, 1987).

GX 339-4 was observed with the Mark III telescope on seven occasions in May 1987. When the hardware-selected data were combined statistically, an effect was found close to the period of Imamura et al, with a chance probability of 3×10^{-3}. It was found that data taken during two observations (29th and 30th May 1987) contributed

Selection		No. events	Prob.	R (%)
1		2724	2.3×10^{-5}	6.2
2		1993	3.1×10^{-5}	7.2
3	50%	1526	3.6×10^{-6}	9.1
	45%	1471	2.0×10^{-6}	9.5
	40%	1323	1.1×10^{-5}	9.1
	35%	1182	2.3×10^{-4}	8.2
	30%	707	3.7×10^{-3}	8.9
	25%	444	8.0×10^{-5}	14.3

Table 5.7

The effects of hardware and pulse integral selections on data on PSR 1855+09. The data come from a single observation made on 11/10/88, which shows very significant periodicity at the pulsar spin period. There is a maximum enhancement of the signal at a cut of 45%. The event selections are:

(1) All events which have exceeded the hardware threshold in the centre channel, regardless of the guard ring responses.

(2) Events which have exceeded the hardware threshold only in the centre channel.

(3) Events which are in (2) and also have no guard ring pulse integral above the shown percentage of the central one.

particularly strongly to this effect. These two datasets were subjected to the enhancement technique.

The results of periodicity tests after pulse integral selections are shown in Table 5.8. Unlike the success seen in the four sources previously tested, there is no enhancement of the signal. The magnitude of the Rayleigh vector remains approximately constant throughout the series of cuts, as would be expected for a random or unfavourable selection of events. If the selection is an efficient enhancer of γ-ray signals, as the results on the previous objects imply, then the decline in the Rayleigh probability is indicative of a periodicity which has arisen by chance in the original dataset, and the effect may be rejected as spurious. Interestingly, the 1.13 ms period was not detected in later optical observations of GX 339-4, and an alternative period of 190 s was put forward (Steiman-Cameron et al, 1990). The rejection of the 1.13 ms periodicity in VHE data on this object demonstrates that selection on the basis of relative pulse integrals is as effective in rejecting spurious effects as it is in enhancing genuine ones.

5.9) Identification of lightning-induced events

In summer months, temperatures near the Narrabri site can exceed 40° C. In these high temperatures, it is common for thunderstorms to develop. Although night-time storms very rarely occur at the site, distant storms are sometimes seen on the horizon. The Mark III telescope is optically sensitive to these storms if the lightning can be seen by the photomultiplier tubes, either directly or by reflection in

Selection		No. events	Prob.	R(%)
1		35853	9.1×10^{-4}	1.5
2		19878	1.6×10^{-5}	2.4
3	50%	15959	3.3×10^{-4}	2.5
	45%	15093	1.2×10^{-4}	2.7
	40%	14393	1.2×10^{-4}	2.6
	35%	13132	2.5×10^{-3}	2.5
	30%	11700	6.7×10^{-3}	2.4
	25%	9901	6.7×10^{-3}	2.6

Table 5.8

The effects of hardware and pulse integral selections on data on GX339-4 taken on 29/05/87 and 30/05/87. There is no enhancement of the candidate signal with any pulse integral cut. The event selections are:

(1) All events which have exceeded the hardware threshold in the centre channel, regardless of the guard ring responses.

(2) Events which have exceeded the hardware threshold only in the centre channel.

(3) Events which are in (2) and also have no guard ring pulse integral above the shown percentage of the central one.

the telescope mirrors. Direct illumination is greatly reduced by hexagonal canvas covers spread across the mirror backs. By the nature of the telescope, reflection of lightning in the mirrors cannot be prevented, but is a lesser problem. The telescope is sensitive to distant, faint lightning only when it is observing a source low on the sky (zenith angle $> \sim 30^{o}$). Since observations are generally made near the time of culmination of an object, the telescope is only affected by storms to the north or south of the site. The major sites for storms in these directions are the nearby Mount Kaputar range to the north, and the Warrumbungles mountains, which lie approximately 100 km to the south.

As mentioned in Chapter 3 (section 3.5.2), lightning produces bursts of spurious events in the data. Although lightning need not always affect periodic analysis of the data, a burst may cause a peak in a light curve at any period much greater than its duration. The false events also make the data unsuitable for tests of unpulsed emission and γ-ray bursts. Lightning bursts must be removed before analysis of affected data. If there is any doubt about the quality of the data, it will not be analysed.

The pulse integrals reveal how faint lightning is seen by the telescope. Figure 5.14 shows a list of events from data taken at a time when distant lightning was noted by the observers. The two lightning-induced events are recognised by their pulse integrals, which have saturated in one *dish*. Such saturation may occur in any of the three dishes and is probably the geometric effect of a particular detector package's being exposed to the lightning. This pattern of PMT responses bears no similarity to the normal, channel dependent Cerenkov events.

```
 96752.851791 C_____
 25   3   5   7   7   0   5
 21   5   5   8   5   1   1
 10  12   9   7   8   3   5

 96753.943940 C123456
 31  12  27  55   8   3   3
 15  25  23  77   4   1   0
255 255 255 255 255 255 255      <—

 96756.298847 C_____
 35   5   5   9   6   0   7
 28   8   6   5   8   5   4
 25  11   9   4  12   4   5

 96757.318765 C_____
 41   1   8   5   7   2   5
 29   5  15  10   8   7   2
 31   6  14   9  10   5  11

 96757.570411 C_____
 28   2   6   6   6   7   9
 31   6   8   7   5   5   3
 23   4  11   7   6   3   6

 96758.114779 C123456
 10   7   7   0   6   1   4
255 185 255 255 213 255 255      <—
  5   7  15  10   6   5   4


      Time (s),  Fire Pattern
QT's: Left dish   (tubes C - 6)
      Centre dish (tubes C - 6)
      Right dish  (tubes C - 6)
```

Figure 5.14

A few events from a dataset taken during a distant electrical storm. The selection shows two events induced by the lightning (arrowed). The difference between these dish-dependent events and the channel-dependent events characteristic of Cerenkov events is obvious.

Although the two events shown would be rejected by the hardware discrimination system, this is not always the case. As some light may also be seen by the other dishes, the hardware discrimination system will register a random fire pattern, including single channel events, and will not be effective in rejecting such events.

Using the pulse integrals, it is simple to filter the data to reject any large events which are dish rather than channel dependent. This can be done specifically or by use of the standard percentile cuts described above. Clearly, the integrals near saturation will dominate in any channel, and a series of very similar averaged integrals will result. The on-/off-source ratio will therefore be close to unity, and the event will be rejected.

The efficiency of lightning rejection has been investigated using data taken in January 1991. Centaurus X-3 was observed in the early evening in this month and distant lightning was observed towards the south during one observation (19^{th}). An inspection of the events shows that the data include some lightning-induced events (Figure 5.14). This dataset is used here to test the efficiency of lightning rejection.

If the data conformed to a Poissonian series of times, then (for one sample per Fourier interval) the distribution of Rayleigh probabilities should be of inverse exponential form. If there is significant periodicity in the data, then the distribution of probabilities will depart from the expected form. Testing for non-statistical behaviour over a wide range of periods can thus be used to observe the effects of lightning.

The data were tested for periodicity over a series of period ranges spanning periods from 10 ms to 90 s. Three subsections of the data were

tested. Figure 5.15 shows the periodograms for all data which has exceeded the hardware threshold in the centre channel. This dataset includes a total of 8543 events. The effects of lightning are seen over a wide range of periods: it is evident that although no single period is outstanding, there is a high level of non-statistical periodicity over all ranges down to a period of 25 ms. Figure 5.16 shows the corresponding periodograms for the 4563 events which have been accepted by the hardware cut as on-axis events. The same excess of small probabilities can be seen. In both cases, the deviation appears as an excess of probabilities $\sim 10^{-1} - 10^{-2}$. In a limited period search, the non-random peaks would be hard to identify.

In Figure 5.17 are shown the same periodograms again, but for data which has been subjected to the 30% selection threshold, which is standard for this object. Under this cut, an a fairly low fraction (27%) of the events in Figure 5.15 has been retained, none of which have the characteristic form illustrated in Figure 5.14. Most reduced data files contain around 30% of the original events. It can be seen that the reduced dataset now behaves as a random Poissonian dataset in all period ranges. This implies that all the dish-dependent events have been removed by the cut. It can therefore be assumed that they are indeed spurious, and that an insignificant number of events (if any) which do not have these unusual characteristics are induced by lightning. The data can now be analysed with caution.

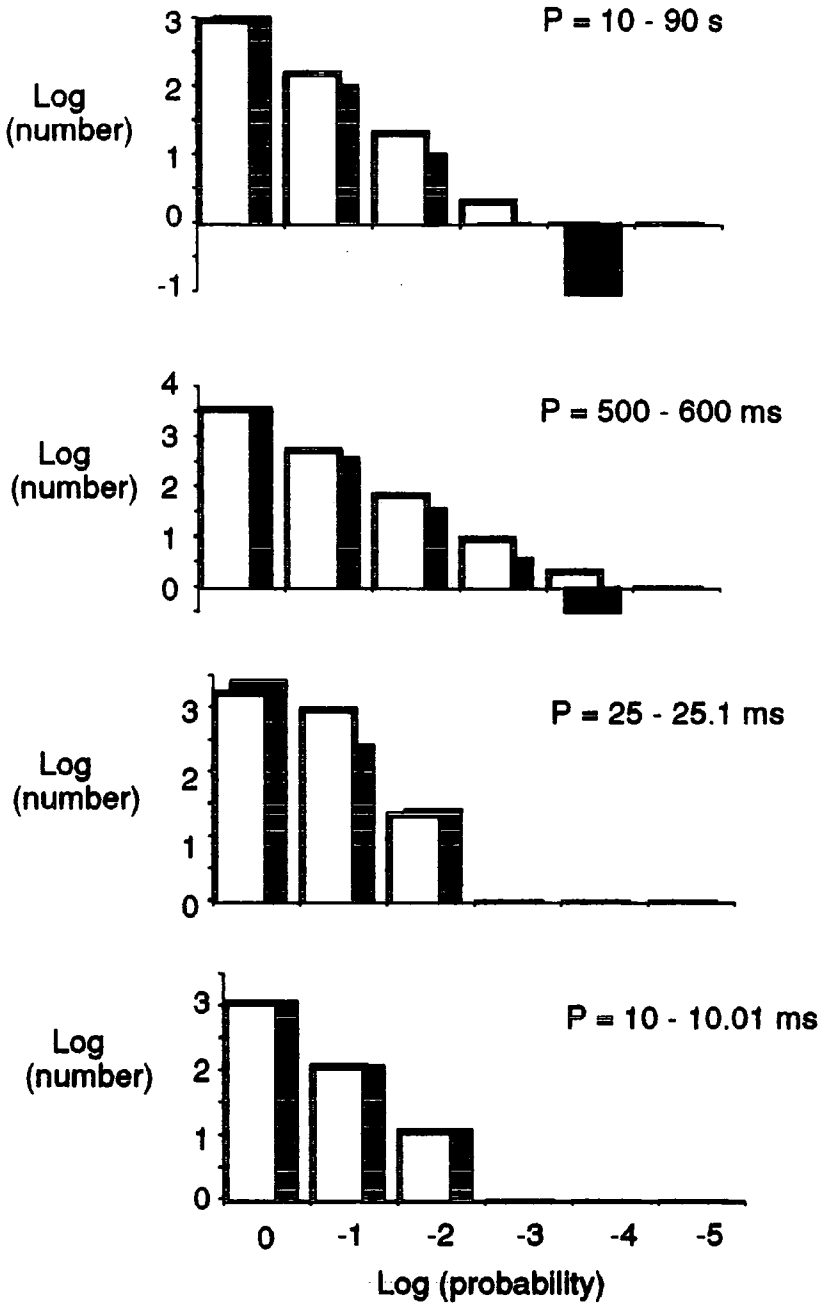

Figure 5.15

The distributions of Rayleigh probabilities for a series of period ranges for all centre channel data taken on Cen X-3 on 19th January 1991. The expected frequencies of occurence are shown in black; observed frequencies are in white. Expected abundances of less than 1 are shown only where that probability did occur.

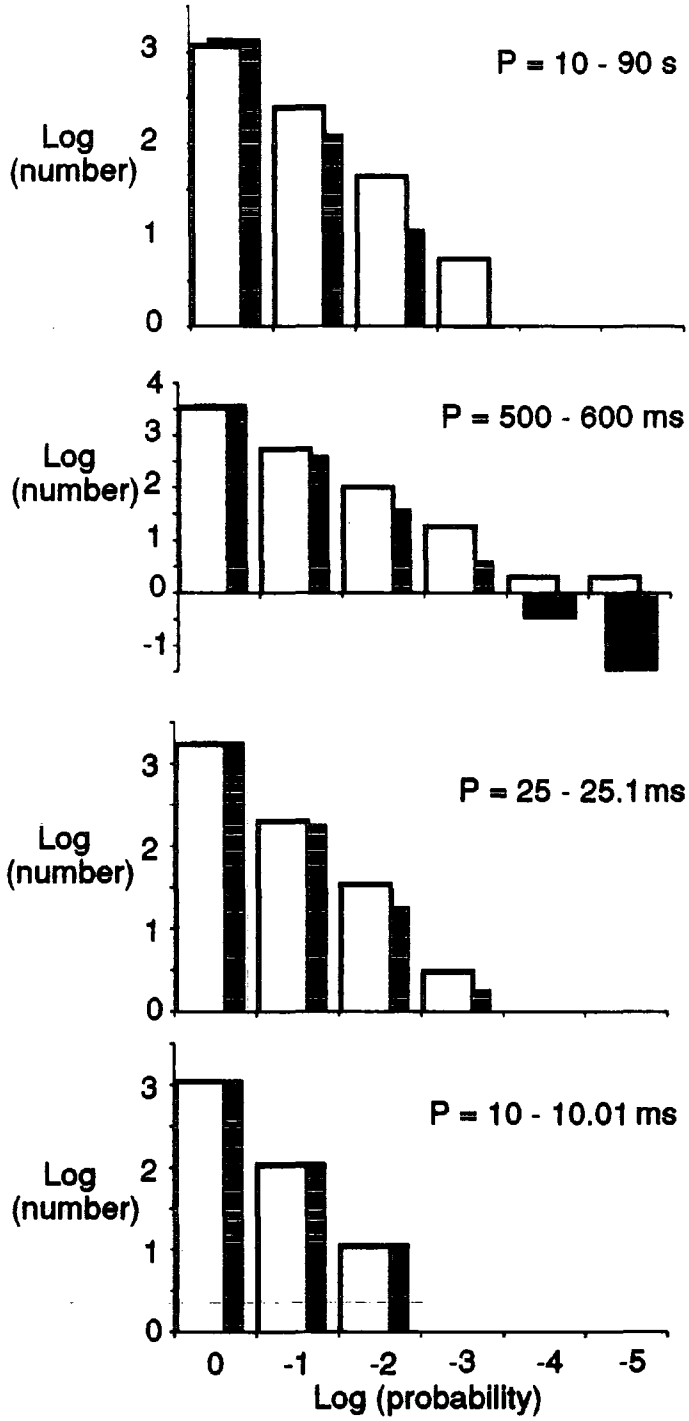

Figure 5.16

The distributions of Rayleigh probabilities for a series of period ranges. The data are the subset of the data used in Figure 5.15 which includes only events which do not exceed the hardware threshold in any guard ring channel. The expected and observed frequencies are distinguished as in Figure 5.15.

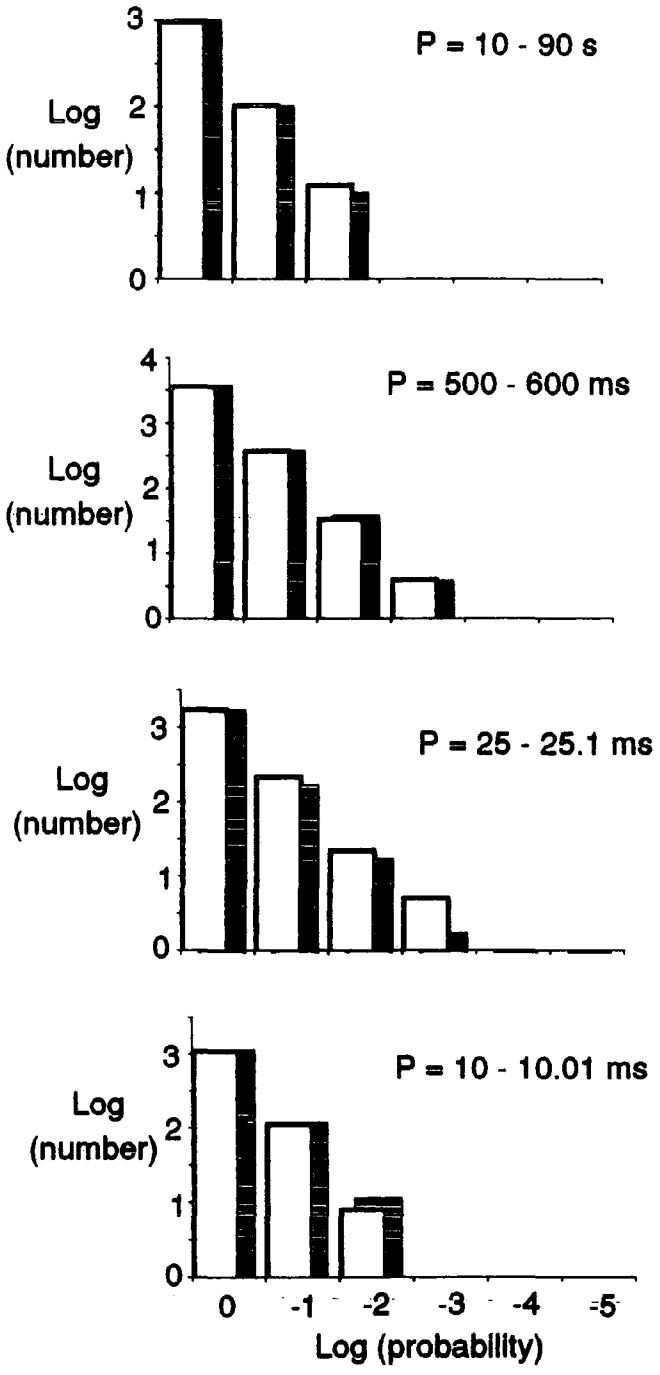

Figure 5.17

The distributions of Rayleigh probabilities at a series of test periods for data which has been accepted by both the hardware discrimination system and a 30% QT cut. The expected and observed frequencies are distinguished as in Figure 5.15.

5.10) Conclusions

Rejection of background cosmic rays by their arrival direction is a tested and efficient method of maximising the source component in a TeV Cerenkov dataset. A simple form of this is provided by the hardware discrimination installed in the Durham Mark III and Mark IV telescopes. Careful design of the telescopes' geometry has ensured that the hardware discrimination is efficient, but an inevitable bias towards accepting small off-axis showers remains. The pulse integrals have been shown to contain much valuable information concerning the direction of incidence of incoming showers. This further information has been used to extend the hardware discrimination system, removing a bias towards small Cerenkov flashes. Taking the simple case in which the Cerenkov light must be biassed towards the direction of the source by more than a certain fraction, it has been shown that a considerable and reproducible enrichment of a signal may be achieved over the standard discrimination system. The enhancement technique is particularly useful in removing the selection bias towards small showers present in the standard selection, and leads to the rejection of half of the hardware-selected events, with very little loss of the signal strength. Enhancement of signals has been shown in data on LMC X-4, SMC X-1, PSR 1855+09 and Cen X-3, each of which exhibits the behaviour expected for an effective selection and for a signal from the target source. In addition, pulse integral selection has been used to reject a spurious signal in data on GX 339-4. The optimum percentage threshold is not the same for all sources, and may be a function of the zenith angle of observation (optimum threshold ~ zenith angle). This is probably a real effect, but

in the absence of a strong, constant source, such dependences cannot be tested.

Despite the simplicity of the technique, directional discrimination is remarkably powerful. The discrimination is achieved via a superposition of the narrow telescope aperture, the hardware threshold and the relative response selection process. The enrichment of the data by this combination is put into context when it is compared with results from another technique. Given the narrow aperture of the Durham telescopes (1°) relative to that of e.g. the Whipple imaging telescope (~3°), the relative size of the enhanced Durham datasets are comparable to those obtained by the Whipple collaboration using the much more intricate imaging technique. The pulse integral selection technique is used routinely on all data taken with the Mark III telescope.

In addition, it has been demonstrated that the pulse integrals can be used to identify and remove spurious events caused by distant lightning. The technique should release for periodic analysis most data affected by faint lightning.

It is hoped that the quality of the Mark IV digitisation electronics will be improved, so that the benefits of further enhancement of the dataset will then be gained by this telescope. The recording of pulse integrals in future telescopes is obviously of paramount importance. The efficiency of both the hardware and relative response selections will also be improved in chopped observations, when a new detector package is introduced. The new design will incorporate three extra channels, so that both on-source chopping channels have a full guard ring.

CHAPTER 6

Pulsed TeV γ-rays from millisecond and binary pulsars

6.1) Introduction

Until recent years, the population of known pulsars had a lower period limit in the tens of milliseconds region, a limit artificially introduced to restrict computing times when searching data for unknown periods. This has changed in the last ten years with the use of supercomputers and the discovery of a new class of very fast pulsars. The new pulsars are characterised by rotation periods of only a few milliseconds, extreme rotational stability and unusually low derived magnetic field strengths of the order of 10^8 G, several orders of magnitude lower than the strengths observed in other pulsars. They do not seem to be merely the tail of the main population, but form a separate class. The concept that they are intrinsically different from canonical pulsars is lent support in that the majority of these 'millisecond pulsars', in contrast with nearly all other known pulsars, are in binary systems. It is this last characteristic which has provided the basis for models which explain the origin of these stars.

In this chapter, we will review some of the progress made on understanding how the millisecond pulsars have evolved, and will summarise two current theories describing the high energy emission from pulsars. Finally, we shall consider the implications for TeV observations of millisecond and binary pulsars. A detailed description

of the whole field of pulsar astronomy, especially in the radio region, is beyond the scope of this work. The reader is referred to the work of Lyne and Graham-Smith (1990) for an excellent review.

6.2) Evolutionary scenarios

It is generally believed that millisecond pulsars were once slower pulsars or white dwarves, which have been 'recycled' in binary systems via mass accretion from a companion. X-ray experiments have observed many accreting binaries, in which the accretion powers strong emission from the locality of the neutron star. The angular momentum gained by the neutron star in this manner can be sufficient to spin a pulsar to millisecond rates. Mass transfer can occur either through a stellar wind, or, more commonly, by Roche lobe overflow.

It is assumed in evolutionary scenarios that the millisecond pulsar was originally the more massive member of a binary system and evolved first to form a main population, relatively slow pulsar or a rotating, magnetised white dwarf. The evolution of the binary once the primary has evolved then depends mainly on the mass of the companion star.

6.2.1) High mass binaries

In a high mass system ($M_c > 3M_\odot$), the companion can evolve much as a solitary star until the onset of mass transfer to the neutron star. In the giant stage of its evolution, the star will shed its outer material. The star may overflow its Roche lobe or/and develop a strong

stellar wind which cocoons the system. Both of these will cause a transfer of matter onto the pulsar. Frictional drag causes a marked decrease in the separation of the two stars. If the star is sufficiently massive, it will eventually undergo a supernova explosion and form a neutron star. If a large fraction of the total mass of the system is lost in the supernova, the binary will be disrupted, ejecting the now solitary, fast pulsar at a high velocity. If not, a pair of neutron stars in a highly elliptical orbit is likely to result. PSR 1913+16, a binary pulsar with a neutron star companion, has an extremely high orbital eccentricity of 0.6. The recently discovered 38 ms pulsar, PSR 1534+12, is in a similar system and has an orbital eccentricity of 0.27 (Wolszczan, 1991). The two systems may well be examples of binaries which have undergone this evolution.

If the companion star is of intermediate mass (M_c ~ 5 - 8 M_x), no supernova occurs. The remnant in this case will be a neutron star orbiting the evolved core of the companion in a tight, circular binary system with an orbital period as short as a few hours.

6.2.2) Low mass binaries

Low mass binaries are more common than high mass ones. The companion mass is less than around 1 $M_\odot$ in this second class of systems and mass transfer occurs via Roche lobe overflow. The mass and the angular momentum of the system are conserved, and the orbit tends to circularise and widen. The companion star is insufficiently massive to form a supernova, and eventually leaves only its degenerate helium core as a helium white dwarf (van den Heuvel and Taam, 1984). PSR 1953+29,

which has a highly circular orbit ($e = 3.3 \times 10^{-4}$) and a low mass ($M_c \sim 0.3\ M_\odot$) companion, is likely to have followed this path.

The evolution of millisecond pulsars has been a matter of discussion for some years, as, if the precursors were also neutron stars, then the estimated population of millisecond pulsars would appear to require a population of low mass X-ray binaries significantly higher than observed. However, if most millisecond pulsars were instead formed directly in the accretion-induced collapse of rapidly spinning white dwarf stars, then the population of low mass X-ray binaries is no longer a problem (Ruderman, 1991). It should also be noted, however, that it has been suggested that the supposed deficiency of low mass X-ray binaries is not real (Ruderman et al, 1989, Tavani, 1991a, 1991b).

The history of a pulsar should also explain its present magnetic field. Most millisecond pulsars have been found to have magnetic fields strengths of around 10^7 G. The very small values can be explained in general terms by the decay of the magnetic field with time, either for a neutron star or white dwarf precursor, but the close similarities between the observed pulsars has prompted some interest. The evolution of pulsar magnetic fields remains an open issue.

6.3) Pulsar emission

6.3.1) Introduction

As we have already seen in Chapter 1, a solitary pulsar is powered by the rotation and the magnetic field of a neutron star. The apparently pulsed nature of the emission does not arise from a true

pulse, but is the intersection of a lighthouse-like, rotating beam with the Earth. This much is certain. In the 20 years since their discovery, a wealth of data on pulsars has been collected at many different wavelengths, and much effort has been devoted to understanding exactly how they accelerate particles to very high energies and how the pulsar beams are formed.

6.3.2) General observations

An upper limit to the luminosity of a rotation-powered pulsar is derived from its rate of loss of rotational energy,

$$\dot{E} = I\omega\dot{\omega} \qquad - 6.1$$

where I is the moment of inertia of the neutron star ($\sim 3 \times 10^{45}$ gcm^2) and ω is its angular rotational frequency. Both ω and $d\omega/dt$ are observable and so dE/dt is easily calculated from pulse timing data. Typically, dE/dt $\sim 10^{32} - 10^{36}$ ergs s^{-1} for an isolated pulsar. Note that for accreting pulsars, $dE/dt \neq I\omega(d\omega/dt)$ because the emission is powered by accretion, not by the pulsar's rotation. In this case, the radiated power may be very much greater than that available to an isolated pulsar. For instance, the X-ray luminosity of some accreting binary pulsars is as much as 10^{39} ergs s^{-1}.

The fraction of the total power which is radiated as high energy photons is less simply derived. Details of the particle acceleration and photon production mechanisms taking place in isolated pulsars have been described in two theories, each taking one part of the

magnetosphere as the acceleration region. These are the 'outer gap' and 'polar gap' models, which will be discussed below.

Before the emission from pulsars is discussed, it is necessary to know something of their structure. A pulsar is not merely the central neutron star, but the volume immediately surrounding it. This volume takes the form of a plasma-filled cylinder, in which magnetic forces are predominant. This is known as the magnetosphere. The magnetosphere corotates with the neutron star out to a radius at which the corotation velocity of a particle would approach the velocity of light. This radius defines the velocity of light cylinder. It is within this that all 'pulsed' emission originates.

6.3.3) Deductions from radio observations

Isolated pulsars are almost always discovered by their radio emission. Around 500 radio pulsars are now known. There is a main population of pulsars with periods ranging from a few tens of milliseconds to several seconds and magnetic fields of the order of 10^{12} G, and a smaller population of pulsars with magnetic fields of only ~ 10^{8} G and rotation periods of just a few milliseconds. This latter class is the subject of Chapter 7.

Some of the most influential information for the development of pulsar theory has come from observations of pulse polarisation. It is found that the pulsed radio radiation is highly linearly polarised. Some pulsars also show a high level of circular polarisation. The position angle of the linear polarisation is observed to vary smoothly across the pulse, typically in an 'S' shape. The explanation was first

proposed by Radhakrishnan and Cooke (1969).

If particles are accelerated near the polar cap, then the strong magnetic field there will constrain their motion to be along the open magnetic field lines. As they follow the diverging, curved field lines, the particles will emit curvature radiation at radio wavelengths. Curvature radiation is linearly polarised parallel to the projected magnetic field. The observed radio polarisation curves therefore merely reflect the projected geometry of the magnetic field lines near the polar cap. Together with the pulse spectrum in the radio region, this observation has led to the conclusion that the radio emission must come from near to the polar cap of the neutron star (Lyne and Graham-Smith, 1990, Srinivasan, 1989).

The above has been refined by Ruderman and Sutherland (1975), who considered a neutron star in which the spin and magnetic axes were antiparallel. This configuration is thought to give a pulsar; an opposite alignment may give another type of object. They pointed out that the binding energy on the neutron star surface is too high for positive ions to be pulled out by the electric field. The outflow of negative particles from the pole, however, causes a charge-depleted gap to form above the pole, across which will be a potential difference of $\geq 10^{12}$ V. A charged particle in the gap will experience strong acceleration and will emit high energy γ-rays via curvature radiation. These in turn will be unstable against pair production in the magnetic field, and so on. The positrons will move out of the gap and away along the open field lines. They cannot accelerate outside the gap, but do give rise to further photons. Subsequent electron-positron pairs are now the source of the radio emission, via curvature radiation in the

lower field further away from the pole. The electrons will return to the stellar surface and replenish the lost negative charges. The gap will discharge in this manner every few microseconds.

6.4) VHE γ-ray emission from millisecond pulsars

6.4.1) The polar gap model

The polar gap model of high energy emission is a direct extension of the radio model outlined above. The gap discharge cascade continues until the curvature photons have energies low enough to allow them to escape from the magnetosphere without interaction. The energy radiated in the form of high energy γ-rays as a result of this process has been calculated by Usov (1983). The argument is as follows.

Consider a positron created near the lower surface of the polar gap. In travelling to the upper surface, it is accelerated to an energy of ~ eEH, where E is the component of the electric field parallel to the magnetic field and H is the height of the gap, given by (Ruderman and Sutherland, 1975)

$$H \approx 1.7 \times 10^4 \ (p/B_p)^{4/7} \qquad - \ 6.2$$

Here p is in seconds and B_p is in units of 10^{12} G. This energy corresponds to a Lorentz factor

$$\gamma = \frac{eEH}{mc^2} = \frac{2\Pi eH^2 B_p}{pmc^3} \qquad - \ 6.3$$

with $E = 2\Pi HB_p/pc$. In following the diverging field lines, the

particle radiates curvature photons, which can escape from the magnetosphere without pair production if they have less than a critical energy E_c,

$$E_c = 10^{10} B_p^{-1} r^2 p \text{ eV} \quad - 6.4$$

where r is the distance from the centre of the star to the region of photon emission, in units of 10^6 cm.

If they exceed E_c, they will be absorbed in the magnetosphere via pair production. The pair will be accelerated in the gap, giving out more curvature radiation, and the process repeats in an electromagnetic cascade. The cascade propagates until the photon energies are small enough for them to escape. The emergent curvature radiation is therefore concentrated close to E_c.

The γ-ray luminosity from the polar gap region is estimated to be (Usov, 1983, Cheng and de Jager, 1990)

$$L \approx 8.5 \times 10^{11} \; p^2/\gamma B_p \quad - 6.5$$

which reduces to

$$L \approx 1.6 \times 10^{20} \; B_p^{6/7} p^{-13/7} \text{ erg s}^{-1} \quad - 6.6$$

In fact, the height of the gap may be smaller than indicated by equation 6.2, so that the Lorentz factor γ of accelerated particles is reduced. The smaller energy means that the number of cascade particles above E_c diminishes. The minimum height is determined by the conditions required for radio emission. In order for a neutron star to be a radio pulsar, there must be electron-positron pairs in the magnetosphere. Their generation by pair production requires that at the stellar surface

(where the magnetic field is greatest), particles will give off curvature photons above the critical energy. These photons are then absorbed and generate the electron-positron pairs required. Since the maximum energy for the curvature photons is

$$E_{max} = \frac{3hc\gamma^3}{4\pi R_c} \qquad - \ 6.7$$

where R_c is the radius of curvature of the field lines, we can use (6.4) and (6.7) to derive a minimum Lorentz factor, γ_{min}. γ_{min} is found in practice to be approximately an order of magnitude lower than the factor derived in (6.3), with a slow dependence on B_p and p. This leads to a minimum gamma ray luminosity approximately an order of magnitude below the maximum.

The beam of radiation will sweep a fraction $(\omega R/c)^{1/2} \approx (2 \times 10^{-4} p^{-1})^{1/2}$ of the sky. Because the beam width is proportional to $p^{-1/2}$, the probability of observing both poles, i.e. both pulse and interpulse, is very high for short period pulsars. This is, of course, dependent on the inclination of the magnetic axis with respect to the spin axis. A nearly aligned pulsar will be expected to show only a single pulse, whereas one rotating with the two axes orthogonal will be seen twice per revolution. In general, we would expect the similar emission regions for radio and TeV photons to make the light curves broadly similar.

Although the model therefore does not predict any very high energy radiation for main population pulsars, it is easily calculated that the low magnetic fields and fast rotation of the millisecond pulsars

conspire to make this mechanism highly efficient in them.

It would be difficult to reject the polar gap acceleration model completely. However, it does suffer from one potentially catastrophic flaw. The electrons and associated cascade particles created and accelerated in the polar gap will return to the pole and heat the stellar surface. It may be expected, therefore, that there would be an intense X-ray luminosity from this region (Cheng and de Jager, 1990). No X-ray fluxes have been detected from pulsars other than the Crab and Vela pulsars, but both of these are very young and are clearly not representative of the main body of pulsars, much less of the millisecond pulsars. A second theory of high energy pulsar radiation has emerged which does not suffer from this problem. This is the semi-empirical 'outer gap' model of Cheng, Ho and Ruderman (1986a, 1986b).

6.4.2) The outer gap model

As well as above the polar gap, charge depleted regions occur near the velocity of light cylinder, on the outside of the last open field lines. In the outer gap model, these are the source of high energy photons. The location of the gaps is shown in Figure 6.1. Through these 'outer gaps' pass streams of both charged particles and photons, well aligned with the magnetic field lines. If a high energy photon interacts in the gap with a lower energy photon or with the magnetic field, an electron-positron pair is created. The two charges are accelerated along the length of the gap and radiate γ-rays by curvature radiation or by inverse Compton interactions with infrared photons. Other charged particles passing through the gap are also accelerated.

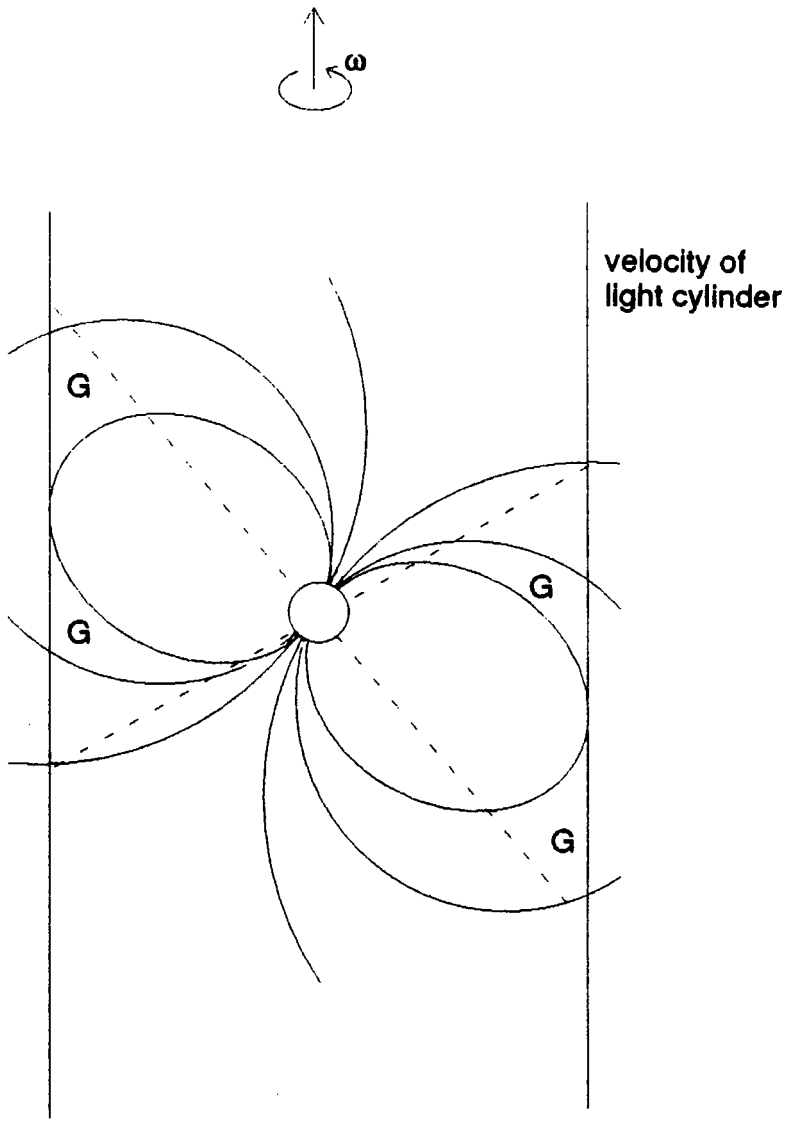

Figure 6.1

A model pulsar magnetosphere. The null surfaces which separate like charges (dashed lines) and the positions of the outer magnetospheric gaps (G) are indicated. (After Cheng, Ho and Ruderman, 1986a.)

Since the gap is large enough for charges to reach energies near to the accelerating potential of more than 10^{12} V, the emergent γ-rays are of correspondingly high energies of up to Tera electron volts (Cheng, Ho and Ruderman, 1986a).

This model has been highly successful in explaining the emission seen from young pulsars, such as the Crab and Vela pulsars. Cheng and de Jager (1990) have recently extended its predictions to cover the millisecond pulsars, whose magnetic fields are several orders of magnitude lower than those of the main population. The criterion for the existence of stable outer gaps is $B_p/p^2 > 10^{13}$ Gs^{-2}. The millisecond pulsars just satisfy this criterion (see Table 6.1). According to their values of B_p and p, Cheng and de Jager have classified six millisecond pulsars with well-measured parameters as 'Vela-like' or 'post-Vela-like'. The most distinctive difference between the two types of pulsar is that Vela-like pulsars are poor emitters of TeV gamma rays, whereas post-Vela-like ones are extremely efficient. Post-Vela-like pulsars will have outer gaps filling nearly the whole of the open magnetosphere and will emit up to half of their radiation in the form of a fan-like beam of TeV gamma rays. Vela-like pulsars, on the other hand, will have a TeV luminosity of less than about 8×10^{-4} of the spin down power.

The final predictions of luminosity rest on a free parameter $\Delta\Phi/\beta$, where $\Delta\Phi$ is the solid angle of radiation and β is the duty cycle of the pulse. $\Delta\Phi/\beta$ can be varied by an order of magnitude, leading to minimum luminosity estimates roughly one tenth of the upper limits quoted above. The freedom in this parameter makes it difficult to make comparisons between observed and expected fluxes in an attempt to discriminate

between the two postulated models (see Chapter 6).

In principle, there may be four outer gaps, as in figure 6.1, but it seems likely that the longer, and therefore more powerful gaps will produce sufficient γ-rays and electron-positron pairs to quench the shorter ones. Because they are short, the latter produce well-collimated γ-ray beams and can only be seen from positions nearly perpendicular to the spin axis of the pulsar. The chance of observing four pulses per revolution is very small (Cheng, Ho and Ruderman, 1986a). We are left with two gaps, giving two similar, observable pulses, whose observed separation is determined by the position of the emitting region and the inclination towards the observer.

Despite the great success of this model in treating the emission from the Crab and Vela pulsars, its extension to the millisecond pulsars is not necessarily viable. It is not certain, for instance, how the model is affected by the inclination between the magnetic and spin axes. There are also some doubts as to the existence of stable outer gaps in millisecond pulsars with low rates of energy loss.

6.4.3) Emission from binary pulsars

Binary pulsars may be divided into those which are accreting mass from their companions and those which are not. Millisecond pulsars generally fall into the categories of non-accreting or ablating pulsars.

6.4.3.1) Non-accreting systems

In this case, the neutron star and companion are assumed to behave as isolated stars except for their orbital motion. This situation

generally occurs in a late stage of the binary's evolution, when both stars have evolved to form white dwarves or neutron stars. There is unlikely to be an eclipse, and modulation of the γ-ray flux with the orbital period is not expected. Since the pulsar is powered by its rotation and not by accretion, flux estimates may be made on the basis of isolated pulsar models for these systems.

6.4.3.2) Accreting pulsars

Interacting binary pulsars are frequently discovered through their thermal X-ray emission. A substantial fraction of a companion's mass may be lost to the pulsar during a giant stage, by Roche lobe overflow or by the capture of a stellar wind, and this accretion powers a very strong flux of high energy photons. Particles accelerated by an accreting pulsar may give rise to gamma rays in an accretion disc, if one is present, or in a gaseous wake trailing from the pulsar to the companion. The γ-ray visibility of the central pulsar depends on the inclination of the accretion disc and photon-photon cross-sections with ultraviolet photons from the disc.

These systems are dominated by effects associated with accretion and are therefore not similar to isolated pulsars in their emission. Their γ-ray luminosities depend on the accretion geometry and are subject to large fluctuations in both amplitude and perceived period, reflecting the irregular nature of the accretion which powers them. It is therefore very difficult to predict the TeV luminosity expected from these objects.

6.4.3.3) Ablating binaries

A third class of binary pulsar includes those whose high energy emission evaporates matter from their companions. One certain example of this type is known - PSR 1957+20, the 'black widow' pulsar (e.g. Fruchter et al, 1988) - and the recently discovered eclipsing pulsar PSR 1744-24A remains a candidate, although the stellar wind in this system which causes the eclipse may be due to Roche lobe overflow instead of pulsar-induced evaporation (Lyne et al, 1990, Nice et al, 1990). In this class, matter is thought to be ablated from the companion by X-rays, the synchrotron radiation from TeV particles emitted by the pulsar and moving in the pulsar magnetic field (Phinney, 1988). The evaporated matter forms a dense, slow wind and is eventually lost from the binary. A bow shock forms between the stars and will be a source of incoherent gamma rays through first order Fermi acceleration of charged particles (Harding, 1989). Although these pulsars are not accreting, it is unlikely that flux predictions based on isolated pulsar models are valid when the interaction of a pulsar with the evaporated matter and attenuation of the radiated γ-rays in its immediate environment is included. The detection of periodicity in γ-rays will be further hindered by the incoherent element of the flux generated in the shock. For PSR 1957+20, this latter element is predicted to dominate the flux (Harding, 1989).

6.4.4) Predicted TeV fluxes from known millsecond pulsars

There are six millisecond pulsars for which good ephemerides are available. Several others have been discovered, but generally only the

pulse period is known, plus the period of any binary orbit. This information is sufficient for period analysis, but there is often only a poor upper limit to the period derivative, precluding estimates of the magnetic field, and no distance estimate. The lack of these pieces of information precludes theoretical predictions of the flux. Table 6.1 lists the relevant parameters of six millisecond pulsars, together with the limited information available on seven others.

Since they are powered by their rotation and are not accreting, flux estimates for the millisecond pulsars may be made on the basis of isolated pulsar models. These pulsars are the only ones for which two acceleration mechanisms are both plausible. In Table 6.2, we apply the polar and outer gap models to each of the six pulsars with complete ephemerides, and estimate the fluxes expected at the Earth. It will be seen that the two models give different, but not dissimilar fluxes for any given pulsar, with the exception of PSR 1620-26. Note that the fluxes shown are upper limits in both cases. The lower limits are around an order of magnitude smaller. The flux estimated for PSR 1957+20 may not be valid for the whole of its orbit if the radiation is attenuated in the stellar wind of the companion star (see section 6.5.3).

All the fluxes depend critically on the distances estimated from radio dispersion measures, and on assumptions made about the spectrum of the source. For the polar gap estimates (Table 6.2a), we have assumed that all emitted photons have the energy of the spectral peak, E_c. A steep spectrum with an index comparable to the background cosmic ray index of -2.6 (+2.6 below the peak) will not substantially change the values quoted. It is of interest to note that the very powerful source

Pulsar	Period (ms)	Period derivative (ss^{-1})	Polar magnetic field (G)	Distance (kpc)	Comments	Refs
1937+21	1.6	1×10^{-19}	4×10^{8}	5.0	Isolated	1,2
1953+29	6.1	3×10^{-20}	4×10^{8}	2.7	Binary	3,2
1855+09	5.4	2×10^{-20}	3×10^{8}	0.4	Binary	4,2
1957+20	1.6	1×10^{-20}	1×10^{8}	0.8	Binary	5,6
1620-26	11.1	8×10^{-19}	3×10^{9}	2.2	Binary	7,8
1821-24	3.1	2×10^{-18}	2×10^{10}	3.9	Isolated	9,10,11
1516+02A	5.5	?	?	5.8	Isolated	12,19
1516+02B	7.2	?	?	5.8	Isolated	12
0021-72A	4.5	$<1 \times 10^{-15}$	6×10^{10}	?	Binary	13,14
0021-72B	6.1	?	?	?	Binary?	13
0021-72C	5.8	$<1 \times 10^{-17}$	$<7 \times 10^{9}$	4.0	Isolated	15
1257+12	6.2	?	?	<0.5	Binary?	16,17
1744-24A	11.6	$<5 \times 10^{-20}$	$<7 \times 10^{8}$	7.1	Binary	18

References:

1. Backer et al, 1982
2. Rawley et al, 1988
3. Boriakoff et al, 1983
4. Segelstein et al, 1986
5. Fruchter et al, 1988
6. Fruchter et al, 1990
7. Lyne et al, 1988
8. McKenna and Lyne, 1988
9. Lyne et al, 1987
10. Foster et al, 1988
11. Foster and Backer, 1990
12. Wolszczan et al, 1990
13. Ables et al, 1988
14. Ables et al, 1989
15. Manchester et al, 1990
16. Wolszczan, 1990
17. Wolszczan, 1991
18. Lyne et al, 1990
19. Wolszczan, priv. comm.

Table 6.1

Observed parameters of thirteen millisecond pulsars

Pulsar	$\dot{I}\omega\omega$ (10^{33}erg s^{-1})	E_c (GeV)	Luminosity (10^{32}erg s^{-1})	Beaming factor	Dist. (kpc)	Flux at E_c* ((10^2m)$^{-2}$hr^{-1})
1937+21	3100	160	50	1/3	5.0	18
1953+29	15	610	5	1/5	2.7	2.5
1855+09	15	710	4	1/5	0.4	140
1957+20	280	640	10	1/4	0.8	42
1620-26	69	150	6	1/26	2.2	245
1821-24	8000	6	400	1/7	3.9	18790

* In the absence of any spectral information, we have assumed here that the flux is contained entirely at E_c.

Table 6.2a

The polar gap model applied to six millisecond pulsars. Note that the apparently high fluxes for PSR's 1620-26 and 1821-24 will be considerably reduced at energies comparable to those of the other pulsars considered.

Pulsar	B_p/p^2 ($10^{13}Gs^{-2}$)	Type	Luminosity* (10^{32}erg s^{-1})	Distance (kpc)	Flux+ ((10^2m)$^{-2}hr^{-1}$)
1937+21	20	Vela	22	5.0	1
1953+29	1	Post-Vela	75	2.7	8
1855+09	1	Post-Vela	75	0.4	373
1957+20	5	Vela	2.2	0.8	3
1620-26	3	Post-Vela	345	2.2	57
1821-24	21	Vela	56	3.9	3

* From Cheng and de Jager, 1990

+ Assuming all emission is at a nominal threshold of 400 GeV.

Table 6.2b

The outer gap model applied to six millisecond pulsars. Note that all the pulsars satisfy the criterion $B_p/p^2 > 10^{13}Gs^{-2}$ for the existence of outer gaps, but that the case is marginal for PSR's 1953+29 and 1855+09. The derived fluxes are to be compared with those in Table 6.2a.

PSR 1821-24 is unlikely to have a high luminosity in the TeV region, but that all the other pulsars listed will have spectra peaking near the energies covered by most Cerenkov telescopes.

For the flux estimates made using the outer gap model (Table 6.2b), there is no information available on the spectrum of a source. In this case, we have taken a nominal photon energy of 400 GeV. This may introduce a small systematic error, but the induced errors are unlikely to alter the flux estimates by more than a factor of three. Cautious comparisons between the models and with observations are thus possible.

It is clear that at least some of the millisecond pulsars are potentially observable TeV sources. Note especially that if the polar gap model holds for these stars, then the detection of radio pulses indicates that the γ-ray beam will also sweep across the Earth. Beaming considerations are less important in the outer gap mechanism, where the emitted beam is very wide. Since the fluxes are in general similar and flux estimates made using TeV observations are notoriously inaccurate, the implications of the number of pulses observed per revolution become highly significant. The outer gap model predicts two, or possibly four pulses. The polar gap, however, suggests either one or two, depending on the geometry of the source. Thus, the observation of either one or four pulses may help us to determine the location of the accelerating gap region of the magnetosphere and thus to understand better the mechanisms which drive the millisecond pulsars.

CHAPTER 7

TeV observations of Millisecond Pulsars

7.1) Introduction

Millisecond pulsars are of great interest to both theoretical and observational astronomers because of the unusually high fraction of their radiated power which may be emitted as high energy photons. Two mechanisms accounting for the emission have been outlined in Chapter 6. In this chapter, the results obtained from observations of eight millisecond pulsars with periods of less than 15 ms will be presented. Four of the pulsars are Galactic, and the remaining four are in globular clusters. In particular, the analysis of data on binary Galactic millisecond pulsars will be described. The implications of a TeV millisecond pulsar in the multi-wavelength source Cygnus X-3 will be discussed briefly. In a concluding section, the observational results will then be compared with those predicted by the current emission models.

7.2) PSR 1937+21

7.2.1) Background information

The nature of the radio source 4C21.53 was a matter for speculation for some time before timing analysis showed that it contained a

millisecond pulsar, PSR 1937+21. The radio light curve showed a clear pulsar signature, with a pulse and an interpulse separated by close to 180°. PSR 1937+21 was the first millisecond pulsar to be discovered (Backer et al, 1982), and at a period of 1.558 ms, it is still the fastest known pulsar.

Despite its speed of rotation, this pulsar emits no detectable optical or X-ray emission, and this combined with the very slow, steady rate of period decrease force the conclusion that it is not a young pulsar. Instead, it is thought to have been spun up during a period of accretion from a binary companion (Backer et al, 1982). However, unlike many millisecond pulsars, PSR 1937+21 is now solitary. Whether an erstwhile companion was evaporated by high-energy emission from the pulsar or coalesced with the neutron star, or whether the binary was disrupted in some catastrophic event such as a supernova, has not yet been established (Rawley, Taylor and Davis, 1988).

Because of its solitude, extremely precise timing measurements of the pulsar have been possible. The ephemeris from a recent measurement is given in Table 7.1. The measurements (Davis et al, 1985) show that the pulsar has unprecedented timing stability, competing with the most stable clocks available on Earth. The prospect of using pulsars as time standards has raised further general interest in millisecond pulsars, and in PSR 1937+21 in particular.

7.2.2) Early VHE observations and results

Soon after its discovery, it was realised that PSR 1937+21 was a likely source of TeV γ-rays (Usov, 1983, Cheng, Ho and Ruderman, 1985a,

Rotation period (ms)	1.5578064488724(2)
Period derivative (10^{-19} ss^{-1})	1.05110 $\pm$ 0.00008
Pulse epoch (JED)	2445303.2731658

Table 7.1

The pulsar ephemeris for PSR 1937+21, as given in Davis et al, 1985. Later ephemerides (see, for example, Rawley et al, 1988) are fully consistent with the above measurements.

1985b), and observations were begun accordingly. Such a fast pulsar presented a new challenge to the event timing in the Durham telescopes in Dugway, which had been designed for pulsars no faster than the Crab (33 ms). However, PSR 1937+21 was observed with the Mark I telescopes in 1983 and 1984. The small dataset from 1983 was discarded because of timing uncertainties, leaving the larger 1984 dataset for analysis. These data comprised 85 hours of observations, taken in the months of July, August and September of that year. Because of the extreme stability of the pulsar, it was theoretically possible to combine all the data and retain relative pulse phase. By regular synchronisation of the crystal timebase with an off-air radio signal, event timing was also made sufficiently accurate to enable a coherent combination of the data.

The data were combined on two timescales. Firstly, the data within each month were combined in phase, forming three datasets. Each of the combined datasets was tested for periodicity at half the radio period (0.7789032265 ms), with a search range of 4×10^{-8} ms allowed to take into account the timing uncertainties in the data. The data were tested at half the rotation period because a radio interpulse is seen in the pulsar's light curve, and because models of TeV emission suggested a TeV interpulse. Periodicity was detected in each of the individual months, with Rayleigh chance probabilities of $\sim 10^{-2} - 10^{-3}$ (Figure 7.1). It is significant that the periodicity arose at exactly the same period in each independent dataset.

The complete 1984 dataset was then merged and tested for periodicity in the same manner. Within the search range, the minimum Rayleigh probability was found to be 1×10^{-4}, at a period of 0.778903219 ms. The strength of the γ-ray signal was 1% of the cosmic

ray flux, or around 3 x 10^{-11} $cm^{-2}s^{-1}$. (This assumes an integral spectral index of -1.6, but the dependence on spectral index is slow). Assuming also that the distance to the source is 5 kpc, the (isotropic) luminosity of the source above ~ 1 TeV was estimated to be 3 x 10^{35} erg s^{-1}.

7.2.3) Recent observations from Narrabri

Observations of PSR 1937+21 from Narrabri are hindered by the large zenith angles at which it is seen (> 51°). Nevertheless, a pilot study of the pulsar was made for a total of 22 hours, on two nights in July 1990 and on six nights in September of that year. The data were combined in phase within each month and tested for periodicity. The results are shown in Figure 7.1 (after Bowden et al, 1990). The chance probabilities of periodicity in each of the months are marginally significant, but the probability minima do not lie precisely at the predicted half-period, nor do they appear at the same period in both months. The result is therefore treated conservatively as an upper limit. It is hoped that an extended series of observations of this source will confirm the earlier detection.

7.3) PSR 1953+29

7.3.1) Background information

A systematic search for fast radio pulsars in the error boxes of COS-B point γ-ray sources led to the discovery of the 6.1 ms pulsar PSR

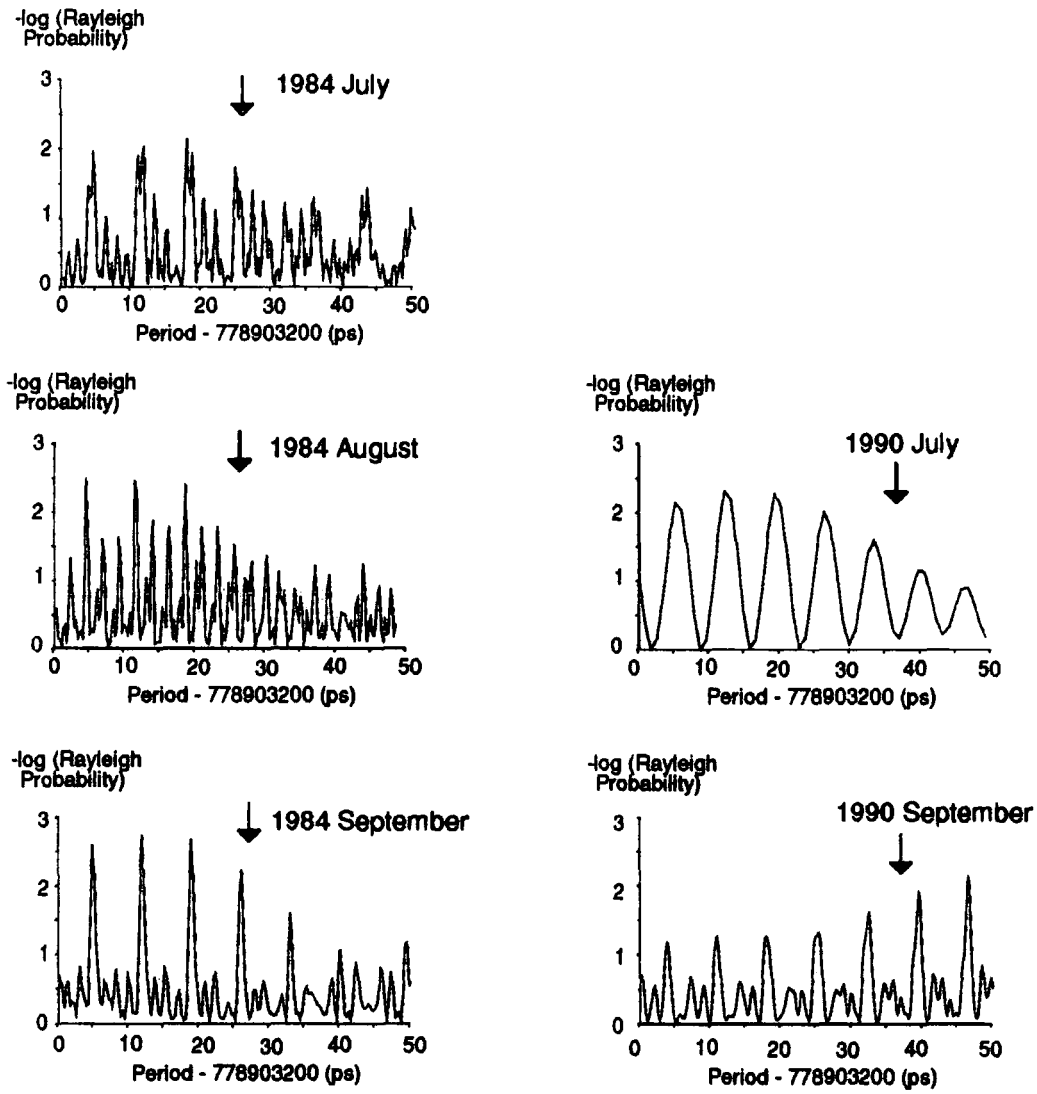

Figure 7.1

The probabilities of chance origin as a function of trial period for data on PSR 1937+21 taken in July - September 1984 and in July and September 1990. The expected pulsar half-period is indicated by arrows.

1953+29 in the direction of the γ-ray source 2CG065+0 (Boriakoff, Buccheri and Fauci, 1983). The pulsar was in a long-period, wide binary orbit, and the companion was thought to be most probably a 0.2 $M_\odot$ white dwarf (Boriakoff et al, 1984). The parameters of the binary system are given in Table 7.2.

PSR 1953+29 has a radio light curve with only a single peak. This has implications for the number of peaks in the VHE light curve: according to the polar gap model, it would mean that only one pulse per revolution of the pulsar would be seen, whereas the outer gap model predicts a minimum of two pulses per revolution. Thus, the single-peaked radio light curve may provide an opportunity to distinguish between the two possible models of high energy emission.

7.3.2) Early VHE observations and results

PSR 1953+29 was observed with the Mark I and Mark II telescopes on 20 occasions in July - October, 1983, and in July 1984. The durations of the observations varied from 1 to 6 hr. From these data, a homogeneous dataset was formed from the 8 observations which lasted for more than four hours. This enabled the datasets to be combined with approximately equal statistical weights. The cumulative uncertainties in the telescope timing and in the binary ephemeris available at the time precluded the combination of any two observations in phase, but a statistical combination of the Rayleigh probabilities was possible. The data were tested for periodicity over a search range of 8 ns about the pulse period. The range was chosen to include all possible deviations from the true period induced by systematic errors in the event timing or

Ephemeris.....	1+	2*
Pulse period (ms).....	6.133166	6.133166488729(9)
Period derivative..... ($10^{-20}ss^{-1}$)	< 4200	2.95 ± 0.03
Semi-major axis (lt-sec)....	31.29	31.412686(5)
Orbital period (days).....	117.3 ± < 0.1	117.349109(3)
Eccentricity.....	< 0.001	3.304 ± 0.003) x 10^{-4}
Longitude of periastron.....	-	29.51° ± 0.09°
Epoch of periastron.....	-	2446112.99 ± 0.03

+ Buccheri, private communication

* Rawley, Taylor and Davis, 1988.

Table 7.2

The orbital and pulse parameters of PSR 1953+29. The early measurements of Buccheri et al are stated, along with the more recent and more accurate ones of Rawley et al.

in the binary ephemeris, or statistical fluctuations in the Rayleigh vector.

The two most sensitive datasets were used in the analysis. The first of these comprised all 14286 events which had been registered on two of the four telescopes, since the effective aperture of the telescope array was smaller for such events. The second, independent dataset consisted of the 17302 events which had been registered by the Mark II telescope alone. The narrow field of view of this single telescope gave it a sensitivity comparable to the two-telescope responses.

The results of this early analysis were described by Chadwick et al, (1985a), and are reproduced in Figure 7.2. Two strong features are evident. Both datasets show a high degree of periodicity near the rotation period. It is significant that emission only appears at the full rotation period, as this is not possible in the outer gap model. The probability minimum for the Mark II events lies within the period search range, but is more than half a Fourier interval away from the probability minimum of the two-telescope events. An inconsistency would be difficult to explain in the two datasets because they were taken simultaneously and are thus subject in general to the same timing uncertainties.

The signal strengths in the two datasets are 3.5% for the two-telescope events and 3.2% for the Mark II events. From these, the flux is estimated to be 3×10^{-11} $cm^{-2}s^{-1}$, and hence the luminosity (assuming a distance of 3.5 kpc, a source spectral index of -1.6 and isotropic emission) is approximately 3×10^{35} erg s^{-1}.

It is difficult to draw any conclusions about orbital effects on

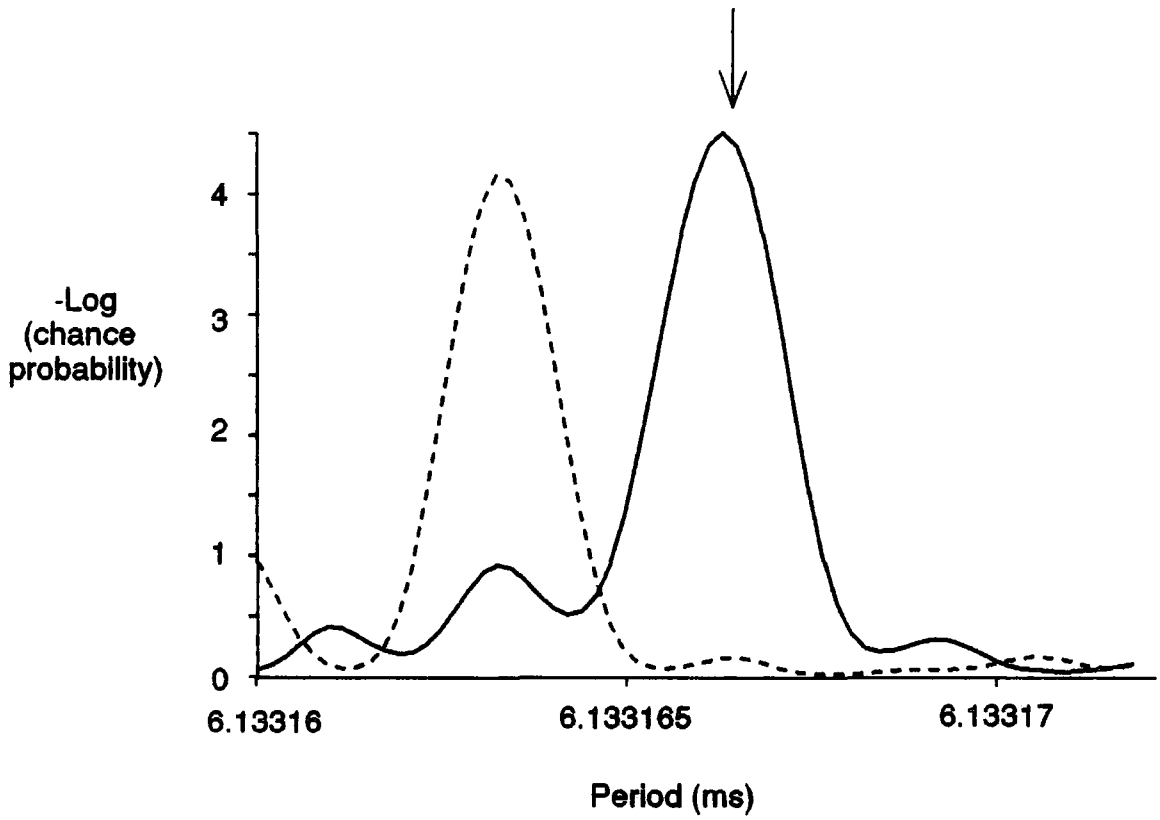

Figure 7.2

The probability of chance occurrence of periodicity about the pulsar period of PSR 1953+29 for 1983 data. The expected period is indicated by the arrow. The two-telescope responses and the data from the Mark II telescope are shown as a full and dashed line respectively.

the flux. The eight observations were taken between phases 0.30 and 0.82 of the orbit (with respect to the ascending node), each one covering only ~0.15%. With such a limited sample, it is not possible to determine whether the flux is modulated by the pulsar's binary orbit.

7.3.3) Reanalysis of the data with a recent ephemeris

The analysis above relied on an early and relatively inaccurate measurement of the orbital parameters. Following the publication of a much more accurate ephemeris in 1988 (Rawley et al, 1988), the data were reanalysed, partly in an attempt to align better the two effects seen in Figure 7.2. The new ephemeris is described in Table 7.2, and it is easily calculated that it is compatible with the original measurement. The correction to event times is different by only ~ $\pm$ 0.1 s, which, although it represents many pulsar spin periods, makes a very small difference to the relative phases which determine the periodicity. The new orbital ephemeris is sufficiently accurate that no orbital sampling is necessary. When the data are analysed after reduction to the barycentre of the new orbit, the periodograms shown in Figure 7.2 change very little. The revised periodograms are displayed in Figure 7.3. Since the signal strengths are almost identical to those obtained before, the flux estimates based on the original analysis remain valid.

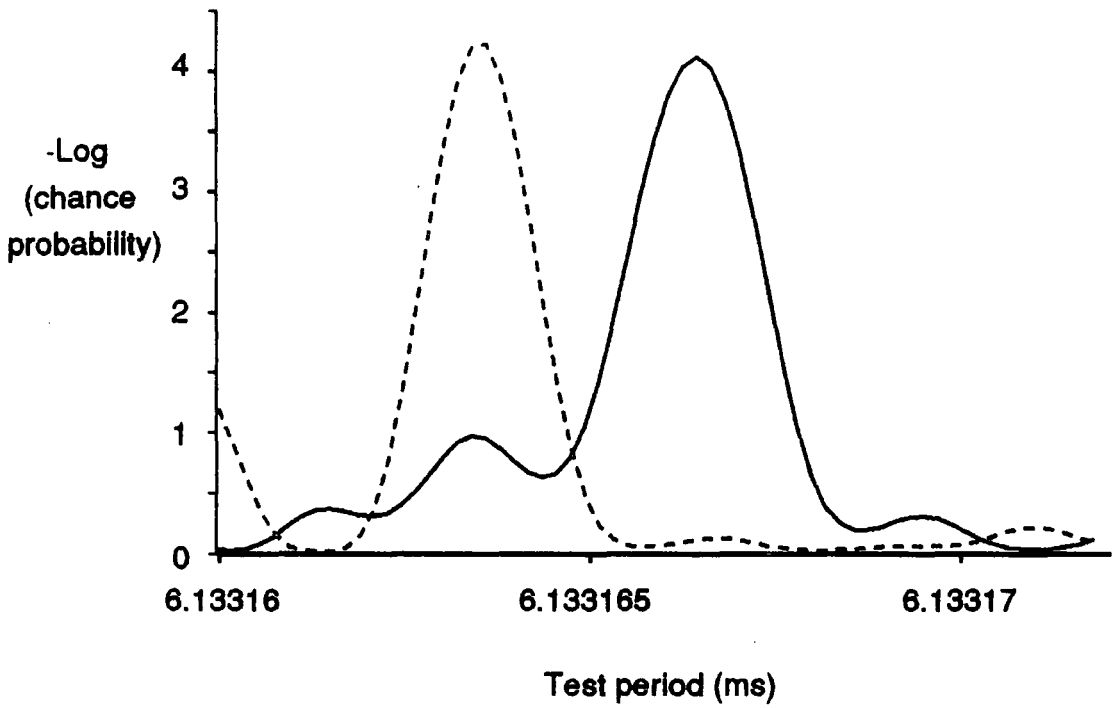

Figure 7.3

The probability of chance occurrence of periodicity as a function of test period for data on PSR 1953+29. The data have been focussed according to the ephemeris of Rawley et al (1988). The dashed and solid lines correspond to the two-telescope responses and the Mark II data respectively.

7.4) PSR 1855+09

7.4.1) Background and motivation

PSR 1855+09 was the third millisecond pulsar to be discovered (Segelstein et al, 1986a, Stokes et al, 1986). Its period was determined to be 5.36 ms, and it was found, like PSR 1953+29, to be in a binary system (Segelstein et al, 1986b). The orbital parameters of the pulsar's binary orbit are presented in Table 7.3 (after Rawley, Taylor and Davis, 1988). The optical companion was expected from timing measurements to be a ~ 0.2 $M_\odot$ white dwarf, and a nearby star was identified optically as being compatible with a 0.3 $M_\odot$ white dwarf, whose low surface temperature of ~5900 K implied an age of >2 x 10^9 years (Wright and Loh, 1986). This candidate companion was, however, some 4" away from the position of the radio source. More recent attempts to confirm the identity of the companion (Callanan et al, 1989, Kulkarni et al, 1991) have looked closer to the radio position. Callanan et al found no star within the error box of the radio position, and concluded that the companion was probably much older than the derived pulsar age,

$$\tau = p/2\dot{p} = 5 \times 10^9 \text{ years} \qquad - \ 7.1$$

Since the pulsar forms before the white dwarf in evolutionary scenarios, this would mean that the above formula was probably not valid for 'recycled' pulsars. Kulkarni et al studied another nearby star (different from that observed by Wright and Loh), but concluded that it could not be the pulsar's companion. The identity of the companion has therefore not yet been established.

Pulse period (ms).....	5.362100452367(10)
Period derivative..... (10^{-20}ss^{-1})	1.71 $\pm$ 0.05
Semi-major axis (lt-sec).....	9.2307850(2)
Orbital period (days).....	12.32717111(3)
Eccentricity.....	(2.14 $\pm$ 0.04) x 10^{-5}
Longitude of periastron.....	277.3° $\pm$ 1.5°
Epoch of periastron.....	JD 2446433.31 $\pm$ 0.05

Table 7.3

The orbital and pulse parameters of PSR 1855+09, after Rawley et al (1988).

The distance to the pulsar has not been firmly established. Dispersion measure estimates place it at ~ 400 pc, but a recent study by Ryba and Taylor (1991) included a marginal detection of the annual parallax of the pulsar, placing it nominally at ~ 1 kpc, and certainly no closer than ~ 400 pc. For calculations of flux or luminosity in this chapter, the usually accepted distance of 400 pc will be assumed.

The detection of PSR's 1937+21 and 1953+29 at distances of 5 and 3.5 kpc respectively bodes well for the detection of PSR 1855+09. At a distance of only 400 pc, this pulsar is ~ 10 times closer to the Earth, so a pulsed luminosity comparable to those from the other two millisecond pulsars would yield a very considerable flux at the Earth. In fact, the emission models outlined in chapter 6 predict a flux of $(10^{-10} - 10^{-9})$ cm^{-2} s^{-1}, or ~ 2 - 15% of the cosmic ray background flux in the Mark III telescope.

7.4.2) The Durham TeV data

PSR 1855+09 has been observed with the Mark III telescope on 56 occasions over the four year period 1987 to 1990, and with the Mark IV telescope on 14 occasions in 1990. On eleven of the latter occasions, both telsecopes observed the source simultaneously, so the data from the less sensitive Mark IV telescope were reserved to confirm effects seen in data taken with the more sensitive Mark III telescope. A catalogue of the data is given in Table 7.4. The twelve day binary period ensures that a wide selection of orbital phases is covered in any one month of observations, with the result that after four years, a fairly uniform and comprehensive sample of the orbit has been gained. This is

Table 7.4

Catalogue of observations of PSR 1855+09. All observations except one (indicated) were taken in the tracking mode. Orbital phases have been derived from the ephemeris of Rawley, Taylor and Davis (1988)

Date	Duration (hrs)	# events[$]	Orbital phase
250487	1.0	1471	0.29
290487	1.0	1779	0.62
230587	3.7	4941	0.56
240587	3.7	5911	0.64
250587	3.3	6779	0.72
260587	3.7	5979	0.81
290587	1.5	1677	0.06
300587	3.0	2368	0.13
310587	3.0	5479	0.21
020687	2.5	5023	0.37
030687	3.3	5664	0.45
040687	3.7	5998	0.54
180787	6.0	2691	0.10
190787	3.0	1473	0.12
200787	5.0	2739	0.25
230787	5.0	5713	0.50
240787	4.7	5655	0.58
160987	2.0	2681	0.95
180987	2.3	3515	0.11
190987	2.3	2799	0.19
200987	2.3	2526	0.27
070988	2.0	2518	0.90
080988	2.5	2324	0.00
090988	2.0	2487	0.07
100988	2.7	5370	0.15
120988	3.3	1706	0.32
290988	1.0	1869	0.69
071088	1.0	1642	0.34
091088	1.3	2046	0.50
101088	1.3	1634	0.58
111088	1.0	1470	0.67
121088	1.0	959	0.75

290589	2.0	2174	0.34
300589	2.5	2441	0.42
310589	4.7	1669	0.51
070689	3.7	6315	0.08
230989	1.5	2825	0.82
240989	2.0	3431	0.90
260989	1.7	3211	0.06
270989*	2.0	1707	0.14
280989	1.7	2948	0.22
290989	1.5	2778	0.30
300989	1.3	1638	0.38
011089	1.0	1236	0.46
300490	2.0,1.7	3399,4670+	0.61
010590	3.0,2.7	5304,7073+	0.69
020590	2.0,2.7	3847,6155+	0.77
030590	3.0,3.0	4472,5366+	0.85
190590	1.7,1.7	1849,2556+	0.14
200590	2.5,2.5	3355,3205+	0.22
250590	4.0,4.0	5980,4831+	0.63
190690	4.0,3.7	5538,7011+	0.65
280690	3.7,3.0	751,1070+	0.38
210790	2.5,2.7	5075,5255+	0.24
230790	2.3,2.5	1714,2197+	0.40
090990	0,2.7	0,5388+	0.29
100990	0,3.7	0,6945+	0.37
140990	0,2.0	0,3505+	0.69
200990	1.7, 0	1300, 0+	0.18
Totals	145,39	181443,65227+	

$ After hardware selection and pulse integral selection at a threshold of 45% (Mark III data); hardware selection only (Mark IV data)

* This observation was taken in the chopping mode

+ Event totals refer to datasets taken with the Mark III and Mark IV telescopes respectively

important if a search for orbital modulation of any emission is to be made. As an observation of 3 hours covers only 1% of the orbit, however, complete coverage of the orbit has not been achieved.

Because the pulse period is very much shorter than the average interval between cosmic ray events, the quality of the data is very little affected by observing conditions, and the passage of clouds across the field of view on a timescale of minutes does not affect periodic analysis of a dataset except by the reduction in event total. All datasets were therefore analysed, except those with fewer than 750 on-source events. The datasets analysed are catalogued in Table 7.4. The optimal threshold of 45% for pulse integral selection was determined from the observation of the 11th October 1988 alone, as described in chapter 5.

7.4.3) Analysis technique

Just as event times must be reduced to the solar system barycentre, it is essential for the recovery of periodicity in data on any binary star that the travel time incurred by each γ-ray in crossing the binary be removed. The complications which can arise during this procedure have been described in detail in Chapter 4. PSR 1855+09 is especially sensitive to the orbital ephemeris applied. Typical sampling intervals in the projected orbital radius (asini) and orbital phase (Φ) for recovery of periodicity at p/2 in a three hour observation are:

At a node: Δasini = 0.04 ls $\Delta\Phi = 3.8^{\circ}$

At conjunction: Δasini = 12.0 ls $\Delta\Phi = 0.2^{\circ}$

The sampling intervals for intermediate positions in the orbit are between the limits above. Although the fractional inaccuracy in asini may therefore be quite large before the true period is lost, the sensitivity to orbital phase, Φ is very high. The significance of this is seen when we consider the reference radio ephemeris for the orbit. The orbit of this pulsar is very nearly circular, with an eccentricity of $(2.14 \pm 0.04) \times 10^{-5}$, and the longitude of periastron, ω, which defines the reference epoch of the ephemeris, is defined to only $\pm 1.5^{\circ}$ (0.42%) in the ephemeris of Rawley, Taylor and Davis (1988). The epoch and position of ω are highly covariant, and their combination will be better known than the errors given. However, the ephemeris is quoted only to the tolerance of the errors. At some points in the orbit, and especially for long observations, the uncertainty in phase is more than can be tolerated for the recovery of periodicity.

To overcome this problem, values of asini and Φ within a small area of trial orbital parameters have been used to remove the travel times, instead of a single fixed ephemeris. For simplicity, this area was fixed for all observations at:

$$9.14 \leq \text{asini} \leq 9.30 \text{ (ls)}$$

$$\Delta\Phi \leq 0.6\% \ (2.2^{\circ})$$

Since the sampling interval in each of these quantities was different for each TeV observation and for each test period, the number of significantly different orbits in the range varied, but in all cases it was small enough that any deviation from the radio ephemeris could be considered more likely to indicate the consequences of statistical

sampling than to suggest an emission site remote from the radio one.

It is not necessary in the analysis of this object to sample in all parameters of period, semi-major axis and phase. The equations derived in chapter 4 show that the three parameters are not independent. Indeed, the sampling intervals in asini and Φ describe the shifts needed to move the periodicity away from its true position by one Fourier interval. In the 12.3 day orbit of PSR 1855+09, a three hour observation spans only 1% of the orbit and curves by only 3.7°. The linear case studied in chapter 4 is therefore a good approximation in this case, so only two parameters (asini and Φ) were sampled, while the test period was fixed at the predicted pulsar period. As with period sampling, three samples were made within each independent interval. The Rayleigh test was used to test each dataset for periodicity.

The analysis yielded a three dimensional array of asini x Φ x chance probability. A graphical representation of one of the results is shown in Figure 7.4 as an illustration of typical results. Only the most significant chance probability obtained from such an array was considered further.

A further problem arose in the calculation of the number of degrees of freedom involved in the analysis of each observation. This was a function of the orbital characteristics of the binary, of the orbital position of the neutron star during the observation and of the length of the observation (or, more correctly, the duration of the periodic flux). The most reliable method of calculating the number of degrees of freedom was considered to be a set of Monte Carlo simulations.

A simulation was devised in which each observation was analysed exactly as above, except that the test period was altered to one

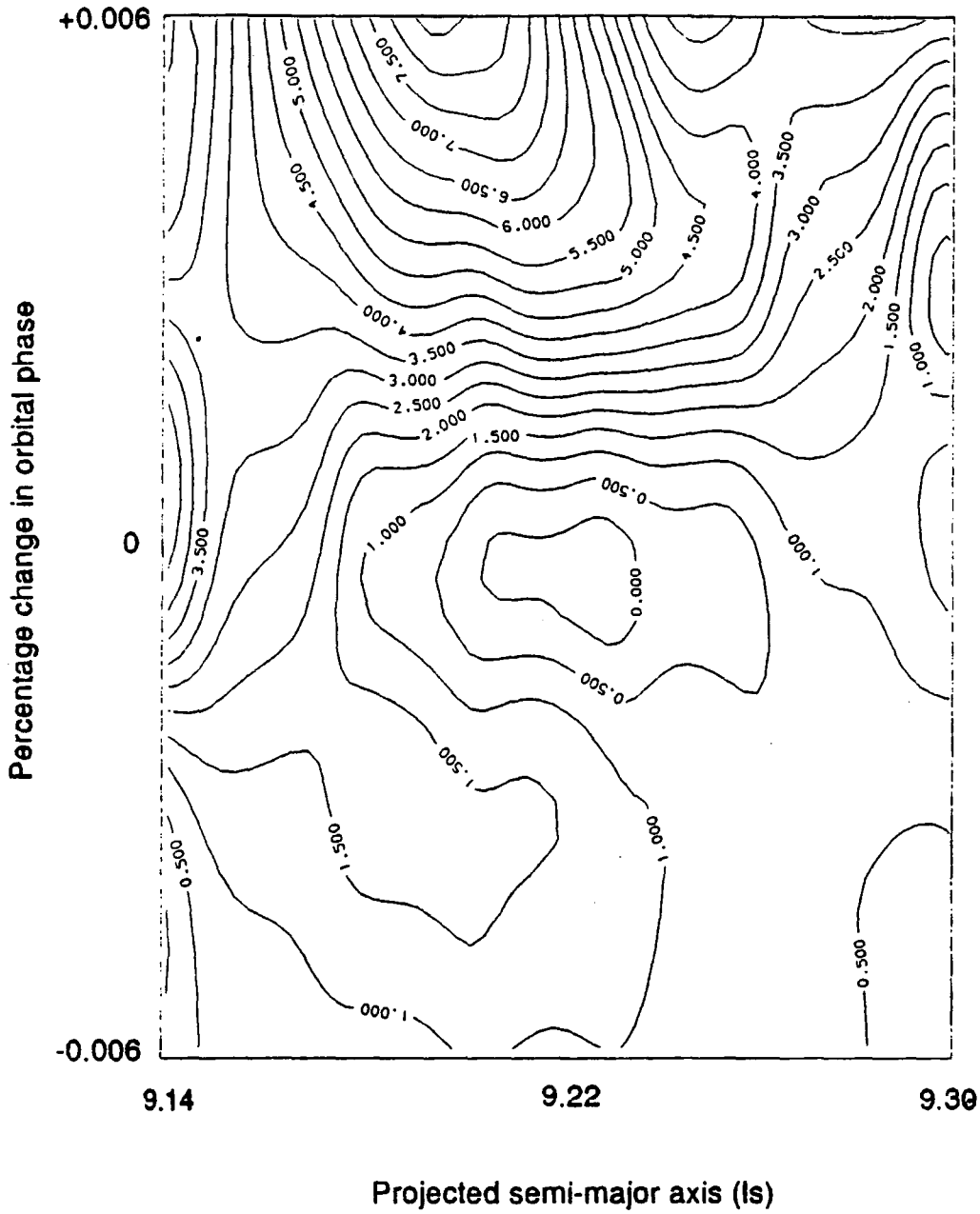

Figure 7.4

An example of the results obtained from orbital sampling. The contours represent levels of constant chance probability of uniformity in pulse phase and are labelled according to the logarithm of the probability (base 10). The reference ephemeris is close to the centre of the plot.

independent of the true test period. The Fourier interval in period for an observation of this pulsar is of the order of nanoseconds in size, so that the test period can be changed by many intervals without the change affecting the sampling intervals in the two orbital parameters. The simulations of a given observation were thus essentially identical in their individual degrees of freedom.

Each simulation yielded a set of Rayleigh probabilities of which only the most significant was noted. After many simulations, a distribution of these Rayleigh probabilities was formed. The fraction of simulation probabilities equalling or exceeding the test value was taken as a measure of the true chance probability of the observed periodicity. For observations in which the observed degree of periodicity could not be reproduced, an exponential function was fitted to the tail of the probability spectrum and used to extrapolate to the observed probability. This method was not necessary for the less significant points, which were easily reproduced. The simulations were accumulated for each observation until there was no ambiguity about the decade in which the probability lay (e.g. $10^{-3} < p < 10^{-2}$).

7.4.4) Results (1): tests at the pulsar period

The minimum Rayleigh probabilities generated by the data at the pulsar period are tabulated in Table 7.5, and the corresponding chance probabilities after allowance for the orbital sampling are given in Table 7.6. There is no evidence that the data are periodic at the full pulse period.

Date	probability
121088	7.1×10^{-2}
020590	1.6×10^{-1}
260587	1.9×10^{-1}
230989	4.3×10^{-1}
030590	8.3×10^{-3}
070988	1.8×10^{-3}
240989	2.2×10^{-2}
160987	1.1×10^{-4}
080988	3.7×10^{-1}
260989	1.2×10^{-1}
290587	1.6×10^{-1}
090988	4.4×10^{-2}
070689	1.5×10^{-1}
180787	1.8×10^{-1}
180987	1.6×10^{-2}
190787	1.2×10^{-3}
190590	1.8×10^{-1}
300587	9.2×10^{-2}
270989	2.2×10^{-1}
100988	1.2×10^{-1}
200990	1.7×10^{-2}
190987	8.0×10^{-3}
310587	7.9×10^{-2}
280989	2.8×10^{-2}
200590	1.0×10^{-1}
210790	2.2×10^{-1}
200787	4.1×10^{-1}
200987	1.8×10^{-1}

Date	probability
250487	4.8×10^{-1}
290989	2.1×10^{-1}
120988	1.9×10^{-1}
290589	2.6×10^{-2}
071088	1.0×10^{-2}
020687	3.6×10^{-2}
300989	1.0×10^{-1}
280690	2.5×10^{-2}
230790	1.7×10^{-3}
300589	1.2×10^{-2}
030687	9.9×10^{-2}
011089	1.8×10^{-1}
230787	1.3×10^{-1}
091088	9.2×10^{-2}
310589	1.5×10^{-1}
040687	2.6×10^{-1}
230587	3.9×10^{-2}
240787	2.5×10^{-2}
101088	9.0×10^{-2}
300490	5.8×10^{-2}
290487	4.5×10^{-1}
250590	1.6×10^{-2}
240587	2.8×10^{-2}
190690	1.2×10^{-1}
111088	2.7×10^{-1}
010590	1.2×10^{-1}
290988	4.1×10^{-1}
250587	5.0×10^{-3}

Table 7.5

Summary of results for PSR 1855+09 at the pulsar spin period. The observations have been ordered by orbital phase, beginning at phase = 0. The probabilities quoted here are the best Rayleigh probabilities generated in the orbital sampling region. Probabilities corrected for the orbital sampling freedom are given in Table 7.6.

Date	probability
121088	3.9×10^{-1}
020590	2.0×10^{-1}
260587	9.9×10^{-1}
230989	1.0×10^{-0}
030590	1.8×10^{-1}
070988	7.4×10^{-2}
240989	1.0×10^{-1}
160987	1.1×10^{-2}
080988	1.0×10^{-0}
260989	8.2×10^{-1}
290587	9.0×10^{-1}
090988	2.0×10^{-1}
070689	1.0×10^{-0}
180787	1.0×10^{-0}
180987	8.9×10^{-2}
190787	6.7×10^{-3}
190590	1.0×10^{-0}
300587	7.7×10^{-1}
270989	1.0×10^{-0}
100988	6.2×10^{-1}
200990	5.2×10^{-1}
190987	6.8×10^{-2}
310587	6.3×10^{-1}
280989	9.2×10^{-2}
200590	1.0×10^{-0}
210790	7.5×10^{-1}
200787	1.0×10^{-0}
200987	7.1×10^{-1}

Date	probability
250487	1.0×10^{-0}
290989	1.0×10^{-0}
120988	1.0×10^{-0}
290589	1.4×10^{-1}
071088	7.6×10^{-2}
020687	4.0×10^{-1}
300989	2.8×10^{-1}
280690	3.1×10^{-1}
230790	5.1×10^{-3}
300589	1.1×10^{-1}
030687	8.3×10^{-1}
011089	9.2×10^{-1}
230787	1.0×10^{-0}
091088	3.3×10^{-1}
310589	7.5×10^{-1}
040687	9.8×10^{-1}
230587	1.6×10^{-1}
240787	3.5×10^{-1}
101088	2.8×10^{-1}
300490	4.1×10^{-1}
290487	7.9×10^{-1}
250590	3.3×10^{-1}
240587	2.1×10^{-1}
190690	1.0×10^{-0}
111088	1.0×10^{-0}
010590	7.6×10^{-1}
290988	7.7×10^{-1}
250587	1.7×10^{-2}

Table 7.6

Summary of results for PSR 1855+09 at the pulsar spin period. The probabilities have been corrected for the orbital sampling freedom. Errors due to the finite number of simulations are not shown, but are generally less than 10%, decreasing with the significance of a point.

7.4.5) Results (2): tests at the half-period

The data from each of the observations was tested for periodicity at half the pulsar spin period, in the manner used to test at the full period. Simulations were made to assess the true significances of the observed probability minima as described above. The raw and true chance probabilities are tabulated in Tables 7.7 and 7.8. The null hypothesis to be tested was that there was no unusual periodicity in any of the datasets. Of the 56 datasets, 13 yielded chance probabilities smaller than 0.1, in marked contrast with the six expected. The probability that this arose by chance was only 3×10^{-3}, and the null hypothesis was rejected.

Once it had been established that there was periodicity in the dataset, the data were examined to ascertain whether the periodicity was in any way time dependent. Two cases were considered. Either the emission could be sporadic, appearing only in isolated datasets, or it could be related to the binary orbit, appearing persistently, but for limited sections of the orbit.

i) Sporadic emission

One of the 56 datasets showed particularly strong periodicity, significant at a level of 4.8×10^{-4} after allowance for the orbital degrees of freedom and for the optimisation of the pulse integral selection threshold performed on this dataset. In a sample of 56 observations, the chance probability of such an occurrence was 2.7×10^{-2}. The observation was made on 11th October, 1988, and lasted for 1 $^1/_2$ hours. The observations adjacent to this in time and in

Date	probability
121088	3.0×10^{-2}
020590	2.2×10^{-2}
260587	3.3×10^{-2}
230989	7.4×10^{-2}
030590	1.5×10^{-1}
070988	8.2×10^{-2}
240989	1.2×10^{-1}
160987	1.4×10^{-2}
080988	1.4×10^{-2}
260989	6.1×10^{-2}
290587	5.5×10^{-2}
090988	9.1×10^{-2}
070689	5.0×10^{-2}
180787	5.0×10^{-2}
180987	6.7×10^{-2}
190787	7.4×10^{-2}
190590	2.7×10^{-2}
300587	1.5×10^{-2}
270989	1.7×10^{-2}
100988	7.4×10^{-3}
200990	8.2×10^{-2}
190987	3.7×10^{-3}
310587	1.0×10^{-2}
280989	1.4×10^{-1}
200590	6.1×10^{-3}
210790	4.1×10^{-3}
200787	1.0×10^{-2}
200987	1.2×10^{-2}

Date	probability
250487	7.5×10^{-4}
290989	4.1×10^{-3}
120988	1.8×10^{-3}
290589	6.7×10^{-3}
071088	4.1×10^{-2}
020687	2.2×10^{-4}
300989	1.5×10^{-2}
280690	2.0×10^{-2}
230790	1.5×10^{-1}
300589	1.7×10^{-1}
030687	4.5×10^{-2}
011089	4.1×10^{-1}
230787	3.0×10^{-2}
091088	8.2×10^{-2}
310589	1.8×10^{-1}
040687	1.4×10^{-1}
230587	3.0×10^{-1}
240787	3.3×10^{-2}
101088	4.5×10^{-1}
300490	3.0×10^{-2}
290487	3.3×10^{-1}
250590	9.1×10^{-3}
240587	6.1×10^{-2}
190690	6.1×10^{-3}
111088	2.2×10^{-6}
010590	3.3×10^{-2}
290988	2.2×10^{-1}
250587	1.2×10^{-1}

Table 7.7

The minimum Rayleigh probabilities found on the matrix of orbital sampling points, at the half-period of the pulsar. The observations have been ordered by orbital phase.

Date	probability
121088	3.3×10^{-1}
020590	5.5×10^{-2}
260587	4.2×10^{-1}
230989	5.0×10^{-1}
030590	1.0×10^{-0}
070988	6.7×10^{-1}
240989	8.3×10^{-1}
160987	2.9×10^{-1}
080988	9.2×10^{-1}
260989	8.3×10^{-1}
290587	7.5×10^{-1}
090988	8.3×10^{-1}
070689	9.2×10^{-1}
180787	9.2×10^{-1}
180987	7.5×10^{-1}
190787	8.3×10^{-1}
190590	5.8×10^{-1}
300587	2.5×10^{-1}
270989	3.2×10^{-1}
100988	7.7×10^{-2}
200990	5.0×10^{-1}
190987	6.3×10^{-2}
310587	1.6×10^{-1}
280989	9.2×10^{-1}
200590	1.7×10^{-1}
210790	2.8×10^{-2}
200787	6.1×10^{-2}
200987	9.4×10^{-2}

Date	probability
250487	4.9×10^{-3}
290989	4.4×10^{-2}
120988	2.9×10^{-2}
290589	7.3×10^{-2}
071088	5.0×10^{-1}
020687	4.9×10^{-3}
300989	8.3×10^{-2}
280690	5.0×10^{-1}
230790	9.0×10^{-1}
300589	1.0×10^{-0}
030687	7.5×10^{-1}
011089	1.0×10^{-0}
230787	8.3×10^{-1}
091088	5.8×10^{-1}
310589	1.0×10^{-0}
040687	1.0×10^{-0}
230587	1.0×10^{-0}
240787	9.2×10^{-1}
101088	1.0×10^{-0}
300490	4.2×10^{-1}
290487	1.0×10^{-0}
250590	3.8×10^{-1}
240587	9.2×10^{-1}
190690	3.3×10^{-1}
111088	4.7×10^{-4}
010590	4.2×10^{-1}
290988	8.3×10^{-1}
250587	8.3×10^{-1}

Table 7.8

True chance probabilities corresponding to the raw figures in Table 7.7.

orbital phase showed no significant periodicity, and the periodicity was present throughout the observation, leading to the conclusion that this was an isolated episode of emission of between 1 $^1/_2$ and 24 hours' duration.

This single incidence of emission did not account for the general excess of observations with individually small, but cumulatively significant periodicity. A second hypothesis was therefore also tested, that the emission was linked to the orbital phase of the pulsar.

ii) Orbital modulation of the flux

Chance probability is plotted as a function of orbital phase in Figure 7.5. With the notable exception of the single observation mentioned above, the periodic data are clearly clustered about the descending node. It is not simple to quantify the significance of the clustering, because it appears not as an accumulation of identical points in a limited region of the orbit, but as an association of similar points in a distribution. Tests considering the integral and linear departures from expectation were considered. A test was finally devised which was similar to the non-parametric Kolmogorov-Smirnov (K-S) test (Conover, 1980). This latter test considers the departure from expectation as illustrated in Figure 7.6. It is applicable to data for which each point carries equal weight and the points are combined into bins. However, an analogous test was made as follows for the alternative case here in which the points were not combined, but carried dissimilar weights. This test was considered preferable to other tests considered because it was less affected by the dissimilarity of the points.

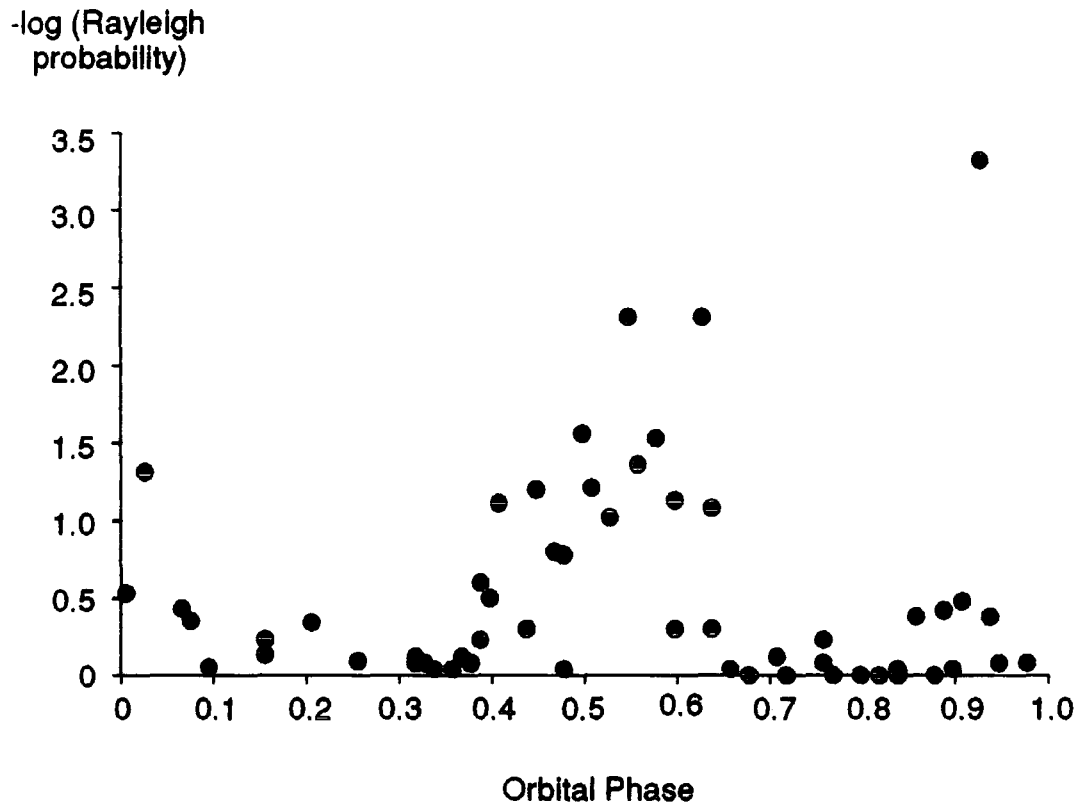

Figure 7.5

Chance probability of observed periodicity at p/2 as a function of orbital phase. Orbital phase is with respect to the ascending node. The probabilities have been corrected for the freedom allowed in the orbital parameters.

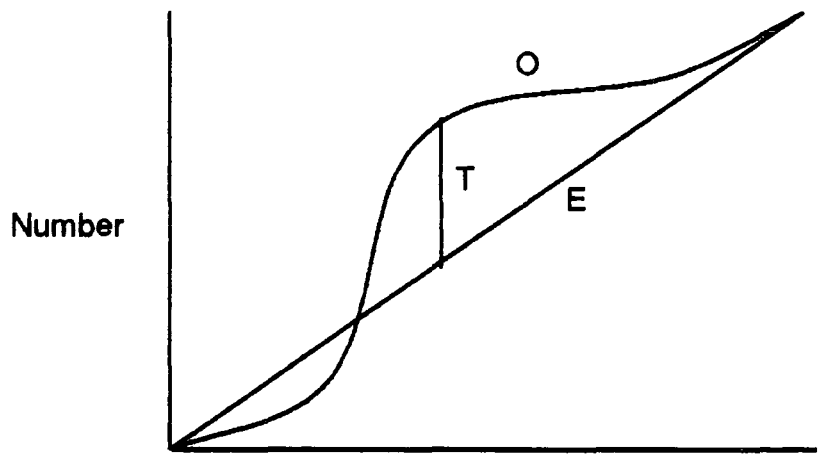

Figure 7.6

Application of the Kolmogorov-Smirnov test. The curve O is the observed distribution, and E is the expected one. The statistic T is defined as the maximum percentage difference (vertically) between the two distributions.

The chance probabilities obtained for the individual datasets were ordered by orbital phase and plotted in a cumulative fashion (Figure 7.7). In a random ordering of the points, the accumulating power (-log(probability)) would not be expected to depart significantly from a straight line. The K-S test uses the maximum absolute deviation from expectation as a measure of the clustering of the data. In the analogous test used here, the deviation from uniformity, T (see Figure 7.7) was used to test for clustering of significant probabilities in orbital phase. This yielded a deviation of 28.8%. In order to assess the significance of this value of T, the test was also applied to a large number of random re-orderings of the same points. The resultant distribution of T then gave the frequency with which any value of T was observed in random orderings of the data. The random number generator and the clustering test were both tested and performed correctly. Thus, the chance probability of the original clustering was found to be 0.027 (with a computational error of $\pm$ 0.004).

This result and the probability of overall emission are independent and can therefore be combined. The final probability of chance occurrence is 8.2×10^{-5}.

The above clustering test includes the strongly periodic data of the 11th October 1988. As mentioned before, these data are more strongly periodic than most, and the observation dominates the power/orbital phase plot of Figure 7.5. The clustering test was chosen partly because it was not greatly affected by this, but it *is* affected to some extent by the single significabt point. Its effect on the clustering simulations is to increase the apparent average chance clustering. Since the test is for a single-peaked distribution, this

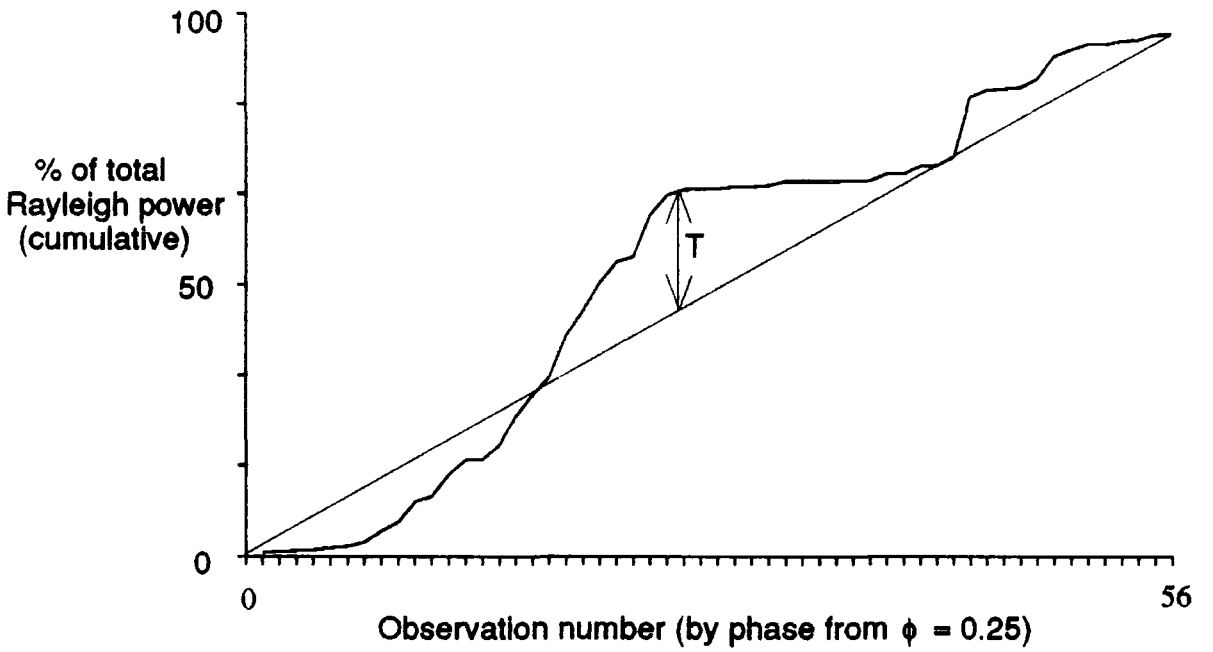

Figure 7.7

Cumulative power plotted as a function of orbital phase. There is a marked deviation from expectation, measured by the statistic T.

night's strong periodicity at a different orbital phase reduces the overall result. The derived chance probability must therefore be considered a very conservative upper limit. If the observation were excluded, the clustering probability would decrease to 3.7×10^{-4} (with a computational error of $\pm 0.9 \times 10^{-4}$). However, although this is an interesting comparison, such ad hoc exclusion of some datasets cannot be permitted. The test for a single diversion from uniformity in all the data has been used to calculate the final chance probability.

The orbital modulation of the flux does not vary detectably on long time scales. When the data from each year are plotted separately, the modulation is seen in each subset (Figure 7.8). This reproducibility is important in aiding the independent verification of the result by other groups. Note that the observations made in 1990 were biassed towards the ascending and descending nodes of the orbit, so that the orbital coverage was less even in that year.

The peak flux occurs in the single strong observation, and forms 18% of the cosmic ray flux above 400 GeV (calculated using equation 4.3). The strongest flux in data taken near the descending node is 14%. From the former, the (isotropic) luminosity of the star is estimated to be 1×10^{33} erg s^{-1}.

The result from this extensive series of observations is lent support by the limited number of observations made with the Mark IV telescope. The data taken with this telescope are less sensitive to a source flux, because of the lower overall count rate and because pulse integral selection cannot be used to reduce the number of background counts. They were therefore analysed separately and the results were compared with those from the corresponding observations made with the

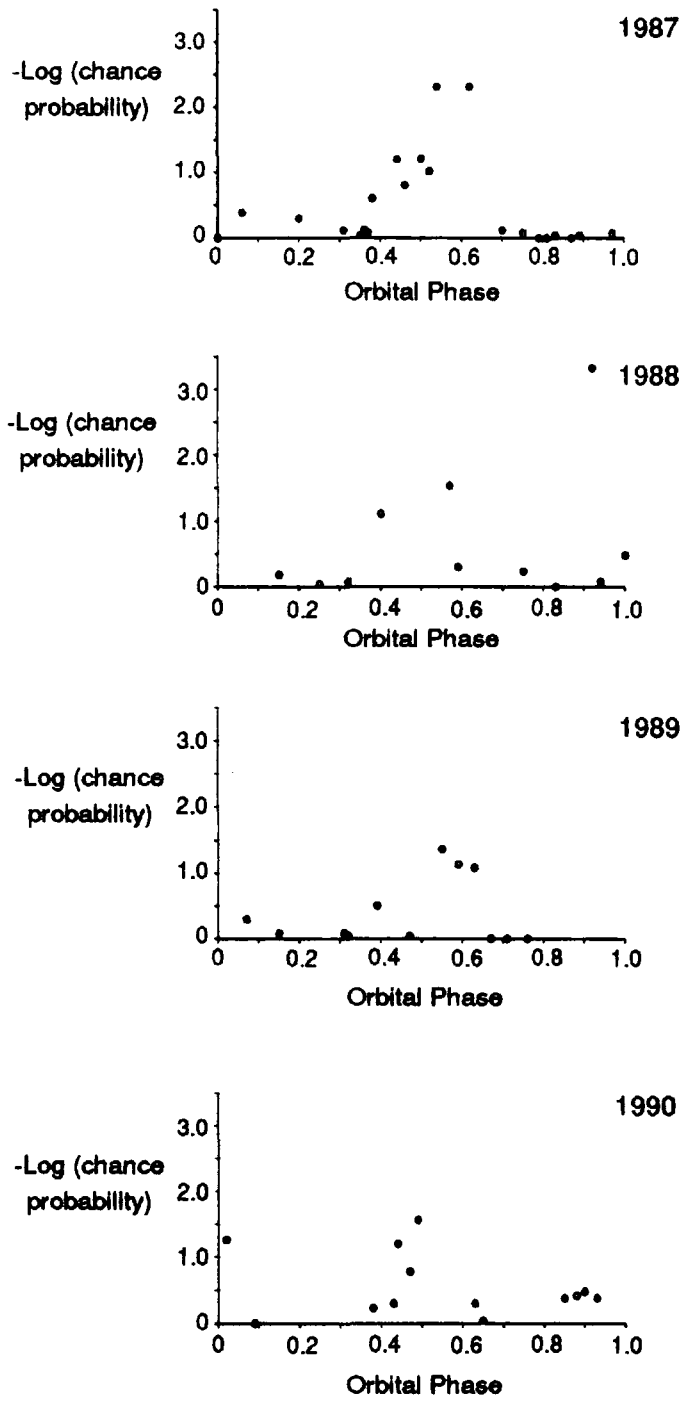

Figure 7.8

The orbital modulation of the signal from PSR 1855+09 displayed for the data from each year of observations. The modulation is apparent in data from each of the four years.

Mark III telescope. Table 7.9 shows the results of periodicity analysis of the Mark IV data. Two observations contain significant periodicity - those from 21st July 1990 and 2nd May 1990. These coincide with the two most significantly periodic observations taken that year with the Mark III telescope. This is independent confirmation that the periodicity and modulation originate in a genuine stellar signal and are not a statistical fluctuation.

7.4.6) Analysis with a recent orbital ephemeris

A more precise orbital ephemeris for the 1855+09 system has recently become available (Ryba and Taylor, 1991). It is summarised in Table 7.10. The new ephemeris is very little changed from its predecessor, except for a considerable improvement in precision. Using the new ephemeris, orbital sampling is unnecessary and the data were therefore refocussed according to the new ephemeris. The results of periodicity testing at the half period are shown in Figure 7.9, which should be compared with Figure 7.5. The figure is largely unchanged from the one obtained previously, and the overall probability of chance occurence is now 8.4×10^{-3}. The orbital distribution now appears more bimodal, although it should be remembered that some low probabilities are expected by chance in a sample of 56 datasets. Applying the clustering test to this figure yielded a chance probability of 5.8%, and so the final probability of the observed features arising by chance is estimated to be 4.9×10^{-4}.

Date	Orbital Phase	Chance probability
190590	0.13	9.0×10^{-1}
200590	0.22	9.0×10^{-1}
210790	0.24	7.0×10^{-2}
090990	0.29	1.0×10^{-1}
100990	0.37	2.0×10^{-1}
280690	0.38	3.0×10^{-1}
230790	0.40	9.0×10^{-1}
300490	0.60	1.5×10^{-1}
250590	0.63	5.0×10^{-1}
190690	0.65	3.0×10^{-1}
010590	0.68	4.0×10^{-1}
140990	0.69	2.1×10^{-1}
020590	0.77	1.6×10^{-2}
030590	0.84	5.0×10^{-1}

Table 7.9

Chance probabilities of periodicity at half the pulsar spin period in the data taken using the Mark IV telescope. The probabilities have been corrected for the freedom allowed in the orbital parameters. The two datasets with probabilities smaller than 0.1 correspond to the two most significantly periodic datasets taken with the Mark III telescope in 1990.

Pulse period (ms).....	5.36210045404065(10)
Period derivative..... (10^{-20}ss^{-1})	1.7738(3)
Semi-major axis (lt-sec)....	9.2307807(3)
Orbital period (s).....	1065067.59082(12)
Eccentricity.....	$(2.167 \pm 0.004) \times 10^{-5}$
Longitude of periastron.....	$276.299335^{\circ} \pm 0.9^{\circ}$
Epoch of periastron.....	JD 2447530.39335870 $\pm$ 0.09

Table 7.10

The orbital and pulse parameters of PSR 1855+09, as recently measured by Ryba and Taylor (1991). The parameters are very similar to the previously published values of Rawley, Taylor and Davis (1988), except for a considerable gain in precision.

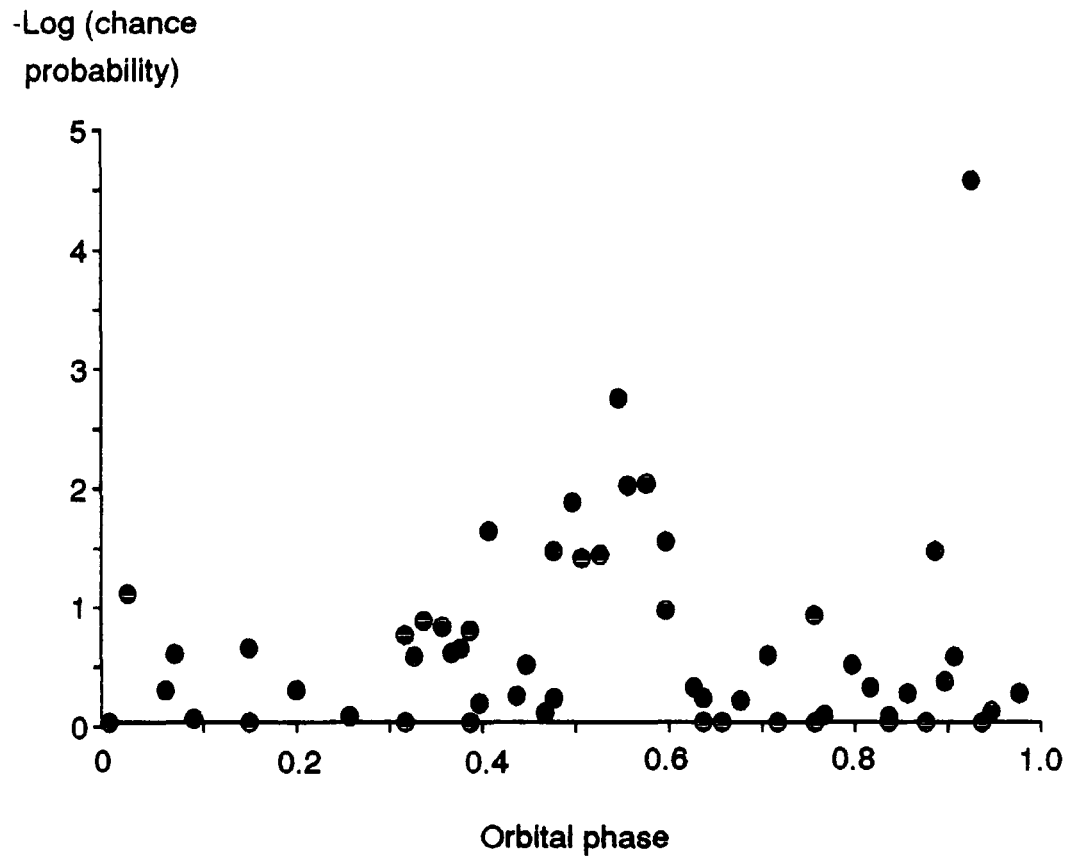

Figure 7.9

Chance probability in each of the observations of PSR 1855+09 plotted as a function of orbital phase. The modulation seen in analysis using a previous ephemeris is still visible.

7.4.7) Discussion

The signal detected from PSR 1855+09 is clear and reproducible from year to year. In the light of the earlier results on PSR's 1937+21 and 1953+29, both of which matched the presence or absence of an interpulse in their radio counterparts, it is not surprising that the signal is seen at the half-period. The unexpected feature of the result is the orbital modulation. Such modulation of the VHE flux from a non-accreting pulsar with a degenerate companion was not predicted and is difficult to explain, especially since radio observations of the object do not reveal any similar modulation (Ryba and Taylor, 1991). Plausible explanations fall into two categories. Either the modulation could be due to some geometrical effect, or a steady flux is affected by intervening matter. Some possible explanations are discussed below.

i) Geometric effects

If TeV and radio beams from pulsars are paraxial, geometric and beaming causes of the TeV orbital modulation are difficult to reconcile with the constancy of the radio flux. In order to postulate that the observed effect is due to a favourable alignment of the beam, it would be necessary to have a γ-ray beam which is narrower than the radio beam. Since the radio beam is generally accepted to be $\sim 10^{\circ}$ wide, the γ-ray beam would have to be extremely narrow, in contrast with the very wide beams predicted by the two VHE emission theories.

ii) Intervening matter

Intervening matter may have one of two effects on a TeV flux. Either it may attenuate a beam, or it may provide the target for γ-ray production from high energy hadrons. Again, the lack of intensity modulation or excess dispersion in the radio flux places constraints on the extent and quantity of material present in the binary system. Because TeV γ-rays are penetrating, it would be more plausible that the observed modulation be associated with the creation of γ-rays than with their attenuation. We will consider here only material associated with the binary orbit. A column density of a few hundred grams is sufficient for the high energy interactions, but would have to be very localised to escape detection in radio measurements. Neutral matter in the binary would not be detected in radio measurements but is unlikely to be present in large quantities.

The location and nature of the target material remain to be determined. In X-ray binaries, orbital modulation at high energies is ascribed to matter being accreted by the neutron star. In the 1855+09 system, however, the possibility of accretion may be ruled out by the extreme speed of the pulsar's rotation. A second possibility might be the existence of 'Trojan' matter at the Lagrange points L4 and L5, as postulated for the 1957+20 binary (see section 7.5.5). This possibility may also be ruled out, because the mass ratio of the two stars is too low for stable Trojans to exist.

The modulation could be plausibly explained if PSR 1855+09 were slowly ablating its companion and a wake of evaporated material trailed this second star. A γ-ray production mechanism similar to that proposed in X-ray binaries might then operate in the wake, provided that there

was a source of energetic hadrons. However, radio observations of a pulse delay around superior conjunction of the pulsar (phase 0.25) have been interpreted as the effects of space-time curvature close to the companion star, rather than an extended atmosphere (Ryba and Taylor, 1991). After correction for the general relativistic effect, no significant delays (i.e. > 3 μs) are seen, and a very low upper limit to the column density of ionised matter in the binary can be placed at around 10^{-12} g cm^{-2}.

None of the possible explanations discussed here are in full agreement with observations of the 1855+09 binary. The cause of orbital modulation of the TeV flux therefore remains an enigma.

7.4.8) Other TeV observations of PSR 1855+09

PSR 1855+09 has also been observed by the Potchefstroom group (de Jager et al, 1989). They detected emission in the orbital phase band 0.92 - 0.02 (0.15 - 0.25 with respect to periastron) at the 0.05 significance level. None of their data in the descending node region showed significant periodicity (Raubenheimer, private communication). The group plan further observations to confirm their result.

7.5) PSR 1957+20

7.5.1) Background information

The discovery of this binary pulsar in 1988 (Fruchter, Stinebring and Taylor, 1988) caused much excitement. Eclipses were observed for

10% of the orbit, suggesting that a substantial amount of ionised matter lay outside the Roche lobe of the 0.022$M_\odot$ white dwarf companion. It was proposed that the eclipsing matter was a dense stellar wind, driven by high energy irradiation of the white dwarf by the pulsar (Phinney et al, 1988). This suggestion led to conclusions on the nature of the pulsar emission. The evaporation of the companion would be most efficiently achieved by MeV photons, but it was unlikely that these were produced inside the pulsar magnetosphere. Instead, it was proposed that they were the synchrotron radiation of TeV particles moving in the pulsar magnetic field near the companion (Kluzniak et al, 1988). This in turn implied a substantial flux of TeV particles present in the binary. These could be produced either in the pulsar magnetosphere, or by pulsar wind shock acceleration. In a binary with a strong, evaporated stellar wind, a standing shock will be set up between the two stars (Phinney et al, 1988), in which particles may be accelerated via first order Fermi acceleration. In the PSR 1957+20 system, protons may be accelerated to TeV energies and the average flux over an orbital period of (unpulsed) gamma rays > 1TeV is estimated to be 8.9×10^{-11} $cm^{-2}s^{-1}$ (Harding, 1989). In addition, the polar and outer gap models predict pulsed TeV gamma ray fluxes from the pulsar of 2×10^{-10} and 2×10^{-11} cm^{-2} s^{-1} respectively. The source is therefore a potentially detectable source of either coherent or incoherent emission, depending on whether the overall flux is dominated by the incoherent or the pulsed element.

7.5.2) The Durham VHE data

PSR 1957+20 was observed on 15 occasions from La Palma in 1988-89 and a further 11 occasions from Narrabri in 1990. Eight of the latter observations were made with both the Mark III and Mark IV telescopes; the rest were made with the Mark III telescope only. All the data were taken in the tracking mode. A catalogue of the data is given in Table 7.11.

As the pulsar's binary period is only 9.1 hours, full coverage of the orbit was possible. All observations were analysed unless their event totals were very small (< 500 events).

7.5.3) Analysis technique

The orbital parameters of PSR 1957+20 are reproduced in Table 7.12 (from Fruchter et al, 1990). As with PSR 1855+09, the accurate removal of photon travel times within the binary is essential for the recovery of periodicity in the data. In this case the orbital parameters are extremely well known and a single, fixed ephemeris could be used.

The data were tested for periodicity at both the full and half period of the pulsar. No search was made for an unpulsed flux, since the data were taken in the tracking mode. The object's declination (+20°) meant that it was always observed at very large zenith angles from Narrabri, and the simultaneous observations with both telescopes in 1990 yielded few more independent events than observations with the Mark III telescope alone. Only the datasets from the more sensitive Mark III telescope have been used when both telescopes observed the source.

Table 7.11

Catalogue of observations of PSR 1957+20. All observations were taken in the tracking mode. Orbital phases have been derived from the ephemeris of Fruchter et al (1990)

Date	Duration (hrs)	# events[$]	Orbital phase[+]
080788	3.5	2657	0.28
090788	2.0	1263	0.80
170788	2.0	1419	0.20
180788	2.0	2583	0.83
190788	1.3	1117	0.56
200788	2.0	2353	0.08
270689	2.3	567	0.14
050789	2.0	4341	0.03
060789	2.0	3916	0.62
010989	1.7	4061	0.61
020989	2.0	4796	0.21
030989	2.0	4643	0.83
040989	2.0	4428	0.45
011089	1.7	3313	0.06
021089	1.7	3374	0.69
240490	0 *	0	-
	3.0*	2229	0.33
270490	2.0	2010	0.24
	2.5	1845	0.21
280490	1.7	1396	0.89
	2.2	1404	0.84
290490	2.0	2254	0.49
	2.3	2058	0.46
170690	2.3	1222	0.38
	2.7	2021	0.41
180690	0	0	-
	1.5	1956	0.21

200690	1.7	2659	0.32
	2.0	2352	0.36
210690	2.0	1487	0.96
	2.0	1416	0.98
220690	3.3	926	0.69
	3.7	809	0.62
230690	3.7	1913	0.14
	3.3	1949	0.18
290690	2.5	1269	0.86
	0	0	-
Totals: Mark III	22.7	19321	-
Mark IV	52.9	58685	-

$ After hardware selection (both telescopes)

* For the 1990 observations, the two rows refer to Mark III and Mark IV data respectively.

+ At the beginning of the observation.

Pulse period (ms).....	1.6074016836502(8)
Period derivative..... (10^{-20}ss^{-1})	1.61 $\pm$ 0.09
Semi-major axis (lt-sec).....	0.0892267(15)
Orbital period (s).....	33001.9167(4)
Eccentricity.....	$< 2 \times 10^{-5}$
Epoch of ascending node.....	JED 2447402.0729653(12)

Table 7.12

The orbital and pulse parameters of PSR 1957+20, as measured by Fruchter et al (1990)

7.5.4) Results

The data were first combined to search for a steady flux from the source. Pulse phase was not retained between observations because the telescope timing is not sufficient to hold phase in such a short period pulsar over the three years covered by the data. The Rayleigh probabilities within one Fourier interval of the full and half rotation periods are given in Table 7.13. The 1988 and 1989 data show marginal evidence of periodicity at half the pulsar rotation period, but this is not supported by the 1990 data. Treating the result therefore as negative, a 3σ upper limit to the pulsed flux of 3×10^{-11} cm^{-2} s^{-1} is calculated.

The failure to detect a pulsed flux from PSR 1957+20 does not necessarily imply that the total flux from the source is low. The pulsed flux may be low, but the unpulsed flux suggested by Harding (1989) may be much larger. All of the observations made so far have been made in the tracking mode and so are sensitive only to pulsed fluxes. It is hoped that future observations of this object will include some made in the chopping mode, in order to search for an overall or unpulsed TeV flux from the source.

7.5.5) Trojans

It is also hoped that a detailed investigation will be made into the feasibility of 'Trojan' matter at the fourth and fifth Lagrange points of the orbit. It was first noted by Shapiro and Teukolsky (1988) that the mass ratio of the binary stars in this system was high enough to support stable Trojans, and observations by other TeV groups have

Period	1.6 ms	0.8 ms
All 1988 and 1989 data (La Palma, Mark IV)	3.0×10^{-2}	7.5×10^{-3}
All 1990 data (Narrabri, Mark III)	3.7×10^{-1}	4.1×10^{-1}

Table 7.13

Summary of results of a search for periodicity in data on PSR 1957+20. The period of 1.6 ms is the rotation period of the pulsar. Although there is some evidence for periodicity at 0.8 ms in the early data taken using the Mark IV telescope in La Palma, this is not supported by later data taken with the more sensitive Mark III telescope.

concentrated on searching for unpulsed emission from these points in the orbit.

Lagrange's restricted 3-body problem considers the situation in which two large bodies form a binary orbit and a third test particle, small enough to have a negligible effect on the binary, is introduced into the system. It is found that five points exist in which the test particle is in gravitational equilibrium in the rest frame of the binary. These are termed the 'Lagrange points', L_1 - L_5. L_4 and L_5, which are each equidistant from the two larger masses, are of particular interest. These are points of stable equilibrium if the ratio of the two larger masses is greater than ~30, a condition satisfied in the 1957+20 binary by the observed ratio of $1.4M_\odot/0.022M_\odot \sim 64$ (Shapiro and Teukolsky, 1988). The Trojan asteroids in the orbit of Jupiter are the only observed example of this.

It is to be expected that Trojan matter in 1957+20 will experience some level of evaporation by the pulsar. Trojans and the companion star are equidistant from the pulsar, so if the MeV photons which cause the companion's ablation are created by synchrotron radiation in the pulsar magnetic field, it is a valid assumption that similar photons will be created near a Trojan. It will be assumed in the following calculations that this flux acts equally efficiently to evaporate the Trojans and the atmosphere of the companion.

Consider a sphere of Trojan matter of initial radius r and constant and uniform density ρ, being evaporated by the same flux of MeV photons as the companion. The rate of change of mass, $\dot{M}$ will depend on the cross sectional area, πr^2, presented to the MeV flux, so

$$\dot{M} = 4\pi\rho r^2 \dot{r} \propto \pi r^2 \qquad - \ 7.1$$

This will also apply to the companion star, and so

$$\dot{M} = \frac{\dot{M}_c r^2}{R_c^2} \qquad - \ 7.2$$

where M_c is the mass of the companion star.

To counteract this loss of matter, the Trojan could be replenished by capturing stellar wind particles. The Trojan will not accrete more matter than would pass through it in an isotropic wind. If the Trojan is of radius r, then the fraction of the companion star's wind passing through it (assuming an istropic wind) is

$$f = \pi r^2 / 4\pi a^2 \qquad - \ 7.3$$

where a is the separation of the companion star and the Trojan. If all of this mass is accreted by the Trojan, then from equations 7.2 and 7.3, the combined rate of mass loss is

$$\dot{M} = \dot{M}_c \left[\frac{1}{R_c^2} - \frac{1}{4a^2} \right] r^2 \qquad - \ 7.4$$

Now, since the radius of the companion, R_c, must be smaller than the orbital separation, a, $\dot{M}$ must be negative, amd the Trojan must eventually be evaporated.

7.5.6) Other TeV observations of PSR 1957+20

This unusual binary has also been observed by a number of other VHE and UHE groups. Following the proposal of Trojan matter at the Lagrangian points L_4 and L_5, the Potchefstroom group claimed a detection of unpulsed emission in a 10 minute time interval when the pulsar was directly behind the Lagrange point L4. No emission was detected from the corresponding point for L5, and the final significance was quoted at 1×10^{-3}. The luminosity was calculated to be 3×10^{32} erg s^{-1}. The data were also tested for periodicity, yielding an upper limit to the pulsed flux of 4×10^{-10} cm^{-2} s^{-1} (de Jager et al, 1989).

The TeV astronomy group based at the Tata Institute in Bombay also made observations of the pulsar and searched for evidence of emission at the orbital phases described by the South African group. They found no evidence for emission above 4.3 TeV at these phases, and placed a 3σ upper limit at 2×10^{-10} cm^{-2} s^{-1} (Acharya et al, 1990). Assuming a distance to the source of 800 pc, this corresponded to an isotropic luminosity of 1×10^{35} erg s^{-1}. The total dataset yielded a smaller limit of 4.1×10^{-11} cm^{-2} s^{-1}. A time-averaged upper limit to periodic emission was placed at 1.4×10^{-11} cm^{-2} s^{-1}.

A second group at the Tata Institute claimed detection of an episode of emission of 10^{14} eV radiation lasting for 57 minutes (Gupta et al, 1991). The emission was detected on one occasion out of 682 observations, and occurred at a phase of around 0.1 - 0.2. The significance of the detection was estimated to be 3.1×10^{-3}. The group did not detect any emission during eclipse, and therefore could not support the result of Sinha et al (1988), who claimed detection of PeV emission in the eclipse region.

7.6) Millisecond pulsars in globular clusters

The Durham millisecond pulsar database also includes observations of four globular cluster pulsars whose parameters are well enough known for periodic analysis of the data. These include PSR's 1620-26 (in the globular cluster M4), 1821-24 (in M28), 0021-72C (in 47 Tucanae)[1] and 1516+02A (in M5). The observations have generally been limited, and have not resulted in any positive detections. The results have been presented previously (Brazier et al, 1990e, Bowden et al, 1990), and are summarised in Table 7.14.

The South African group have also observed PSR's 1620-26 and 1821-24, at an energy threshold of ~ 1 TeV. They did not detect emission from either pulsar, and derived flux limits of 2.0×10^{-10} and 1.4×10^{-10} cm^{-2} s^{-1} respectively (de Jager et al, 1989).

7.7) Cygnus X-3

Although it is clearly very different from the other 'recycled' pulsars, Cygnus X-3 is mentioned here because the 12.6 ms pulsar period includes it in the category of millisecond pulsars.

---

[1] Note that a search for PSR 0021-72A is not hampered by poor measurements of the pulsar period, but by the possibility that the orbital parameters are very different from those derived in the original analysis of the data (Podsiadlowski, Naylor and Fabian, 1990).

Pulsar	Globular cluster	Spin Period (ms)	Comments	Flux limit (3σ) ($\times 10^{-11}$ cm^{-2} s^{-1})
PSR 1620-26	M4	11.1	195 day binary	8.2 ± 1.4 (E>300GeV)
PSR 1821-24	M28	3.1	Isolated	9.7 ± 1.7 (E>300GeV)
PSR 0021-72C	47 Tuc	5.8	Isolated	4.4 ± 3.0 (E>400GeV)
PSR 1516+02A	M5	5.5	Isolated	8.3 ± 1.5 (E>350GeV)

Table 7.14

Flux limits for the four globular cluster pulsars observed. Analysis of other globular cluster pulsars is precluded by poor knowledge of their parameters.

7.7.1) Background

Cygnus X-3 has mystified astronomers since its discovery. It is a source of photons from radio to ultra-high energies, but its nature remains a mystery. It exhibits a five-hour sinusoidal modulation in X-rays, which is suggestive of a binary stellar orbit, and it has been suggested that it may contain an accreting neutron star, possibly a pulsar. However, it lies in a heavily obscured, dusty region of the Galaxy, so that coherent pulsations would be considerably smeared by passage through the intervening media. Pulsar searches at X-ray wavelengths have failed to find evidence of coherent emission (Kitamoto et al, 1991).

7.7.2) The 12.6 ms pulsar

Cygnus X-3 was established as a TeV source in the early 1980's (e.g. Danaher et al, 1981, Gibson et al, 1982b, Samorski and Stamm, 1983, Lloyd-Evans et al, 1983). The high energy emission showed the 4.8 hr amplitude modulation seen in X-rays, with detection limited to the region of X-ray maximum (phase 0.625 with respect to X-ray minimum).

During an observation in 1983 with the Mark I and Mark II Durham telescopes in Dugway, a 7 minute count rate excess was noted at the time of X-ray maximum. Assuming a distance of 10 kpc, the source luminosity was estimated to be 5×10^{38} erg s^{-1}. The 450 events from this short time interval offered a sufficiently rich sample to warrant a search for the suspected pulsar, and so were tested for periodicity between 10 ms and 50 s. Periodicity was detected at 12.59 ms. Searches in other data taken at the same 'orbital' phase revealed the same periodicity

(Chadwick et al, 1985b).

Subsequent searches have revealed periodicity close to this value in a number of datasets (Brazier et al, 1990f). Between 1981 and 1988, the period changed linearly, with a time derivative of 2.8×10^{-14} ss^{-1}. The emission is detected in only about 10% of observations of a small orbital phase band. This may be one reason why three other groups have failed to detect the pulsations (Resvanis et al, 1987, Bhat et al, 1988, Fegan et al, 1989). Until 1989, detections of the 13 ms pulsar were made only in during a fixed 400 s interval when the source was close to X-ray maximum, but in September 1989, the TeV group based in Adelaide, Australia, detected 13 ms pulsations from Cygnus X-3, at a slightly different period and shortly before the predicted 300 s phase interval (Gregory et al, 1990). The change in period may be related to two large radio bursts observed from Cygnus X-3 not long before the Adelaide observations (Waltman, 1989a, 1989b), or may simply be the effect of orbital motion of the pulsar in a binary orbit.

7.7.3) Physical implications

Assuming that the long-term period derivative is physical, and not an artifact of the poorly defined 'orbital' ephemeris, the parameters determined from the TeV data permit the following calculations. If the emission is rotation-powered, then the total available energy from the rotation is $\sim 10^{39}$ erg s^{-1}. That half of the available energy should be emitted as TeV γ-rays may seem unlikely, but this would be just the prediction of the outer gap model if the pulsar were 'post-Vela-like' (see section 6.4.2). However, in the terms of the authors of that

model, the pulsar is 'Vela-like', and the predicted luminosity is only 10^{36} erg s^{-1}. Beaming considerations could not account for the large difference between theory and observation.

The polar gap model predicts an even lower luminosity of 6×10^{33} erg s^{-1}. The very narrow beaming factor of 0.016 would make the empirical calculation of isotropic luminosity appear artificially too large by a factor of 60, but this is insufficient to explain the discrepancy.

In view of its powerful emission across many orders of magnitude of the electromagnetic spectrum and its apparently orbital cycles, it is more plausible that the emission from Cygnus X-3 is powered by some mechanism other than rotation, such as accretion from a binary companion. The pulsar seems to be either very young, born with its fast rate of rotation, or old and spun up by accretion. If it is an accreting pulsar in the late stages of mass transfer, it provides an important evolutionary link between recycled pulsars and their precursors in X-ray binaries.

7.8) Discussion

In this last section, the fluxes derived from observations of millisecond pulsars will be compared with those expected from the two pulsar theories outlined in chapter 6, in an attempt to establish whether the models are feasible and to identify the location of the emission site. Cygnus X-3 has not been included in this section, because its emission is more likely to be powered by accretion processes

than by its rotation alone and its TeV luminosity cannot easily be predicted. Fluxes or flux limits for eight canonical millisecond pulsars remain for the comparison.

The systematic variations in fluxes estimated by different Cerenkov astronomy groups are notorious. They arise mostly because of differences in the assumed effective collecting areas of the telescopes. The assumed spectral indices of sources are generally similar and do not sig nificantly affect source luminosities. Only fluxes derived by the Durham group will be used here, because they can be intercompared without risk of systematic differences. Random errors remain due to use of the Rayleigh statistic in calculating fluxes.

In Table 7.15, the results described earlier in this chapter are summarised, together with the theoretical predictions made in chapter 6. To avoid complications arising from the conversion of observed fluxes to luminosities, the predicted luminosities have instead been converted to fluxes at the Earth. This eliminates model-dependent parameters such as beaming factors from the empirical calculations. It is worthy of mention here that luminosities calculated from observed fluxes assume isotropic emission from the pulsar and thus are overestimates.

The fluxes expected in each model are defined only to within an order of magnitude. Within these margins, both models can plausibly account for the observations. That the globular cluster pulsars have not been detected is in accordance with expectation. The pulse structure therefore becomes important. If the emission originates in the outer magnetosphere, then two pulses should be seen per pulsar revolution. If, however, the source of the emission is near the magnetic poles of the neutron star, then the pulse multiplicity should

Pulsar	Flux ($(10^2 m)^{-2} hr^{-1}$)		
	Outer gap+	Polar gap*	Observed
1937+21	1	18	10
1953+29	8	3	11
1855+09	373	140	90
1957+20	3	42	<11
1620-26	57	245	<30
1821-24	3	18790	<35

+ Assuming all emission is at a nominal threshold of 400 GeV.

* At the peak energy, E_c. The apparently high flux for PSR 1821-24 is misleading, as E_c is very low for this pulsar.

Table 7.15

The predicted and observed fluxes for six millisecond pulsars. Within the large errors present in both the predictions and observations, both models can plausibly account for the observed fluxes.

match that seen in radio observations. Of the three millisecond pulsars detected (PSR's 1937+21, 1855+09 and 1953+29), the former two both have strong radio interpulses, but the detection of these two pulsars at the half-period of rotation does not identify the emission site. PSR 1953+29, however, has no interpulse either in radio or in TeV measurements. This would indicate that the emission is from the polar region, and that we see only one pole. This is maybe the only strong evidence favouring either emission mechanism, and suggests that, for this pulsar at least, TeV γ-rays are created in and emitted from a charge-depleted gap above the magnetic poles.

CHAPTER 8

Summary and Conclusions

8.1) Signal enhancement and telescope design

TeV γ-ray astronomy is a rapidly advancing field. The telescopes of the current generation have detected a variety of sources. In telescope design, emphasis is now laid on signal enhancement techniques. Three techniques have been put forward as means of rejecting a large fraction of the background events caused by cosmic ray protons. 'Imaging' uses the spatial characteristics of photon-initiated extensive air showers in order to diferentiate between γ-ray source events and cosmic ray proton events. This technique has had considerable success in observations of the Crab nebula, but has yet to prove its universal applicability. A second enhancement technique, 'pulse shape discrimination', achieves a similar goal using the temporal profile of Cerenkov flashes. It is still a largely undeveloped technique, but shows very promising initial results.

An alternative technique is employed by the Durham group. It does not distinguish directly between EAS initiated by photons and other particles. Instead, the the acceptance angle of a telescope is matched to the narrow width of the Cerenkov light flash to achieve a high signal to noise ratio. Further enhancement is gained by using information from off-axis detectors to reject background events. The technique cannot reject background events coming by chance from the direction of the

source, but is subject to few of the uncertainties inherent in direct discrimination techniques and has proved highly successful. In the Durham Mark III telescope, typically half of the background is rejected on this basis. Since the background is already low because of the small geometrical aperture of the telescope, this results in a high quality dataset. An extension of the original system was considered in chapter 5. Instead of using a fixed discrimination threshold, the new system rejects events on the basis of the *fraction* of the Cerenkov light falling off-axis. This technique results in a more uniform selection of events across the spectrum of event 'sizes'. It was successful in improving event selection, cutting the background counts by a further factor of two. The new technique also makes allowance for the changes in Cerenkov flash characteristics with zenith angle. Empirically, the optimum rejection threshold appears to increase with zenith angle, but the dependence is difficult to study without a strong, steady source.

The technique also has the ability to distinguish between real signals and those which arise by chance in the data. This is possible because only a real signal should be enhanced by the event selection. Establishing early on that an effect of marginal significance is spurious saves much time spent making extensive observations in an attempt to confirm the effect. Since initial detections are frequently of low significance, this is an important tool for aiding observation strategies.

It is concluded that directional discrimination is a simple and efficient means of rejecting a large fraction of background events. Around three quarters of the events registered in a 1° field of view may be rejected on this basis. No signal has been detected in the rejected

events of any known sources, suggesting that a very high proportion of the source events is retained in the accepted data.

8.1.1) The Mark V telescope

Future telescopes designed and operated by the Durham group will also have the capacity to make detailed studies of Cerenkov flashes. The Mark V telescope is currently being built and will be deployed at Narrabri. Like the Marks III and IV, the Mark V telescope will operate on the successful coincidence system. Emphasis in its design has been laid on exploring techniques to reject as many as possible of the background events. Temporal, spatial and angular details of the Cerenkov flashes will be studied. For example, it will be possible to replace the conventional 2" diameter photomultiplier tubes of the centre dish with 24 1" PMT's. The original triple coincidence system will still be operated, and the array of small PMT's will give a coarse image of the Cerenkov flashes. This will allow a simple version of the 'imaging' technique to be applied to the data and compared with the effects of the 'guard ring' approach. It is hoped that such studies of the Cerenkov flash characteristics will lead to a compound method of event selection involving all the available information.

One new feature of the telescope design will be the addition of three extra photomultiplier tubes in each detector package. These will complete the guard ring for the alternate on-source channel used in chopped observations. Their addition will allow chopped observations to benefit fully from signal enhancement techniques. At present, less enhancement is possible for the half of a chopped observation when the

outer channel is on-source, since it has an incomplete guard ring.

8.2) TeV γ-rays from millisecond pulsars

Most TeV detections to date have been of X-ray binary pulsars. The large population of canonical radio pulsars has proved a much less successful subject of study. Only the Crab and Vela pulsars have so far been claimed as sources of TeV γ-rays (Gibson et al, 1982a, Bhat et al, 1980). However, the sub-population of 'recycled', millisecond pulsars may prove to contain some extremely efficient emitters of TeV photons.

The detection of TeV γ-rays from PSR 1855+09 represents the third detection of a millisecond pulsar at these energies. The detection has been made after extensive observations of the source. Curiously, the signal is modulated with the pulsar's binary orbit, appearing almost exclusively at the descending node. It does not vary appreciably in amplitude and appears in each of four years' data. The peak flux of 2.5×10^{-10} cm^{-2} s^{-1} is consistent with theoretical expectations. A fourth millisecond pulsar, PSR 1957+20, has also been observed, but has not yet been detected. The 3σ flux limit of 3×10^{-11} cm^{-2} s^{-1} is too high to conflict with theory.

Although this class of stars does not include any TeV γ-ray emitters as powerful as X-ray binary stars, their predictable behaviour makes them very suitable for study. Furthermore, the number of known millisecond pulsars is increasing rapidly, providing ever more targets for observation. Ten more millisecond pulsars in 47 Tucanae have recently been discovered (Manchester et al, 1991). These point to a

large population of millisecond pulsars in globular clusters. The globular clusters are therefore rich targets for TeV observations. Since they are relatively distant objects, it may not be possible to detect the individual pulsars. However, the summed flux from a cluster may be considerable. At a distance of $4^1/_2$ kpc, the 11 pulsars so far detected in 47 Tucanae could produce a TeV γ-ray flux of $\sim 10^{-10}$ $cm^{-1}s^{-1}$ for an average luminosity of 10^{33} erg s^{-1}. This would be detectable with the Durham Cerenkov telescopes after some tens of hours of observation. Given that these are probably only a subset of the detectable population of millisecond pulsars in the cluster, the actual flux may be much higher. A measurement of the TeV flux from 47 Tucanae would yield an independent estimate of the population of millisecond pulsars in the cluster. Estimates of the pulsar population are needed for studies of stellar evolution, especially of binary stars, and for understanding the physics of stellar associations. For example, the severe lack of gas in globular clusters has not yet been convincingly explained. It is possible that the high energy emission from fast pulsars (in the form of photons or other particles) is sufficient to have expelled the gas (Spergel, 1991). This example underlines the importance of including the effects of high energy emission from pulsars in models of galaxies and stellar clusters. It is interesting that the effects of pulsar radiation have usually been omitted in such models.

Estimates of pulsar populations using TeV fluxes are hindered by the difficulty in comparing the TeV fluxes predicted by theory with those observed. Accurate theoretical predictions are precluded by a lack of knowledge of details of the emitting regions and uncertainties in the distances to sources. For the empirical estimates of fluxes,

systematic errors arise because of assumptions of the collecting areas and energy thresholds of telescopes. These make it generally unwise to compare flux estimates made by different groups. Random errors are caused mainly by use of the Rayleigh statistic to estimate fluxes. These are reduced if the flux is determined using a number of datasets.

A comparison made in chapter 7 of the observed fluxes and those predicted by two emission models does not distinguish between the models. Given the large margins allowable in all the flux estimates, both models could satisfactorily account for the observations. A means agreed by all groups of ascribing fluxes to detections would be welcomed. This would allow flux measurements and limits made by different groups to be compared. Five of the six pulsars considered theoretically yield small but potentially detectable fluxes in the TeV region. The sixth pulsar, PSR 1821-24, has a much higher magnetric field. Consequently, curvature photons produced near the magnetic poles are downgraded further before they can escape. Thus, the emission from this pulsar may be concentrated at GeV energies, and it may not be detectable at TeV energies.

An alternative method of comparison between the emission models and the observed fluxes does not use estimates of the flux. The differences in the form of the TeV light curve predicted by the polar and outer gap models can be used to differentiate between them. The absence of an interpulse can be accommodated only in the polar gap model. Even in this model, an interpulse is expected if the radio light curve contains such a feature. Of the three millisecond pulsars detected, two have interpulses in both the radio and TeV emission. Only one, PSR 1953+29, does not have an interpulse in its radio light curve. The TeV emission

from this pulsar also has only a single peak. This empirical result therefore favours the polar gap model. Further detections of millisecond pulsars are needed if the conclusion is to be confirmed.

A parallel study of millisecond pulsars in the GeV region is likely to answer many of the questions raised by the TeV studies made to date. The high energy instruments aboard the Gamma Ray Observatory satellite (GRO) may provide the observations needed. EGRET is a spark chamber instrument designed to detect γ-rays of between 20 MeV and 30 GeV. The instrument represents a large increase in sensitivity over earlier comparable instruments, and it is hoped that it will be able to detect many of the fastest pulsars (Buccheri and Schoenfelder, 1989). A second instrument, the Compton Telescope (Comptel), is predicted to detect a subset of the EGRET pulsars. Satellite telescopes have the advantage over atmospheric Cerenkov telescopes that their collecting areas are better known. Flux estimates may therefore be considered with some confidence. Observations with the two GRO instruments may well resolve many of the questions about the γ-ray fluxes from millisecond pulsars.

It is clear that there is a great deal to be learnt from millisecond pulsars. It is hoped that much more work, both theoretical and empirical, will be done on the high energy emission from these objects. As the number of known millisecond pulsars grows, the opportunities for empirical research are many. A unified approach to estimating γ-ray telescope collecting areas and energy thresholds is much needed, so that results can be compared. Best possible use must also be made of the opportunities for comparative work afforded by GRO. These may take the form of both flux comparisons and studies of temporal behaviour in the two energy bands. It is hoped that a base of

established and well-studied TeV sources will be set up, from which the field of TeV astronomy can advance in confidence.

References

Ables J.G., Jacka C.E., McConnel D., Hamilton P.A., McCulloch P.M. and Hall P.J. (1988) 'PSR 0021-72A and 0021-72B', I.A.U. Circ. No. 4602

Ables J.G., McConnell D., Jacka C.E., McCulloch P.M., Hall P.J. and Hamilton P.A. (1989) 'A millisecond pulsar in a 32-minute binary orbit', Nature, 342, 158-161

Acharya B.S., Bhat P.N., Gandhi V,N., Ramana Murthy P.V. and Sathyanarayana G.P. (1990) 'Search for TeV gamma ray emission from PSR 1957+20' Astron. Astrophys., 232, L5-L8

Backer D.C., Kulkarni S.R., Heiles C., Davis M.M. and Goss W.M. (1982) 'A millisecond pulsar', Nature, 300, 615-618

Boriakoff V., Buccheri R. and Fauci F. (1983) 'Discovery of a 6.1-ms pulsar PSR 1953+29', Nature, 304, 417-419

Boriakoff V., Buccheri R., Fauci F., Turner K. and Davis M.M. (1984) 'The 6.1 millisecond binary pulsar', Proc. N.R.A.O. Workshop No. 8 (Green Bank, West Virginia, USA) Eds S.P. Reynolds and D.R. Stinebring

Batshelet E. (1981) Circular Statistics in Biology, Academic Press, London

Bhat P.N., Gupta S.K., Ramana Murthy P.V., Sreekantan B.V., Tonwar S.C. and Vishwanath P.R. (1980), 'Pulsed high energy gamma rays from Vela pulsar', Astron. Astrophys., 81, L3-L5

Bhat P.N., Ramana Murthy P.V. and Vishwanath P.R. (1988) 'Search for 12.6 millisecond periodicity in TeV gamma rays from Cygnus X-3', J. Astrophys. Astron., 55, 155-160

Bowden C.C.G., Bradbury S.M., Brazier K.T.S., Carraminana A., Chadwick P.M., Dipper N.A., Edwards P.J., Lincoln E.W., McComb T.J.L., Orford K.J., Rayner S.M. and Turver K.E. (1991) '400 GeV gamma rays from AE Aquarii', *in preparation*

Bowden C.C.G., Bradbury S.M., Brazier K.T.S., Carraminana A., Chadwick P.M., Dipper N.A., Edwards P.J., Lincoln E.W., McComb T.J.L., Orford K.J., Rayner S.M. and Turver K.E. (1990) 'TeV Gamma Rays from Millisecond Pulsars', Proc. Int. Conf. High Energy Gamma-Ray Astronomy (American Institute of Physics, New York), 75-86

Brazier K.T.S., Carraminaña A., Chadwick P.M., Currell T.R., Dipper N.A., Lincoln E.W., Mannings V.G., McComb T.J.L., Orford K.J., Rayner S.M. and Turver K.E. (1989a) 'The University of Durham Southern Hemisphere Gamma Ray Telescope', Experimental Astronomy, 1, 77-101

Brazier K.T.S., Carramiñana A., Chadwick P.M., Dipper N.A., Lincoln E.W., Mannings V.G., McComb T.J.L., Orford K.J., Rayner S.M. and Turver K.E. (1989b) 'VHE Gamma Ray Emission from Southern Hemisphere X-Ray Binaries', Proc. 23rd ESLAB Symposium on X-Ray Astronomy, ed. J. Hunt and B. Battrick, (ESA, Paris), 1, 311-314

Brazier K.T.S., Carramiñana A., Chadwick P.M., Dipper N.A., Lincoln E.W., McComb T.J.L., Orford K.J., Rayner S.M. and Turver K.E. (1989c) 'The detection of VHE Gamma Rays Using the Atmospheric Cerenkov Technique', Proc. 23rd ESLAB Symposium on X-Ray Astronomy, ed. J. Hunt and B. Battrick, (ESA, Paris) 1, 325-329

Brazier K.T.S., Carramiñana A., Chadwick P.M., Dipper N.A., Lincoln E.W., Mannings V.G., McComb T.J.L., Orford K.J., Rayner S.M., Turver K.E. and Williams D.G. (1990a) 'VHE Gamma Ray Emission from Sco X-1 and Cen X-3', Proc. 21st. Int. Cosmic Ray Conf. (Adelaide), 2, 296-299

Brazier K.T.S., Carramiñana A., Chadwick P.M., Dipper N.A., Lincoln E.W., Mannings V.G., McComb T.J.L., Orford K.J., Rayner S.M., Turver K.E. and Williams D.G. (1990b) 'The Performance of TeV Cerenkov Gamma Ray Telescopes', Proc. 21st. Int. Cosmic Ray Conf. (Adelaide), 4, 274-277

Brazier K.T.S., Carramiñana A., Chadwick P.M., Dipper N.A., Lincoln E.W., Mannings V.G., McComb T.J.L., Orford K.J., Rayner S.M. and Turver K.E. (1990c) 'Enhancement of the gamma ray signal in atmospheric Cerenkov light measurements using the University of Durham VHE gamma ray telescopes'. Nucl. Phys. B (Proc. Suppl.), 14A, 250-255

Brazier K.T.S., Carramiñana A., Chadwick P.M., Dipper N.A., Lincoln E.W., Mannings V.G., McComb T.J.L., Orford K.J., Rayner S.M. and Turver K.E. (1990d) '400 GeV emission from extragalactic X-ray binary pulsars', Proc. 21st Int. Cosmic Ray Conf. (Adelaide), 2, 300-303

Brazier K.T.S., Carramiñana A., Chadwick P.M., Dipper N.A., Lincoln E.W., Mannings V.G., McComb T.J.L., Orford K.J., Rayner S.M. and Turver K.E. (1990e) 'A search for VHE emission from pulsars', Proc. 21st Int. Cosmic Ray Conf. (Adelaide), 2, 304-307

Brazier K.T.,Carramiñana, Chadwick P.M., Dipper N.A., Lincoln E.W., Mackie P.C., Mannings V.M., McComb T.J.L., Orford K.J., Rayner S.M., Turver J.H. and Turver K.E., (1990f) 'New Measurements of the 12.6 ms pulsar in Cygnus X-3', Astrophys. J., 350, 745-753

Browning R. and Turver K.E. (1977) 'Cerenkov radiation from computer simulations of the γ-ray initiated atmospheric showers', Nuovo Cimento, 38A, 223-238

Buccheri R. and Schoenfelder V. (1989) 'Prospects for pulsar searches with the gamma ray observatory GRO', in Timing Neutron Stars, Kluwer, eds. Ogelman H. and van den Heuvel E.P.J., pp419-428

Callanan P.J., Charles P.A., Hassel B.J.M., Machin G., Mason K.O., Naylor T., Smale A.P. and van Paradijs J. (1989) 'A search for the optical counterpart of the binary millisecond pulsar PSR 1855+09', Mon. Not. R. Astr. Soc., 238, 25p-28p

Carramiñana A., Chadwick P.M., Dipper N.A., Lincoln E.W., Mannings V.G., McComb T.J.L., Orford K.J., Rayner S.M., Turver K.E. and Williams, D.G. (1989a) '300 GeV gamma rays from Vela X-1', Astrophys. J., 346, 967-970

Carramiñana A., Chadwick P.M., Dipper N.A., Lincoln E.W., Mannings V.G., McComb T.J.L., Orford K.J., Rayner S.M., Turver K.E. and Williams D.G. (1989b) 'VHE gamma ray emission from Centaurus X-3', in Timing Neutron Stars, Kluwer, eds. Ogelman H. and van den Heuvel E.P.J., pp369-374

Chadwick, P.M. (1987) Very high energy cosmic gamma-rays from radio and X-ray pulsars, Ph.D. thesis, University of Durham

Chadwick P.M., Dowthwaite J.C., Harrison A.B., Kirkman I.W., McComb T.J.L., Orford K.J. and Turver K.E. (1985a) 'Association of the 6-ms pulsar PSR1953 with the COS-B γ-ray source 2CG065', Nature, 317, 236-238

Chadwick P.M., Dowthwaite J.C., Harrison A.B., Kirkman I.W., McComb T.J.L., Orford K.J. and Turver K.E. (1985b) 'A 12.6-ms pulsar in Cygnus X-3', Nature, 318, 642-644

Chadwick P.M., Dowthwaite J.C., Harrison A.B., Kirkman I.W., McComb T.J.L., Orford K.J. and Turver K.E. (1985c) '4U0115+63: an energetic gamma ray binary pulsar', Astron. Astrophys., 151, L1-13

Chadwick P.M., Dipper N.A., Kirkman I.W., McComb T.J.L., Orford K.J. and Turver K.E. (1987) 'Simultaneous measurements of VHE gamma rays from Hercules X-1', in Very High Energy Gamma Ray Astronomy (Reidel) ed. K.E. Turver, pp121-123

Cheng K.S., Ho C. and Ruderman M.A. (1986a) 'Energetic radiation from rapidly spinning pulsars. 1. Outer magnetospheric gaps', Astrophys. J., 300, 500-521

Cheng K.S., Ho C. and Ruderman M.A. (1986b) 'Energetic radiation from rapidly spinning pulsars. 2. Vela and Crab', Astrophys. J., 300, 522-539

Cheng K.S. and de Jager O.C. (1990) ' Very high energy gamma rays from millisecond pulsars' Nucl. Phys. B (Proc. Suppl.), 14A, 28- 37

Chevalier C. and Ilovaisky S.A. (1977) 'The binary nature of the LMC X-4 optical candidate', Astron. Astrophys., 59, L9-L12

Chodil G., Mark H., Rodrigues R., Seward F., Swift C.D. and Hiltner W.A (1967) 'Spectral and location measurements of several cosmic X-ray sources including a variable source in Centaurus', Phys. Rev. Lett., 19, 681-683

Conover W.J. (1980) Practical Non-parametric Statistics, Wiley and Sons, New York

Craig M.A.B. (1984) The lateral distribution of Cerenkov light in large cosmic ray showers as a measure of longitudinal development, Ph.D. thesis, University of Durham

Danaher S., Fegan D.J., Porter N.A. and Weekes T.C. (1981) 'γ-ray observations of Cygnus X-3 at energies of 10^{12} eV', Nature, 289, 568-569

Davis M.M., Taylor J.H., Weisberg J.M. and Backer D.C. (1985) 'High-precision timing observations of the millisecond pulsar PSR 1937+21', Nature, 315, 547-550

Djorgovski S. and Evans C.R. (1988) 'Photometry and the light curve of the optical counterpart of the eclipsing millisecond pulsar PSR 1957+20', Astrophys. J. Lett., 335, L61-L65

Dowthwaite J.C. (1987) Very energetic gamma rays from binary X-ray sources and other astronomical objects, Ph.D. Thesis, University of Durham

Dowthwaite J.C., Harrison A.B., Kirkman I.W., Macrae J.H., Orford K.J., Turver K.E. and Walmsley M. (1983) 'The Galactic Plane: A source of 1000 GeV gamma rays', Astron. Astrophys., 142, 55-58

Eadie W.T. et al (1971) Statistical Methods in Experimental Physics, North Holland, Amsterdam

Eichler D. and Levinson A. (1988) 'On black widow evolutionary scenarios for binary neutron stars', Astrophys. J. Lett., 335, L67-L70

Fegan D.J., Cawley M.F., Gibbs K., Lamb R.C., Lewis D.A., Porter N.A., Reynolds P.T., Smyth G. and Weekes T.C. (1989) 'Search for a 12.59 ms pulsar in Cygnus X-3', Astron. Astrophys., 211, L1-L4

Foster R.S. and Backer D.C. (1990) 'Constructing a pulsar timing array', Astrophys. J., 361, 300-308

Foster R.S., Backer D.C., Taylor J.H. and Goss W.M. (1988) 'Period derivative pf the millisecond pulsar in globular cluster M28', Astrophys. J., 326, L13-L15

Fritz G., Henry R.C., Meekins J.F., Chubb T.A. and Friedmann H. (1969) 'X-ray Pulsar in the Crab Nebula', Science 164, 709-711

Fruchter A.S., Berman G., Bower G., Convery M., Goss W.M., Hankins T.H., Klein J.R., Nice D.J., Ryba M.F., Stinebring D.R., Taylor J.H., Thorsett S.E. and Weisberg J.M. (1990) 'The eclipsing millisecond pulsar PSR 1957+20', Astrophys. J., 351, 642-650

Fruchter A.S., Stinebring D.R. and Taylor J.H. (1988) 'A millisecond pulsar in an eclipsing binary', Nature 333, 237-239

Galbraith W. and Jelley J.V. (1953) 'Light pulses from the Night Sky associated with Cosmic Rays', Nature, 171, 349-350

Giacconi R., Gursky H., Kellogg E., Schreier E. and Tananbaum H. (1971) 'Discovery of periodic X-ry pulsations in Centaurus X-3 from UHURU', Astrophys. J., 167, L67-L73

Gibson A.I., Harrison A.B., Kirkman I.W., Lotts A.P., Macrae J.H., Orford K.J., Turver K.E. and Walmsley M. (1982a) 'Transient emission of ultra-high energy pulsed γ-rays from Crab pulsar PSR 0531', Nature, 296, 833-835

Gibson A.I., Harrison A.B., Kirkman I.W., Lotts A.P., Macrae J.H., Orford K.J., Turver K.E. and Walmsley M. (1982b) 'The University of Durham facility at Dugway', Proc. International Workshop on Very High Energy Gamma Ray Astronomy (Ootacamund, India), 97-117

Gilfanov M., Sunyaev R., Churazov E., Loznikov V., Efremov V., Kaniovskiy A., Kuznetsov A., Yamburenko N., Melioranskiy A., Skinner G.K., Al-Emam O., Patterson T.G., Willmore A.P., Brinkman A.C., Heise J., In't Zand J.J.M., Jager R., Pietsch W., Doebereiner S., Englhauser J., Reppin C., Truemper J., Voges W., Kendziorra W., Maisak M., Mony B., Staubert R., Parmar A.N. and Smith A. (1989) 'Observations of the X-ray pulsars from the Kvant module', Proc. 23rd ESLAB Symposium on Two Topics in X-Ray Astronomy, Bologna, Italy (European Space Agency), 1, 71-79

Goeckel (1910), Phys. Zeits., 11, 280

Gold T. (1968) 'Rotating neutron stars as the origin of the pulsating radio sources', Nature, 218, 731-732

Gorham P.W. (1986) Ground-based detection of gamma-rays above 200 GeV from Hercules X-1, Ph.D. thesis, University of Hawaii

Gorham P.W., Cawley M.F., Fegan D.J., Gibbs K.G., Lamb R.C., Liebing D.F., Porter N.A., Stenger V.J. and Weekes T.C. (1986) 'Pulsed TeV gamma rays detected from Hercules X-1 during X-ray source eclipse', Astrophys. J., 308, L11-L15

Gregory A.A., Patterson J.R., Roberts M.D., Smith N.I. and Thornton G.J. (1990) 'Observations of Cygnus X-3 near 100 TeV using the low elevation atmospheric technique', Astron. Astrophys., 237, L5-L8

Gupta S.K., Rajeev M.R., Sreekantan B.V., Srivatsan R. and Tonwar S.C. (1991) 'Episodic emission of UHE radiation from the eclipsing binary pulsar PSR 1957+20: Ooty observations', Astron. Astrophys. 241, L21-L24

Harding A.K. (1989) 'Gamma rays from pulsar wind shock acceleration', in Proceedings of the Energetic Gamma-Ray Experiment Telescope (EGRET) Science Symposium (Goddard Space Flight Center) NASA, pp183-198

Hess V. (1911), Phys. Zeits., 12, 998

van den Heuvel E.P.J. and van Paradijs J. (1988) 'Fate of the companion stars of ultra-rapid pulsars', Nature, 334, 227-228

van den Heuvel E.P.J. and Taam R.E. (1984) 'Two types of binary radio pulsars with different evolutionary histories', Nature, 309, 235-237

Hewish A., Bell S.J., Pilkington J.D.H., Scott P.F. and Collins R.A. (1968) 'Observation of a Rapidly Pulsating Radio Source' Nature 217, 709-713

Hillas A.M. (1985) 'Cerenkov light images of EAS produced by primary gamma rays and by nuclei', Proc 19th International Cosmic Ray Conf. (La Jolla), 3, 445-448

Imamura J.N., Steiman-Cameron T.Y. and Middleditch J. (1987) 'A possible 1.13 millisecond periodicity in GX 339-4', Astrophys. J., 314, L11-L13

de Jager O.C. (1987) The analysis and interpretation of VHE gamma ray measurements, Ph.D. thesis, Potchefstroom University for Christian Higher Education, Republic of South Africa

de Jager O.C., Brink C., Meintjies P.J., Nel H.I., North A.R., Raubenheimer B.C. and van der Walt D.J. (1990) 'VHE gamma rays from radio pulsars and cataclysmic variables' Nucl. Phys. B (Proc. Suppl.), 14A, 169-175

de Jager O.C., Swanepoel J.W.H. and Raubenheimer B.C. (1989) 'A powerful test for weak periodic signals with unknown light curve shapes in sparse data', Astron. Astrophys., 221, 180-190

Jelley J.V. (1958) Cerenkov Radiation and its Applications, Pergamon Press, London

Kelley R.L., Rappaport S., Clark G.W. and Petro L.D. (1983a) 'Orbital Period Changes in Centaurus X-3', Astrophys. J., 268, 790-799

Kelley R.L., Jernigan J.G., Levine A., Petro L.D. and Rappaport S. (1983b) 'Discovery of 13.5s X-ray pulsations from LMC X-4 and an orbital determination', Astrophys. J., 264, 568-574

Kenter A.T. (1989) A Search for Very High Energy Gamma Rays from the Crab Nebula, Ph.D. thesis, Wisconsin-Madison

Kitamoto S., Mizobuchi S., Yamashita K. and Nakamura H. (1991) 'Time variations in the X-rays from Cygnus X-3 observed with Ginga', preprint

Kluzniak W., Ruderman M., Shaham J. and Tavani M. (1988) 'Nature and evolution of the eclipsing millisecond binary pulsar PSR 1957+20', Nature, 334, 225-227

Kulkarni S.R., Djorgovski S. and Klemola A.R. (1991) 'Optical and radio observations of the binary pulsar 1855+09: evolution of pulsar magnetic fields and low-mass white dwarf cooling', Astrophys. J., 367, 221-227

Kulkarni S.R. and Hester J.J. (1988) 'Discovery of a nebula around PSR 1957+20', Nature 335, 801-803

Lang M.J., Cawley M.F., Fegan D.J., Hillas A.M., Kwok P.W., Lamb R.C., Lewis D.A., Macomb D., Reynolds P.T., Vacanti G. and Weekes T.C. (1990) 'Observations of TeV gamma-rays from the Crab Nebula using the Whipple Observatory High Resolution Camera', Proc. 21st International Cosmic Ray Conf. (Adelaide), 2, 139-142

Lawrence M.A., Reid R.J.O. and Watson A.A. (1990) 'A reassessment of the Haverah Park energy spectrum above 3 x 10^{17} eV', Proc. 21st International Cosmic Ray Conf. (Adelaide), 3, 159-162

Lloyd-Evans J., Coy R.N., Lambert A., Lapikens J., Patel M., Reid R.J.O. amd Watson A.A. (1983) 'Observations of γ rays > 10^{15} eV from Cygnus X-3', Nature, 305, 784-786

Lyne A.G., Biggs J.D., Brinklow A. Ashworth M. and McKenna J. (1988) 'Discovery of a binary millisecond pulsar in the globular cluster M4', Nature, 332, 45-47

Lyne A.G., Brinklow A., Middleditch J., Kulkarni S.R., Backer D.C. and Clifton T.R. (1987) 'The discovery of a millisecond pulsar in the globular cluster M28', Nature, 328, 399-401

Lyne A.G. and Graham-Smith F. (1990) Pulsar Astronomy, Cambridge University Press, Cambridge, England

Lyne A.G., Manchester R.N., D'Amico N., Staveley-Smith L., Johnston S., Lim J., Fruchter A.S., Goss W.M. and Frail D. (1990) 'An eclipsing millisecond pulsar in the globular cluster Terzan 5', Nature 347, 650-652

Macomb D.J., Cawley M.F., Fegan D.J., Hillas A.M., Kwok P.W., Lamb R.C., Lang M.J., Lewis D.A., Reynolds P.T., Vacanti G. and Weekes T.C. (1990) 'Search for TeV emission from 4U0115+63', Astrophys. J. (in the press)

Makino F. et al (1987) 'X-ray pulsars', I.A.U. Circ. No. 4459

Manchester R.N., Lyne A.G., D'Amico N., Johmston S. Lim J. and Kniffen D.A. (1990) 'A 5.75-millisecond pulsar in the globular cluster 47 Tucanae', Nature, 345, 598-600

Manchester R.N., Lyne A.G., Robinson C., D'Amico N., Bailes M. and Lim J. (1991) 'Discovery of ten millisecond pulsars in the globular cluster 47 Tucanae', Nature, 352, 219-221

Mardia K.V. (1972) Statistics of Directional Data, Academic Press

McKenna J. and Lyne A.G. (1988) 'Timing measurements of the binary millisecond pulsar in the globular cluster M4', Nature, 336, 226-227

Millikan R.A. and Bowen I.S. (1926) 'High frequency rays of cosmic origin. i. Sounding balloon observations at extreme altitudes', Phys. Rev., 27, 353-361

Millikan R.A. and Otis R.M. (1926) 'High frequency rays of cosmic origin. ii. Mountain peak and airplane observations', Phys. Rev., 27, 645-658

Nice D.J., Thorsett S.E., Taylor J.H. and Fruchter A.S. (1990) 'Observations of the eclipsing binary pulsar in Terzan 5', Astrophys. J., 361, L61-L63

North A.R., Raubenheimer B.C., de Jager O.C., van Tonder A.J. and van Urk G. (1987) 'Pulsed TeV gamma-rays from Vela X-1', Nature, 326, 567-569

North A.R., Brink C., Cheng K.S., de Jager O.C., Nel H.I. and Raubenheimer B.C. (1989) 'Orbitally modulated VHE gamma-rays from Cen X-3', Proc. 23rd ESLAB Symposium on Two Topics in X-ray Astronomy, European Space Agency, 1, 563-566

North A.R., Brink C., Cheng K.S., de Jager O.C., Nel H.I. and Raubenheimer B.C. (1990) 'TeV gamma ray observations of Cen X-3', Proc. 21st International Cosmic Ray Conf., 2, 275-278

Orford K.J. (1990) 'Analytical treatment of oversampling', *submitted to* Experimental Astronomy

Patterson J.R. and Hillas A.M. (1989) 'Optimising the design of very high energy gamma ray telescopes', Nucl. Instr. Meth. Phys. Res., A278, 553-564

Phinney E.S., Evans C.R., Blandford R.D. and Kulkarni S.R. (1988) 'Ablating dwarf model for eclipsing millisecond pulsar 1957+20', Nature 333, 832-834

Podsiadlowski Ph., Naylor R. and Fabian A.C. (1990) 'The effects of dispersion on the apparent orbital parameters of close binary millisecond pulsars and PSR 0021-72A', Mon. Not. R. Astr. Soc., 247, 523-528

Pounds K.A., Cooke B.A., Ricketts M.J., Turner M.J. and Elvis M. (1975) 'An extended observation of Cen X-3 with the Ariel-5 sky survey', Mon. Not. R. Astr. Soc., 172, 473-481

Protheroe R.J. (1977) Computer simulations of large cosmic ray showers using recent models of hadronic collisions, Ph.D. thesis, University of Durham

Radhakrishnan V. and Cooke D.J. (1969) 'Magnetic poles and the polarization structure of pulsar radiation', Astrophys. Lett., 3, 225-229

Raubenheimer B.C., North A.R., de Jager O.C., Meintjes P.J., Brink C., Nel H.I., van Urk G. and Visser B. (1991) 'TeV gamma-rays from accreting binary systems' Proc. Int. Conf. High Energy Gamma-Ray Astron. (American Institute of Physics, New York), 70-74

Rawley L.A., Taylor J.H. and Davis M.M. (1988) 'Fundamental Astrometry and Millisecond Pulsars', Astrophys. J. 326, 947-953
Rayner, S.M. (1989) Very high energy gamma rays from isolated pulsars and non-pulsating objects, Ph.D thesis, University of Durham

Resvanis L., Learned J. Stenger V., Weeks D., Gaidos J., Loeffler F., Olson J., Palfrey T., Sembroski G., Wilson C., Camerini U., Finley J., Fry W., Jaworski M., Jennings J., Kenter A., Koepsel R., Lomperski M., Loveless R., March R., Matthews J., Morse R., Reeder D., Sandler P., Slane P and Szentgyorgyi A. (1987a) 'VHE gamma rays from Cygnus X-3', in Very High Energy Gamma Ray Astronomy (Reidel), ed. K.E. Turver, pp105-110

Resvanis L., Learned J. Stenger V., Weeks D., Gaidos J., Loeffler F., Olson J., Palfrey T., Sembroski G., Wilson C., Camerini U., Finley J., Fry W., Jaworski M., Jennings J., Kenter A., Koepsel R., Lomperski M., Loveless R., March R., Matthews J., Morse R., Reeder D., Sandler P., Slane P and Szentgyorgyi A. (1987) 'VHE gamma rays from the X-ray pulsar 4U0115+63', in Very High Energy Gamma Ray Astronomy (Reidel), ed. K.E. Turver, pp135-138

Resvanis L.K., Szentgyorgyi A., Hudson J., Kelley L., Learned J.G., Sinnis C., Stenger V., Weeks D.D., Gaidos J., Kertzman M., Loeffler F., Palfrey T., Sembroski G., Wilson C., Camerini U., Finley J.P., Fry W., Jennings J., Kenter A., Lomperski M., Loveless R., March R., Matthews J., Morse R., Reeder D. and Slane P. (1988) 'VHE gamma rays from Hercules X-1', Astrophys. J., 328, L9-L12

Reynolds P.T., Cawley M.F., Fegan D.J., Hillas A.M., Kwok P.W., Lamb R.C., Lewis D.A., Macomb D., Vacanti G. and Weekes T.C. (1990) 'Observations of Hercules X-1 at TeV energies', Proc. 21st International Cosmic Ray Conf. (Adelaide), 2, 99-102

Roberg J. and Nordheim L.W. (1949) 'The angular and lateral spread of cosmic ray showers', Phys. Rev., 75, 444-457

Ruderman M.A. (1991) 'Neutron star crustal plate tectonics. 1. Magnetic dipole evolution in millisecond pulsars', Astrophys. J., 366, 261-269

Ruderman M., Shaham J., Tavani M. and Eichler D. (1989) 'Late evolution of very low mass X-ray binaries sustained by radiation from their primaries', Astrophys. J., 343, 292-312

Ruderman M.A. and Sutherland P.G. (1975) 'Theory of pulsars: polar gaps, sparks, and coherent microwave emission', Astrophys. J., 196, 51-72

Rutherford and Cooke (1903), Phys. Rev., 16, 183

Ryba M.F. and Taylor J.H. (1991) 'High-precision timing of millisecond pulsars. 1. Astrometry and masses of the PSR 1855+09 system', Astrophys. J., 371, 739-748

Samorski M. and Stamm W. (1983) 'Detection of 2 x 10^{15} eV to 2 x 10^{16} eV gamma rays from Cygnus X-3', Astrophys. J., 268, L17-L21

Schreier E., Levinson R., Gursky H., Kellogg E., Tananbaum H. and Giacconi R. (1972) 'Evidence for the binary nature of Centaurus X-3 from Uhuru X-ray observations', Astrophys. J., 172, 179-L89

Schreier E., Schwartz K., Giacconi R., Fabbiano G. and Morin J. (1976) 'The long-term intensity behaviour of Centaurus X-3', Astrophys. J., 204, 539-547

Segelstein D.J., Taylor J.H., Rawley L.A. and Stinebring D.R. (1986) 'New millisecond binary pulsar', I.A.U Circ. No. 4162

Segelstein D.J., Rawley L.A., Stinebring D.R., Fruchter A.S. and Taylor J.H. (1986) 'New millisecond pulsar in a binary system', Nature, 322, 714-717

Shapiro S.L. and Teukolsky S.A. (1988) 'Are Trojans pursuing the eclipsing pulsar', Nature 333, 213

Sinha S., Acharya B.S., Bhat P.N., Khairatkar S.G., Rajeev M.R., Rao M.V.S., Sivaprasad K., Sreekantan B.V., Vishwanath P.R. and Viswanathan K. (1990) 'UHE gamma rays from the recently discovered eclipsing binary pulsar PSR 1957+20', Proc. 21st International Cosmic Ray Conf. (Adelaide), 2, 370-374

Spergel D.N. (1991) 'Evacuation of gas from globular clusters by winds from millisecond pulsars', Nature, 352, 221-222

Srinivasan G. (1989) 'Pulsars: their origin and evolution', Astron. Astrophys. Review, 1, 209-260

Steiman-Cameron T., Imamura J., Middleditch. J. and Kristian J. (1990) 'A 190 second periodicity in the optical emission of the enigmatic X-ray source GX 339-4', Astrophys. J., 359, 197-203

Stokes G.H., Segelstein D.J., Taylor J.H. and Dewey R.J. (1986) 'Results of two surveys for fast pulsars', Astrophys. J., 311, 694-700

Tavani M. (1991a) 'Birthrates of Galactic millisecond pulsars and their low-mass X-ray binary precursors', Astrophys. J., 366, L27-L31

Tavani M. (1991b) 'Orbital evolution of low-mass X-ray binaries due to radiation driven mass transfer', Nature, 351, 39-41

Tuohy I.R. and Cruise A.M. (1975) 'Observation of an accretion wake and pre-eclipse dips on Centaurus X-3', Mon. Not. R. Astron. Soc., 171, 33P-39P

Tumer O.T., Hammond J.S., White R.S. and Zych A.D. (1990a) 'Analysis of VHE gamma rays from the Crab nebula using pulse shape discrimination', in Proceedings of the 21st International Cosmic Ray Conference (Adelaide) University of Adelaide, 2, 155-158

Tumer O.T., Hammond J.S., Zych A.D. and MacCallum C. (1990b) 'VHE gamma-ray observation of the Crab Nebula with pulse shape discrimination to reduce the cosmic-ray background', Nucl. Phys. B (Proc. Suppl.), 14A, 176-180

Usov, V.V. (1983) 'Expected high-frequency radiation from the 1.5-ms pulsar', Nature, 305, 409-410

Waltman E.B., Fiedler R.L. and Johnston K.J. (1989a) 'V1521 Cygni (Cygnus X-3)', I.A.U Circ. No. 4798

Waltman E.B., Fiedler R.L. and Johnston K.J. (1989b) 'V1521 Cygni (Cygnus X-3)', I.A.U Circ. No. 4817

Wasserman I. and Cordes J.M. (1988) 'Physical implications of the eclipsing binary pulsar', Astrophys. J. Lett., 333, L91-L94

Weekes T.C., Cawley M.F., Fegan D.J., Gibbs K.G., Hillas A.M., Kwok P.W., Lamb R.C., Lewis D.A., Macomb D., Porter N.A., Reynolds P.T. and Vacanti G. (1989) 'Observation of TeV gamma rays from the Crab nebula using the atmospheric Cerenkov imaging technique', Astrophys. J., 342, 379-395

Wolszczan A. (1990) 'PSR 1257+12 and PSR 1534+12', I.A.U. Circ. No. 5073

Wolszczan A. (1991) 'A nearby 37.9-ms radio pulsar in a relativistic binary system', Nature, 350, 688-690

Wolszczan A., Anderson S., Kulkarni S. and Prince T. (1990) 'Two millisecond pulsars in M5', I.A.U. Circ. No. 4880

Wright G.A. and Loh E.D. (1986) 'Companion star of a binary millisecond pulsar', Nature 324, 127-128